Journal of Cellular Physiology

Complement 3 is Involved in Changing the Phenotype of Human Glomerular Mesangial Cells

JIAN-XIN WAN,[1] NOBORU FUKUDA,[1,2]* MORITO ENDO,[1,3] YOSHIKO TAHIRA,[1] EN-HUI YAO,[1] HIROYUKI MATSUDA,[1,2] TAKAHIRO UENO,[1] AND KOICHI MATSUMOTO[1]

[1]*Department of Medicine, Division of Nephrology and Endocrinology, Nihon University School of Medicine, Tokyo, Japan*

[2]*Advanced Research Institute for the Science and Humanities, Nihon University, Tokyo, Japan*

[3]*Faculty of Human Health Science, Hachinohe University, Aomori, Japan*

Complement activation contributes to tissue injury in various forms of glomerulopathy and is characterized by deposition of complement components, which accelerates the progression of chronic renal damage. We recently reported that complement 3 (C3), a critical component of the complement system, is associated with the synthetic phenotype of vascular smooth muscle cells. It is possible that C3 stimulates mesangial cells to assume the synthetic phenotype to, in turn, induce glomerular injury and sclerosis. We investigated the role of C3 in the growth and phenotype of mesangial cells. Cultured human mesangial cells (HMCs) expressed C3 mRNA and protein, and levels were increased in response to IFN-γ and TNF-α. HMCs also expressed C3a receptor mRNA and protein. Exogenous C3a stimulated DNA synthesis in HMCs in a dose-dependent manner. C3a decreased expression *h*-caldesmon mRNA, a marker of the contractile phenotype, and increased the expression of osteopontin, matrix Gla, and collagen type1 α1 (collagen IV) mRNAs, which are markers of the synthetic phenotype. C3a decreased expression of α-smooth muscle actin in HMCs. Small interfering RNA (siRNA) targeting C3 reduced the DNA synthesis and proliferation of HMCs, increased expression of *h*-caldesmon mRNA, and decreased expression of osteopontin, matrix Gla, and collagen IV mRNAs in HMCs. These results indicate that C3 causes HMCs to convert to the synthetic phenotype and stimulates growth of mesangial cells, suggesting that C3 may play an important role in phenotypic regulation of mesangial cells in renal diseases.

J. Cell. Physiol. 213: 495–501, 2007.

Proliferation of glomerular mesangial cells appears to play an important role in the pathogenesis of progressive glomerular abnormalities leading to glomerulosclerosis. In experimental models of glomerulopathy, increased mesangial cell proliferation often precedes the development of glomerulosclerosis with increased extracellular matrix (ECM) deposition in the mesangium (Pesce et al., 1991; Floege et al., 1992). The search for agents which are capable of favorably regulating MC proliferation are, therefore, of considerable clinical importance in the area of progressive glomerular damage. There are known many similarities between the function and structure of the glomerulus and those of the vasculature. Endothelial cells compose both the glomerulus and vasculature, and mesangial cells are modified vascular smooth muscle cells (VSMCs) derived from the same progenitor cells (Bakris et al., 1996). We found that complement 3 (C3) is expressed in spontaneously hypertensive rat (SHR)-derived VSMCs that show the synthetic phenotype and exaggerated growth. We found that C3 causes VSMCs to convert from the contractile to the synthetic phenotype to stimulate growth (Lin et al., 2004).

Complement components, particularly C3, have been detected in glomeruli of patients with a variety of renal diseases (Welch, 2001). It is generally accepted that the complement system is associated with the development of glomerulopathy, and the beneficial effects of complement inhibition have been investigated in cases of acute and chronic renal injury (Johnson, 1997). Moreover, recent studies have suggested that local production of complement significantly influences pathologic conditions in renal disease (Zhou et al., 2001). Complement activation leads to tissue injury in several ways, including generation of anaphylactic and chemotactic peptides C3a and C5a by cleavage of C3 and C5, respectively, and formation of the C5b-9 membrane attack complex. However, little attention has been given to the direct effects of C3, which is a central component of the complement system that acts on human glomerular mesangial cells (HMCs).

In the current study, to examine the contributions of C3 to glomerulopathy, we investigated the role of C3 in phenotype modulation and proliferation of HMCs.

Materials and Methods

Cell culture

HMCs were purchased from Cambrex BioScience (Walkersville, MD). HMCs were maintained in RPMI 1640 (Sigma, St. Louis, MO) with 10% fetal bovine serum (FBS) (Gibco Laboratories, Grand Island, NY) and 0.05 mg/ml gentamicin (Gibco). Experiments were performed on cells between the fifth and tenth passages.

Contract grant sponsor: Ministry of Education, Science, Sports, and Culture of Japan;
Contract grant number: 15590863.

*Correspondence to: Noboru Fukuda, Department of Medicine, Nihon University School of Medicine, Ooyaguchi-kami 30-1, Itabashi-ku, Tokyo 173-8610, Japan.
E-mail: fukudan@med.nihon-u.ac.jp

Received 10 November 2006; Accepted 2 April 2007

DOI: 10.1002/jcp.21129

Determination of DNA synthesis and cell numbers

DNA synthesis in HMCs was assessed by 5-bromo-2-deoxyuridine (BrdU) labeling and detection with an ELISA kit (Cell Proliferation ELISA System, RPN250, Amersham Biosciences, Buckinghamshire, UK). Quiescent HMCs were treated both with and without human complement 3a (C3a, Calbiochem, Spring Valley, CA) for 24 h and then incubated with 10 μM BrdU for 2 h. BrdU uptake was measured according to the ELISA protocol. The optical density was determined in a plate reader at 450 nm (Microplate Reader MPR-A4i-II, Tosoh, Tokyo, Japan).

Quiescent HMCs were incubated for 24 h in 12-well plates with RPMI 1640 with 5% FBS containing 0.05 mg/ml gentamicin (Gibco). HMCs were trypsinized with 0.05% trypsin at 24, 48, and 72 h after inoculation, and cell numbers were counted with a Coulter Counter (Beckman Coulter, Fullerton, CA).

Reverse transcription-polymerase chain reaction (RT-PCR) analysis

Total RNA was extracted from cultured HMCs with ISOGEN (Nippon Gene, Toyama, Japan) according to the manufacturer's instructions. Aliquots of total RNA were reverse transcribed into single-stranded cDNA by incubation with avian myeloblastoma virus reverse transcriptase (Takara Biochemicals, Osaka, Japan). Diluted cDNA products were then subjected to PCR. Primers used to amplify complement 3 (C3), *h*-caldesmon, osteopontin, matrix Gla, and collagen type1 α1 (collagen IV) transcripts are listed in Table 1. Human 18S ribosomal RNA was amplified as an internal control. PCR was performed according to the profiles shown in Table 2. PCR was performed in a DNA thermal cycler (GeneAmp PCR System 2700, Applied Biosystems, Foster City, CA). The quality and concentration of amplified PCR products were determined with the Agilent 2100 Bioanalyzer (Agilent, Palo Alto, CA).

Western blot analysis for C3 and C3a receptor proteins

HMCs or U937 cells (positive control for C3a Receptor) were disrupted with lysis buffer (50 mM Tris-HCl [pH 8.0], 150 mM NaCl, 0.02% sodium azide, 100 μg/ml phenylmethylsulfonyl fluoride, 1 μg/ml aprotinin, 1% Triton X-100). Total proteins were extracted, heated at 95°C for 5 min, subjected to 7.5% SDS–polyacrylamide gel electrophoresis (SDS–PAGE), and electroblotted onto PVDF membranes (Amersham Biosciences, Uppsala, Sweden). Blots were incubated with rabbit polyclonal antibody specific for C3, goat polyclonal antibody specific for C3a receptor (Santa Cruz Biotechnology, Santa Cruz, CA), or mouse monoclonal antibody specific for α-tubulin (Sigma) as an internal control and then with goat anti-rabbit IgG, donkey anti-goat IgG or goat anti-mouse IgG (Bio-Rad Laboratories, Hercules, CA), respectively, as secondary antibodies. Bound antibodies were detected by enhanced chemiluminescence (ECL Kit, RPN2106, Amersham) and exposure to X-ray films. SDS–PAGE molecular weight markers (Prestained SDS–PAGE Standard Broad Range, Bio-Rad) were run to calibrate the gel. Bands were scanned and quantitated by densitometry with NIH Image Software (NIH Image 1.63f).

TABLE 1. PCR primers and product sizes

Target mRNA	Primer	Sequence	PCR product (bp)
C3	5′	5′-GCTGAAGCACCTCATTGTGA-3′	169
	3′	5′-CTGGGTGTACCCCTTCTTGA-3′	
h-caldesmon	5′	5′-TCGCCTACCAGAGAATGAC-3′	300
	3′	5′-TTGTTGGGTCGAACTCCTTC-3′	
Osteopontin	5′	5′-TCAGCTGGATGACCAGAGTG-3′	153
	3′	5′-TGAAATTCATGGCTGTGGAA-3′	
Matrix Gla	5′	5′-CACGAGCTCAATAGGGAAGC-3′	188
	3′	5′-GCTGCTACAGGGGGATACAA-3′	
Collagen IV	5′	5′-TGGTCCAAGAGGATTTCCAG-3′	192
	3′	5′-TCATTGCCTTGCACGTAGAG-3′	
18S	5′	5′-CGACGACCCATTCGAACGTCT-3′	312
	3′	5′-GCTATTGGAGCTGGAATTACCG-3′	

PCR, polymerase chain reaction; C3, complement 3.

TABLE 2. Thermal cycling profiles for PCR

Target mRNA	Denaturation	Primer annealing	Primer extension	Cycles
C3	94°C, 30 sec	58°C, 30 sec	72°C, 30 sec	35
h-caldesmon	94°C, 30 sec	55°C, 30 sec	72°C, 30 sec	30
Osteopontin	94°C, 30 sec	57°C, 30 sec	72°C, 30 sec	30
Matrix Gla	94°C, 30 sec	56°C, 30 sec	72°C, 30 sec	30
Collagen IV	94°C, 30 sec	55°C, 30 sec	72°C, 30 sec	30
18 S	94°C, 30 sec	55°C, 30 sec	72°C, 30 sec	20

Immunofluorescence of α-smooth muscle actin

Immunocytochemical staining was performed for α-smooth muscle actin expression. HMCs were immunostained using monoclonal mouse anti-smooth muscle actin antibody (1A4, 1:200; Dako, Carpinteria, CA), a marker for the contratile phenotype. Incubation with the primary antibody dilution was performed at 4°C overnight. Incubation with secondary FITC-conjugated goat anti-mouse IgG (1:1,000, Invitrogen, Tokyo, Japan) was performed for 60 min in the dark. Coverslips were placed over the cells and sealed with manicure. Cells were visualized by fluorescence microscopy with standard FITC excitation/emission filter combinations.

Application of short interfering RNA (siRNA)

A duplex siRNA was designed to target human C3 (NCBI: NM_000064). The target sequence is CCGAGCCGTTCTCTACAATTA (2,601–2,621 bp). The siRNA nucleotide sequences for C3 were r(GAGCCGUUCUCUACAAUUA)dTdT (Sense) and r(UAAUUGUAGAGAACGGCUC)dGdG (Antisense). Meanwhile, a non-silencing siRNA duplex targeting sequence, AATTCTCCGAACGTGTCACGT, was used as a negative control (control siRNA). Control siRNA nucleotide sequences were r(UUCUCCGAACGUGUCACGU)dTdT (Sense) and r(ACGUGACACGUUCGGAGAA)dTdT (Antisense). The duplex siRNA to C3 and the control siRNA duplex were synthesized by Qiagen (Tokyo, Japan). HMCs were seeded in 12-well plates at a density of 1×10^5 cells per well to obtain 50% confluence. Transfection of the siRNA was performed with RNAiFect Transfection Reagent (Qiagen) in RPMI 1640 (without FBS and antibiotics) per the manufacturer's instructions to yield a final siRNA concentration of 3.3 μg/ml in the culture media. Forty-eight hours after transfection of siRNA, cells were stimulated with 0.1 μM C3a, 10 μg/ml tumor necrosis factor-α (TNF-α, Sigma), or 50 ng/ml interferon-γ (IFN-γ, Sigma) for 24 h. Control cells were transfected with the siRNA buffer alone.

Statistical analysis

Values are reported as mean ± SEM. Statistical analysis was done with Student's *t*-test for unpaired data, two-way analysis of variance (ANOVA), or Duncan's multiple range test. $P < 0.05$ was considered statistically significant.

Results

Expression of C3 and C3a receptor mRNA and protein in cultured HMCs

HMCs expressed both C3 mRNA and protein. IFN-γ and TNF-α significantly increased levels of C3 mRNA and protein in HMCs (Fig. 1A,B). HMCs also expressed C3a receptor mRNA and protein (Fig. 1C,D). C3a receptor mRNA expression was increased by exogenous C3a, TNF-α and IFN-γ.

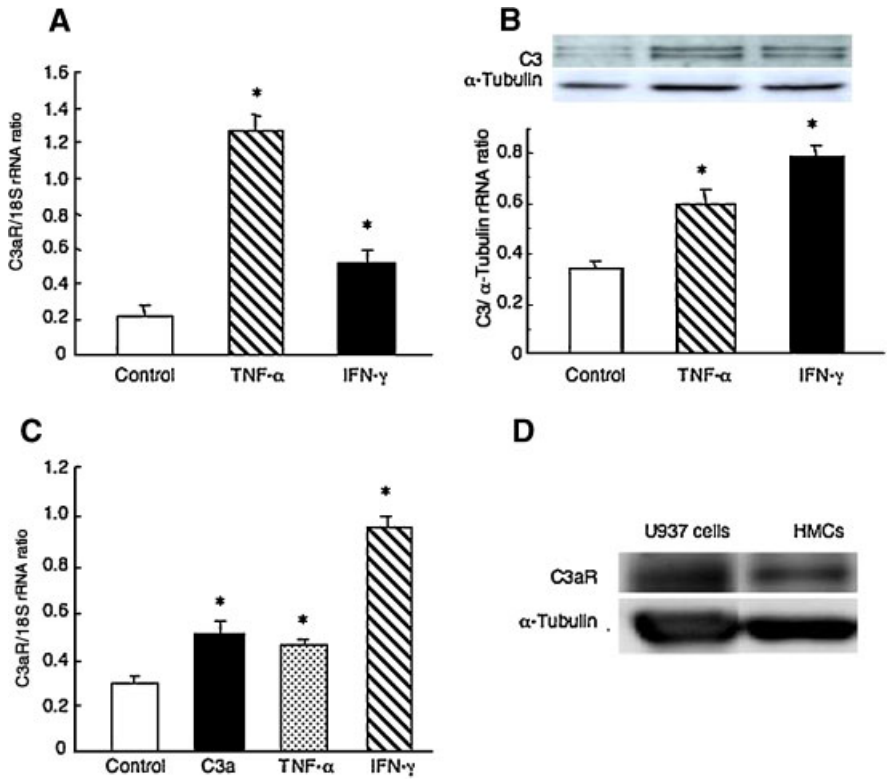

Fig. 1. A: Expression of C3 mRNA by RT-PCR analysis of cultured HMCs treated with TNF-α or IFN-γ. Quiescent HMCs were incubated without (control) or with 10 μg/ml TNF-α or 50 ng/ml IFN-γ for 24 h. The ratio of the abundance of each mRNA to that of 18S rRNA was evaluated by densitometric analysis. B: Expression of C3 protein by Western blot analysis in HMCs cultured without or with TNF-α and IFN-γ. Quiescent HMCs were incubated without (control) or with 10 μg/ml TNF-α or 50 ng/ml IFN-γ for 24 h. The ratio of the abundance of C3 protein to that of α-tubulin was evaluated by densitometric analysis. C: RT-PCR analysis of expression of C3a receptor (C3aR) mRNA by cultured HMCs without or with C3a, TNF-α, and IFN-γ. Quiescent HMCs were incubated without (control) or with 0.1 μM C3a, 10 μg/ml TNF-α, or 50 ng/ml IFN-γ for 24 h. The ratio of the abundance of each mRNA to that of 18S rRNA was evaluated by densitometric analysis. D: Expression of C3a receptor protein by Western blot analysis in HMCs or U937 cells. Data are mean ± SEM (n = 6). *$P < 0.05$ versus control cells.

Effects of exogenous C3a on phenotype and growth of HMCs

C3 convertases, including the spontaneously generated fluid-phase convertase, cleave C3 and release the anaphylatoxin C3a. The effects of exogenous C3a on phenotypic marker mRNAs and DNA synthesis in HMCs are shown in Figure 2. Exogenous C3a significantly decreased the abundance of *h*-caldesmon mRNA in HMCs ($P < 0.05$). Exogenous C3a significantly increased expression of osteopontin, matrix Gla, and collagen IV mRNAs in HMCs ($P < 0.05$). Exogenous C3a (0.001–1.0 μM) significantly increased DNA synthesis in HMCs in a dose-dependent manner ($P < 0.05$). These data suggest that exogenous C3a promotes conversion of HMCs from the contractile phenotype to the synthetic phenotype and stimulates growth of HMCs.

Effect of C3a on morphology and α-smooth muscle actin expression in HMCs

C3a treatment did not considerably change morphology of HMCs. However, C3a treatment for 24 or 48 h markedly decreased immnofluorescence of α-smooth muscle actin in HMCs compared to HMCs without C3a treatment (Fig. 3).

Effects of siRNA against C3 on phenotype and growth of HMCs

To evaluate the contribution of endogenous C3 to the phenotype and growth of HMCs, we designed and synthesized a duplex siRNA against C3. The effects of the duplex siRNA specific for C3 on expression of C3 mRNA and protein in HMCs are shown in Figure 4. siRNA against C3 significantly decreased levels of both C3 mRNA and protein ($P < 0.05$).

The effects of siRNA to C3 on expression of phenotypic marker mRNAs in HMCs are shown in Figure 5. siRNA against C3 significantly increased expression of *h*-caldesmon mRNA in HMCs ($P < 0.05$), whereas siRNA to C3 significantly decreased levels of osteopontin, matrix Gla, and collagen IV mRNAs in HMCs ($P < 0.05$). These data suggest that suppression of endogenous C3 causes HMCs to change from the synthetic to the contractile phenotype in culture.

The effects of siRNA against C3 on growth of HMCs are shown in Figure 6. siRNA to C3 significantly inhibited DNA synthesis in HMCs in a dose-dependent manner ($P < 0.05$). siRNA to C3 significantly suppressed proliferation of HMCs at 48 and 72 h after transfer of siRNA in the presence of 5% calf serum ($P < 0.05$).

Discussion

The mesangial tissue between the glomerular capillaries consists of mesangial cells and an intercellular matrix. Mesangial cells contain contractile processes that attach directly to the capillaries and regulate capillary diameter and provide structural support for the glomeruli through contractions. Mesangial cells contain high levels of myosin and actin filaments and have various functions, including phagocytosis. Mesangial

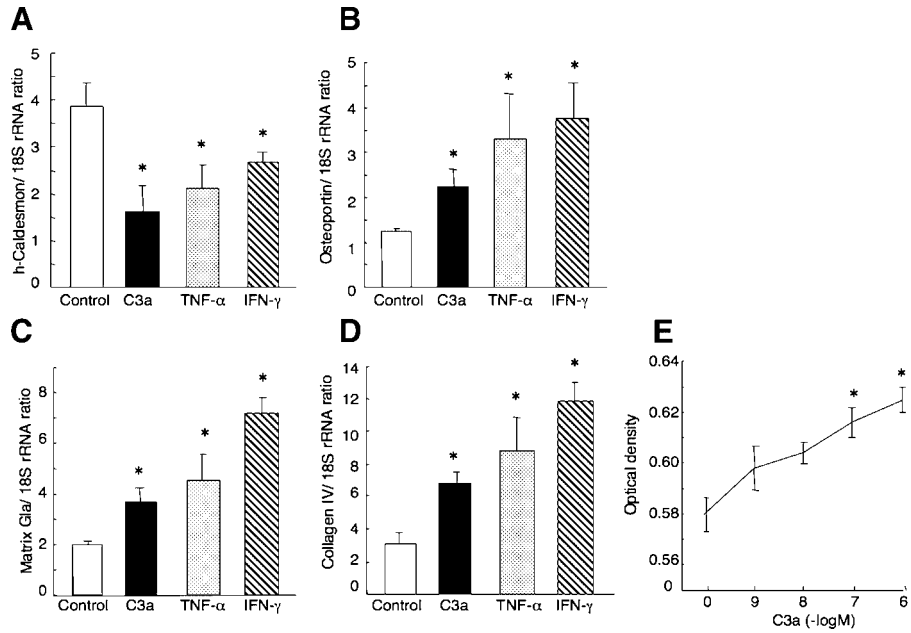

Fig. 2. A–D: Effects of exogenous C3a on expression of phenotype marker mRNAs in cultured HMCs. Quiescent HMCs were incubated with or without 0.1 μM C3a, 10 μg/ml TNF-α, or 50 ng/ml IFN-γ for 24 h. Total RNA was extracted and *h*-caldesmon (A), osteopontin (B), matrix Gla (C), and collagen IV (D) mRNAs were evaluated by RT-PCR analysis. The ratio of the abundance of each mRNA to that of 18S rRNA was evaluated by densitometric analysis. Data are mean ± SEM (n = 6). *$P < 0.05$ versus control cells. E: Effects of exogenous C3a on DNA synthesis in cultured HMCs. Quiescent HMCs were incubated without or with 0.001–1.0 μM C3a for 24 h and incorporation of BrdU into DNA was examined. Data are mean ± SEM (n = 8). *$P < 0.05$ versus control cells.

cells also produce substances, such as extracellular matrix components, hormones, and cytokines (Stockand and Sansom, 1998). The glomerulus is a highly specialized vascular structure in which mesangial cells serve as specialized pericytes sharing properties with VSMCs (Schlondorff, 1987). In fact, progressive glomerulosclerosis shows pathological similarities to arteriosclerosis (Grone et al., 1994; Oda and Keane, 1999), suggesting that these two entities may share pathogenic mechanisms.

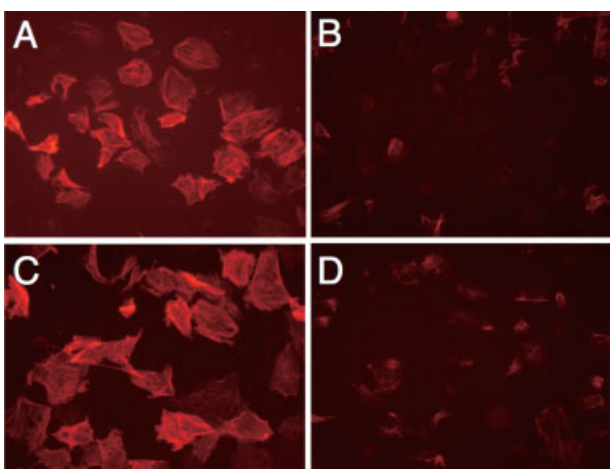

Fig. 3. Representative immunofluorescence of α-smooth muscle actin of HMCs treated without or with C3a (0.1 μM) for 24 h (A,B), or 48 h (C,D). Magnification 100×. [Color figure can be viewed in the online issue, which is available at www.interscience.wiley.com.]

VSMCs show either a synthetic or contractile phenotype. The synthetic phenotype is formed when a cell of the contractile phenotype loses contractile function and begins to proliferate and produce additional proteins, such as extracellular matrix components (Ross, 1993; Schwartz, 1997). Freshly plated VSMCs do not proliferate, and they possess a high volume-fraction of myofilaments, show few biosynthetic organelles, and retain their ability to contract in response to a vasoconstrictor. These characteristics define the differentiated contractile phenotype. After several passages, VSMCs dedifferentiate and display the synthetic phenotype, which is characterized by a reduction in the volume fraction of myofilaments and an increase in synthetic organelles such as Golgi, mitochondria, and endoplasmic reticulum. Cells with the synthetic phenotype produce copious amount of proteases, growth factors, and cytokines (Mosse et al., 1985; Glukhova et al., 1990). Similar to VSMCs, mesangial cells with the synthetic phenotype have increased organelle content and production of extracellular matrix components, such as collagens and fibronectin (Makino et al., 1995).

It has been reported that caldesmon is involved in smooth muscle contraction as an actin-linked regulatory protein (Sobue et al., 1985; Marston and Redwood, 1993). Ueki et al. (1987) reported that *h*-caldesmon is closely associated with phenotypic modulation of smooth muscle cells. Osteopontin and matrix Gla are expressed preferentially in passaged cells that have downregulated production of contractile proteins and are expressed strongly in dedifferentiated VSMCs (Shanahan et al., 1993). Therefore, we used *h*-caldesmon as a marker of the contractile phenotype and matrix Gla and osteopontin as markers of the synthetic phenotype in cultured HMCs treated with exogenous C3a, TNF-α, and IFN-γ. Exogenous C3a decreased expression of *h*-caldesmon mRNA in HMCs, whereas it increased the expression of matrix Gla and osteopontin mRNAs, indicating that C3a promotes HMCs,

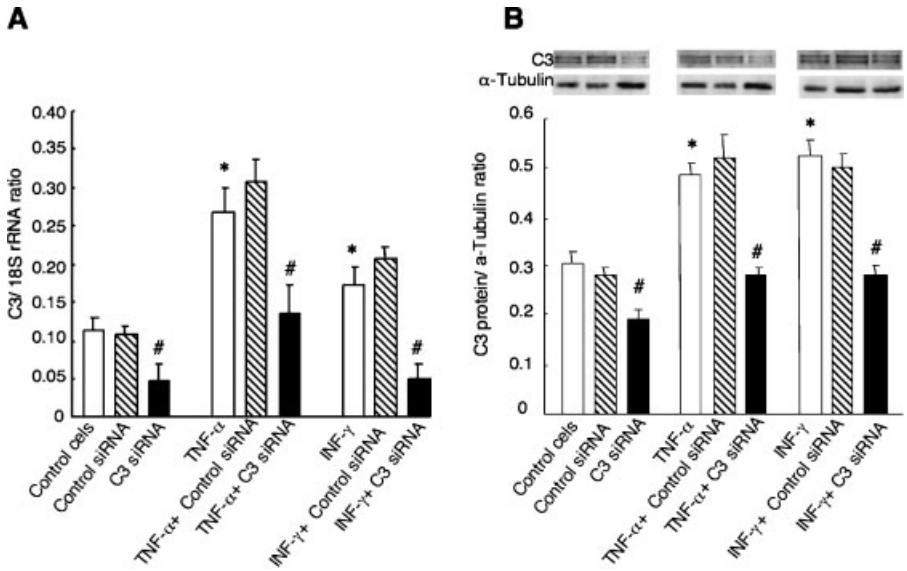

Fig. 4. Effects of siRNA against C3 on expression of C3 mRNA and protein in cultured HMCs. Quiescent HMCs were incubated with 3.3 μg/ml siRNA against C3. Forty-eight hours after transfection of siRNA, cells were incubated with 10 μg/ml TNF-α or 50 ng/ml IFN-γ for 24 h. A: The ratio of the abundance of each mRNA to that of 18S rRNA was evaluated by densitometric analysis. Data are mean ± SEM (n = 4). #P < 0.05 versus cells without C3 siRNA or control siRNA. *P < 0.05, versus untreated control cells. B: The ratio of C3 protein to α-tubulin was evaluated by densitometric analysis. Data are mean ± SEM (n = 4). #P < 0.05 versus cells without C3 siRNA or with control siRNA. *P < 0.05 versus control cells.

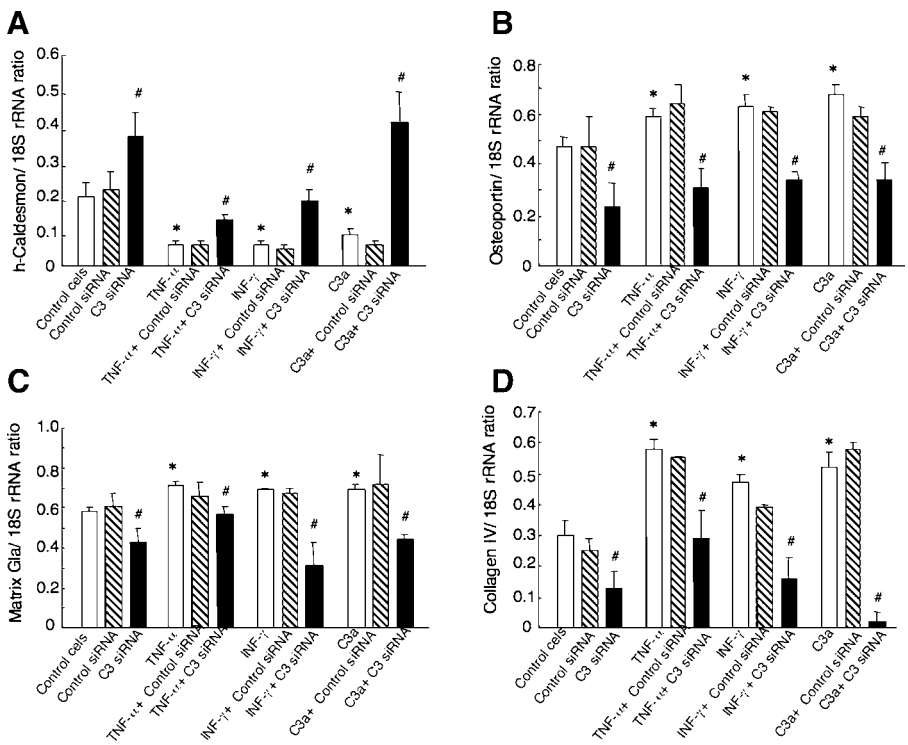

Fig. 5. Effects of siRNA to C3 on expression of phenotypic marker mRNAs in HMCs. Quiescent HMCs were incubated with 3.3 μg/ml siRNA to C3. Forty-eight hours after transfection of siRNA, cells were incubated with 10 μg/ml TNF-α, 50 ng/ml IFN-γ, or 0.1 μM C3a for 24 h. Total RNA was extracted and *h*-caldesmon (A), osteopontin (B), and matrix Gla (C) mRNAs were evaluated by RT-PCR analysis. The ratio of the abundance of each mRNA to that of 18S rRNA was evaluated by densitometric analysis. Data are mean ± SEM (n = 4). #P < 0.05 versus cells without C3 siRNA or with control siRNA. *P < 0.05 versus untreated control cells.

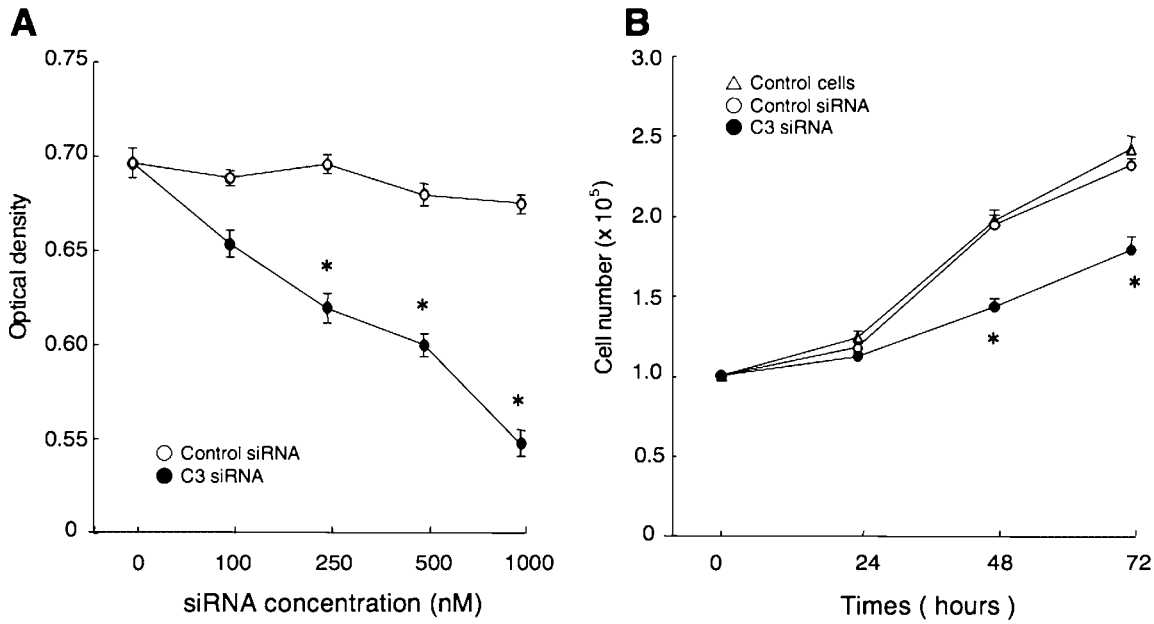

Fig. 6. Effects of siRNA to C3 on growth of HMCs. A: Effects of siRNA to C3 on basal DNA synthesis of cultured HMCs. Quiescent HMCs were incubated with 100–1,000 nM siRNA to C3 or control siRNA and incorporation of BrdU into DNA was examined. *$P < 0.05$ versus control siRNA. B: Effects of C3 specific siRNA on proliferation of HMCs. HMCs were inoculated at 1×10^5 cells/ml in RPMI 1640 containing 5% calf serum and 3.3 μg/ml siRNA to C3, 3.3 μg/ml control siRNA, or no siRNA (control cells). HMCs were replenished with RPMI 1640 containing 5% calf serum and 3.3 μg/ml siRNA to C3 and control siRNA every 24 h. Cells were trypsinized at 24, 48, and 72 h after inoculation, and cell number was determined with a Coulter Counter. Data are mean ± SEM (n = 4). *$P < 0.05$ versus control siRNA or control cells.

transition from the contractile to the synthetic phenotype. Exogenous C3a decreased expression of α-smooth muscle actin in HMCs. In addition, exogenous C3a stimulated DNA synthesis in HMCs. These findings suggest that C3a causes HMCs to convert to the synthetic phenotype and that it stimulates the growth of HMCs.

Exogenous C3a also significantly increased the expression of collagen IV mRNA in HMCs. Collagen IV is the predominant molecule in the matrix surrounding mesangial cells (Setty et al., 1998). Glomerulosclerosis is characterized by excessive deposition and accumulation of ECM components. These findings suggest that the increased production of collagen IV is associated with the increased number of intracellular organelles that occurs with the C3-induced switch to the synthetic phenotype and that is increased production of collagen is associated with deposition of more ECM.

Although the major site of production of complement proteins is the liver, complement biosynthesis has been detected in many other organs and cell types, including indigenous cells in the kidney (Morgan and Gasque, 1997; Daha and van Kooten, 2000). Local production of complement has been reported to be associated with tissue damages against a variety of conditions (Laufer et al., 2001). The complement system plays an important role in host defenses against various pathogens, whereas inappropriate activation of the complement system can damage host tissues. A pivotal step in the complement cascade is generation of activated C3 (Li et al., 1999), which occurs through the classical, alternative, or lectin pathway. The alternative pathway is initiated continuously in plasma by the spontaneous activation of C3, termed "tick-over of C3." Once C3 has been activated, C3 cleavage is amplified and C5 convertases, such as C4b2a3b and C3bBb3b, are formed. Cleavage of C5 by the C5 convertase results in the release of the potent anaphylatoxin C5a and the formation of the membrane attack complex (MAC), which triggers various cellular-metabolic pathways. However, significant cleavage of C5 should not have occurred in the present study because the initial pathway of the complement cascade was not activated. C3 can be synthesized by embryonic cells (Hong et al., 1991) and enhances the growth of cancer cells (Di Renzo et al., 1999). Taken together, these findings suggest that C3 may participate in cell differentiation and proliferation.

In the cardiovascular field, C3 is known to be increased in atherosclerotic lesions and to contribute to the development of atherosclerosis in vivo (Seifert and Kazatchkine, 1988; Buono et al., 2002). Recently, we demonstrated by microarray analysis that C3 mRNA is produced in smooth muscle from SHR in vivo but is not expressed in smooth muscle from Wistar Kyoto rats. In contrast, there were no differences in levels of mRNAs for C4, C8, and C9 in aortic smooth muscle cells from SHR and Wistar Kyoto rats (Lin et al., 2004). These data suggest that expression of C3 in VSMCs is independent of that of other complement system components and that C3 has unique effects on VSMCs.

Synthesis of C3 has been reported in HMCs. A significant increase in C3 expression was found in kidney biopsy specimens from patients with immune-mediated glomerulonephritis and with interstitial nephritis (Sacks et al., 1993a; Welch et al., 1993). Expression of C3 is tissue specific and is regulated by immune complexes and several cytokines. IL-1 and other pro-inflammatory cytokines, such as TNF-α and IL-6, stimulate C3 synthesis in several cell types (Volanakis, 1995). In the present study, synthesis of C3 was detected in cultured HMCs as in previous studies (Sacks et al., 1993b; van den Dobbelsteen et al., 1994) and was increased in the presence of IFN-γ and TNF-α. Thus, endogenous C3 is increased by cytokines such as IFN-γ and TNF-α, which may contribute to the pathogenesis of progressive glomerulosclerosis.

To observe the effects of inhibiting endogenous C3 on expression of the synthetic phenotype and proliferation of HMCs, we designed a duplex siRNA against C3 to inhibit endogenous C3. This siRNA was effective in inhibiting C3 production in HMCs and caused an increase in the expression of *h*-caldesmon mRNA and a decrease in the expression of osteopontin, matrix Gla, and collagen IV mRNAs. These data indicate that C3 contributes directly to the synthetic phenotype of HMCs. Moreover, siRNA to C3 reduced the higher basal DNA synthesis and proliferation observed in HMCs with the synthetic phenotype.

In conclusion, C3 is produced by HMCs and contributes to the exaggerated growth and expression of the synthetic phenotype of HMCs. C3 may underly the synthetic phenotype and exaggerated growth of HMC. A therapeutic approach utilizing siRNA to target C3 may be effective in the treatment of progressive renal disease.

Acknowledgments

This work was supported in part by a Grant-in Aid to Nihon University for the High-Tech Research Center from the Japanese Ministry of Education, Science, Sports, and Culture and by the Ministry of Education, Science, Sports, and Culture of Japan (15590863).

Literature Cited

Bakris GL, Palant CE, Walsh MF, Sowers JR. 1996. Analogy between endothelial/mesangial cell and endothelial/vascular smooth muscle cell interactions: Role of growth factors and mechanotransduction. In: Sowers JR, editor. Endocrinology of the vasculature. Totowa, NJ: Humana Press. pp 341–355.

Buono C, Come CE, Witztum JL, Maguire GF, Connelly PW, Carroll M, Lichtman AH. 2002. Influence of C3 deficiency on atherosclerosis. Circulation 105:3025–3031.

Daha MR, van Kooten C. 2000. Is there a role for locally produced complement in renal disease? Nephrol Dial Transplant 15:1506–1509.

Di Renzo L, Longo A, Morgante E, Mardente S, Prodinger WM, Russo M, Pontieri GM, Lipari M. 1999. C3 molecules internalize and enhance the growth of Lewis lung carcinoma cells. Immunobiology 200:92–105.

Floege J, Burns MW, Alpers CE, Yoshimura A, Pritzl P, Gordon K, Seifert RA, Bowen-Pope DF, Couser WG, Johnson RJ. 1992. Glomerular cell proliferation and PDGF expression precede glomerulosclerosis in the remnant kidney model. Kidney Int 41:297–309.

Glukhova MA, Frid MG, Koteliansky VE. 1990. Developmental changes in expression of contractile and cytoskeletal proteins in human aortic smooth muscle. J Biol Chem 265:13042–13046.

Grone EF, Walli AK, Grone HJ, Miller B, Seidel D. 1994. The role of lipids in nephrosclerosis and glomerulosclerosis. Atherosclerosis 107:1–13.

Hong MH, Jin CH, Sato T, Ishimi Y, Abe E, Suda T. 1991. Transcriptional regulation of the production of the third component of complement (C3) by 1α, 25-dihydroxyvitamin D3 in mouse marrow-derived stromal cells (ST2) and primary osteoblastic cells. Endocrinology 129:2774–2779.

Johnson RJ. 1997. Involvement of complement components in renal disease. Curr Opin Nephrol Hypertens 6:120–127.

Laufer J, Katz Y, Passwell JH. 2001. Extrahepatic synthesis of complement proteins in inflammation. Mol Immunol 38:221–229.

Li W, Tada T, Miwa T, Okada N, Ito J, Okada H, Tateyama H, Eimoto T. 1999. mRNA expression of complement components and regulators in rat arterial smooth muscle cells. Microbiol Immunol 43:585–593.

Lin ZH, Fukuda N, Jin XQ, Yao EH, Ueno T, Endo M, Saito S, Matsumoto K, Mugishima H. 2004. Complement 3 is involved in the synthetic phenotype and exaggerated growth of vascular smooth muscle cells from spontaneously hypertensive rats. Hypertension 44:42–47.

Makino H, Kashihara N, Sugiyama H, Kanao K, Sekikawa T, Shikata K, Nagai R, Ota Z. 1995. Phenotypic changes of the mesangium in diabetic nephropathy. J Diabetes Complications 9:282–284.

Marston SB, Redwood CS. 1993. The essential role of tropomyosin in cooperative regulation of smooth muscle thin filament activity by caldesmon. J Biol Chem 268:12317–12320.

Morgan BP, Gasque P. 1997. Extrahepatic complement biosynthesis: Where, when and why. Clin Exp Immunol 107:1–7.

Mosse PR, Campbell GR, Wang ZL, Campbell JH. 1985. Smooth muscle phenotypic expression in human carotid arteries. I: Comparison of cells from diffuse intimal thickenings adjacent to atheromatous plaques with those of the media. Lab Invest 53:556–562.

Oda H, Keane WF. 1999. Recent advances in statins and the kidney. Kidney Int 56:S2–S5.

Pesce CM, Striker LJ, Peten E, Elliot SJ, Striker GE. 1991. Glomerulosclerosis at both early and late stages is associated with increased cell turnover in mice transgenic for growth hormone. Lab Invest 65:601–605.

Ross R. 1993. The pathogenesis of atherosclerosis: A perspective for 1990s. Nature 362:801–809.

Sacks SH, Zhou W, Andrews PA, Hardley B. 1993a. Endogenous complement C3 synthesis in immune complex nephritis. Lancet 342:1273–1274.

Sacks S, Zhou W, Campbell RD, Martin J. 1993b. C3 and C4 gene expression and interferon-gamma-mediated regulation in human glomerular mesangial cells. Clin Exp Immunol 93:411–417.

Schlondorff D. 1987. The glomerular mesangial cell: An expanding role for a specialized pericyte. FASEB J 1:272–281.

Schwartz SM. 1997. Perspectives series: Cell adhesion in vascular biology. Smooth muscle migration in atherosclerosis and restenosis. J Clin Invest 99:2814–2816.

Seifert PS, Kazatchkine MD. 1988. The complement system in atherosclerosis. Atherosclerosis 73:91–104.

Setty S, Kim Y, Fields GB, Clegg DO, Wayner EA, Tsilibary EC. 1998. Interactions of type IV collagen and its domains with human mesangial cells. J Biol Chem 273:12244–12249.

Shanahan CM, Weissberg PL, Metcalfe JC. 1993. Isolation of gene markers of differentiated and proliferating vascular smooth muscle cells. Circ Res 73:93–204.

Sobue K, Takahashi K, Wakabayashi I. 1985. Caldesmon150 regulates the tropomyosin-enhanced actin-myosin interaction in gizzard smooth muscle. Biochem Biophys Res Commun 132:645–651.

Stockand JD, Sansom SC. 1998. Glomerular mesangial cells: Electrophysiology and regulation of contraction. Physiol Rev 78:723–744.

Ueki N, Sobue K, Kanda K, Hada T, Higashino K. 1987. Expression of high and low molecular weight caldesmons during phenotypic modulation of smooth muscle cells. Proc Natl Acad Sci USA 84:9049–9053.

van den Dobbelsteen ME, Verhasselt V, Kaashoek JG, Timmerman JJ, Schroeijers WE, Verweij CL, van der Woude FJ, van Es LA, Daha MR. 1994. Regulation of C3 and factor H synthesis of human glomerular mesangial cells by IL-1 and interferon-gamma. Clin Exp Immunol 95:173–180.

Volanakis JE. 1995. Transcriptional regulation of complement genes. Annu Rev Immunol 13:277–305.

Welch TR. 2001. The complement system in renal diseases. Nephron 88:199–204.

Welch TR, Beischel LS, Witte DP. 1993. Differential expression of complement C3 and C4 in the human kidney. J Clin Invest 92:1451–1458.

Zhou W, Marsh JE, Sacks SH. 2001. Intrarenal synthesis of complement. Kidney Int 59:1227–1235.

Available online at www.sciencedirect.com
ScienceDirect
Journal of Chromatography B, 859 (2007) 272–275
JOURNAL OF CHROMATOGRAPHY B
www.elsevier.com/locate/chromb

Short communication

Optimization and validation of a high-performance liquid chromatographic method with UV detection for the determination of pyrrole–imidazole polyamides in rat plasma

Akiko Fukasawa [a], Takashi Nagashima [a], Takahiko Aoyama [a], Noboru Fukuda [b], Hiroyuki Matsuda [b], Takahiro Ueno [c], Hiroshi Sugiyama [d], Hiroki Nagase [b], Yoshiaki Matsumoto [a,*]

[a] *Department of Clinical Pharmacokinetics, College of Pharmacy, Nihon University, 7-7-1 Narashinodai, Funabashi, Chiba 274-8555, Japan*
[b] *Advanced Research Institute for the Science and Humanities, Nihon University, Tokyo 102-0073, Japan*
[c] *Department of Medicine, Division of Nephrology and Endocrinology, Nihon University School of Medicine, Tokyo 173-8610, Japan*
[d] *Department of Chemistry, Graduate School of Science, Kyoto University, Kyoto 606-8502, Japan*

Received 18 July 2007; accepted 26 September 2007
Available online 5 October 2007

Abstract

A simple and sensitive high-performance liquid chromatography (HPLC) method utilizing UV detection was developed for the determination of plasma pyrrole (Py)–imidazole (Im) polyamides in rats and applied to the pharmacokinetic study of compounds. After deproteinization of plasma with methanol, Py–Im polyamides were analyzed with a reversed-phase TSK-GEL ODS-80T$_M$ (4.6 mm × 15.0 cm TOSOH Co., Japan) column maintained at 40 °C. The mobile phase solvent A was 0.1% acetic acid and the solvent B was HPLC-grade acetonitrile (0–10 min, A: 100–20%, B: 0–80% linear gradient; 10–15 min, A: 40%, B: 60%). The flow rate was 1.0 ml/min. The detection wavelength was set at 310 nm. The method was used to determine the plasma concentration time profiles of Py–Im polyamides after intravenous injection.

Keywords: Pyrrole–imidazole polyamide; HPLC; Rat plasma; Pharmacokinetics

1. Introduction

Pyrrole (Py)–imidazole (Im) polyamides are small synthetic molecules composed of the aromatic rings of *N*-methylpyrrole and *N*-methylimidazole amino acid [1]. Py–Im polyamides were purified by HPLC using Chemcobond 5-ODS-H column, 0.1% acetic acid and acetonitrile 0–50% linear gradient, 40 min. The detection wavelength was set at 254 nm [2,3]. Synthetic polyamides can bind to specific nucleotide sequences in the minor groove of double-helical DNA with high affinity and specificity. Sequence-specific DNA recognition by Py–Im polyamide depends on the side-by-side paring of Py and Im; the Py/Im pair targets the CG base pair, Im/Py recognizes the GC base pair, and Py/Py binds to both AT and TA base pairs [4]. Various types of sequence-specific DNA-binding Py–Im polyamides have been developed to regulate gene expression by targeting the promoter regions of enhancer and transcription factor binding elements in vitro [5]. Recently, Matsuda et al. [6] reported that the Py–Im polyamide targeting the rat transforming growth factor (TGF)-β_1 is a novel gene-silencing agent for the treatment of progressive renal diseases in Dahl-S rats. These observations suggested that the Py–Im polyamide could be a useful bioprobe for molecular biology and a potential medicine.

The aims of the present study are to develop a sensitive and specific HPLC assay for the quantitation of Py–Im polyamides in rat plasma and to propose its application to pharmacokinetic studies.

2. Experiment

2.1. Chemicals and reagents

Py–Im polyamides (A) and (B) were provided by Gentier Biosystems Co., Ltd. (Japan). Their chemical structures are

* Corresponding author. Tel.: +81 47 465 7182; fax: +81 47 465 7182.
E-mail address: matsuy@pha.nihon-u.ac.jp (Y. Matsumoto).

1570-0232/$ – see front matter © 2007 Elsevier B.V. All rights reserved.
doi:10.1016/j.jchromb.2007.09.032

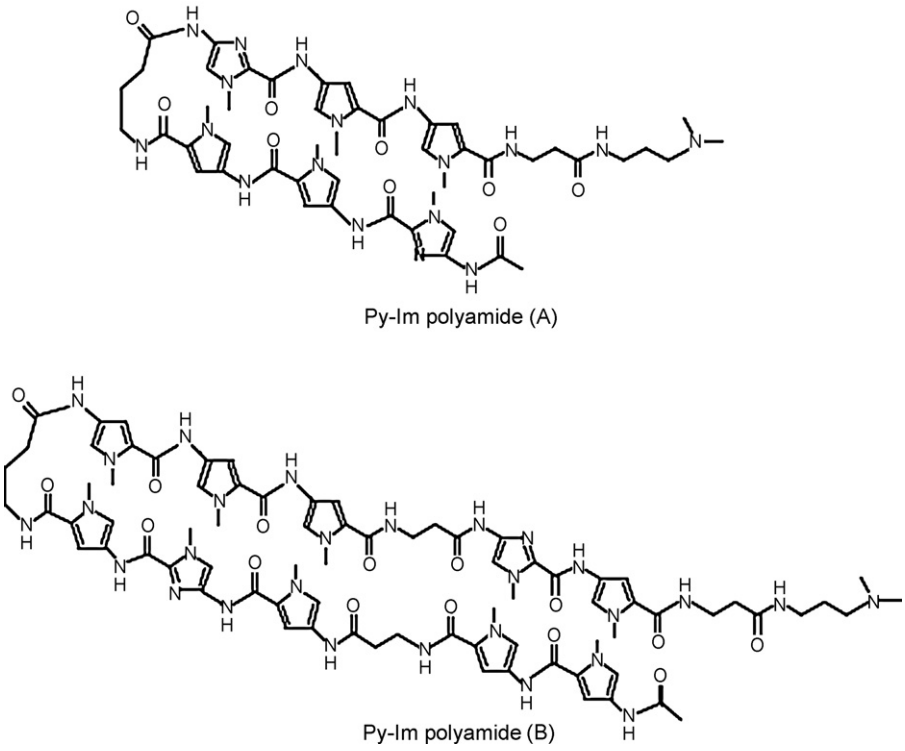

Fig. 1. Chemical structures of Py–Im polyamides (A) and (B). The molecular weight of Py–Im polyamide (A) is 1035.12 and that of Py–Im polyamide (B) is 1665.78.

shown in Fig. 1. Py–Im polyamide (A) was composed of Ac-ImPyPy-ImPyPy-β-Dp (Dp: *N*,*N*-dimethylaminopropylamide). Py–Im polyamide (B) was composed of Ac-PyPy-β-PyIm-Py-PyPyPyβ-ImPy-β-Dp. The molecular weights of Py–Im polyamides (A) and (B) were calculated from the sum of the standard atomic weights of all the atoms [7]. Py–Im polyamide (A) was 1035.12 and Py–Im polyamide (B) was 1665.78. Acetonitrile and methanol were HPLC-grade from Wako Pure Chemical Industries, Ltd. Acetic acid was of the highest quality from Kanto Chemical Co., Inc. The water was purified by distillation.

2.2. Chromatographic system

The analyses of Py–Im polyamides were carried out using a Shimadzu LC-20A HPLC system (Tokyo, Japan) with a reversed-phase TSK-GEL ODS-80T_M (4.6 mm × 15.0 cm, TOSOH Co., Japan) column maintained at 40 °C. The mobile phase solvent A was 0.1% acetic acid and the solvent B was acetonitrile (0–10 min, A: 100–20%, B: 0–80% linear gradient; 10–15 min, A: 40%, B: 60%). The flow rate was set at 1.0 ml/min. The detection wavelength was set at 310 nm. Injection volume was 30 μl.

2.3. Animals and blood sampling

Male Wistar rats (14 weeks old) weighing 280–300 g were obtained from Sankyo Lab Service Corporation. The animals were maintained in a temperature-controlled room on a 12-h light:12-h dark cycle and allowed free access to food and tap water. A polyethylene tube (0.58 mm, I.D. 0.96 mm, O.D.) was inserted into the left femoral artery and right jugular vein of the rat while under anesthesia with pentobarbital sodium (Dainippon Sumitomo Pharma Co.). The cannulation treatment was performed at least 1 day prior to the experiment. A Py–Im polyamide aqueous solution was injected into the jugular vein at a single dose of 2.0 mg/kg. Blood samples (0.5 ml) were collected at 0, 10, 30, 60, 90 and 120 min after the injection. After each sampling, the blood drawn was replaced with an equal volume of saline.

2.4. Preparation of plasma samples

Blood samples were centrifuged in a 1.5 ml microcentrifuge at 10,000 × *g* at 4 °C. Each sample was immediately transferred to a heparinized microcentrifuge tube and centrifuged for 10 min. Collected plasma samples (50 μl) were then vortex-mixed with 100 μl of methanol for 10 s. The mixture was centrifuged for 5 min to precipitate protein. Supernatants were centrifuged for 5 min again and 30 μl of each supernatant was directly injected into the chromatograph.

2.5. Stock solution and standards

Primary stock solutions of Py–Im polyamide (A) or (B) (2.0 mg/ml) were prepared in water and stored at 4 °C until analysis. Working solutions with concentrations of 20 and 200 μg/ml were prepared by adding water. Py–Im polyamide (A) or (B) calibration standards were prepared fresh daily at concentrations of 0, 1, 2, 5, 10, 20, 50, 100 and 200 μg/ml by spiking 45 μl of blank rat plasma with 5 μl of water (for "zero" standard sample) or Py–Im polyamides (A) and (B) working solution. In the same manner, quality control (QC) samples at concentrations of

1, 5, 20, and 100 μg/ml were freshly prepared to evaluate the accuracy and precision of the HPLC method.

2.6. Linearity of calibration curve

Calibration curves were constructed by plotting the peak area of Py–Im polyamide. The linearity of the calibration curves was evaluated by linear regression analysis.

2.7. Recovery

To assess the extraction recovery, two series of Py–Im polyamide QC samples were prepared as described above one with rat plasma and another without plasma. The set without plasma was prepared by adding water instead of plasma. The extraction recovery was determined from the ratio of peak area of water standard to that of the corresponding plasma standard.

2.8. Sensitivity

The lower limit of quantification (LLOQ) was determined during the evaluation of the linear range of the calibration curve. LLOQ was defined as the lowest concentration yielding a precision with coefficients of variation (CV) of less than 20% and accuracy within 15% of the theoretical value (i.e., accuracy between 85 and 115%) for both intra- and inter-day analysis.

2.9. Accuracy and precision

For the intra- and inter-day precision and accuracy of the assay, Py–Im polyamide (A) and (B) QC samples were prepared as described above. The intra-day precision was calculated from the CV for QC samples in three replicate analyzed on the same day, and the inter-day precision was determined by the analysis of QC samples in three consecutive days. The accuracy of each set of measurements was calculated by comparing the means with nominal values, and was expressed in percent. The criterion for the acceptability of precision was that the relative standard deviation for each concentration level did not exceed ±15% except for the LLOQ, which did not exceed ±20%. Similarly, for accuracy, the mean value did not exceed ±15% of the nominal concentration except for the LLOQ, where the limit was the LLOQ.

Table 1
Recovery of Py–Im polyamides (A) and (B) from plasma ($n = 3$)

Theoretical concentration (μg/ml)	Recovery (%)			
	Py–Im polyamide (A)		Py–Im polyamide (B)	
	Mean ± S.D.	CV (%)	Mean ± S.D.	CV (%)
1	83.7 ± 7.5	8.9	109.0 ± 1.2	1.1
5	103.5 ± 4.5	4.4	87.3 ± 4.4	5.1
20	97.4 ± 1.7	1.7	93.4 ± 11.1	11.9
100	97.7 ± 2.7	2.8	92.7 ± 2.8	3.0

2.10. Assay application

The present method was used to determine the concentrations of Py–Im polyamides (A) and (B) in rat plasma after intravenous injection of Py–Im polyamide (A) and (B) aqueous solutions.

3. Results and discussion

3.1. Separation

The UV absorbances of Py–Im polyamides (A) and (B) were determined from wavelengths of 200–400 nm. Py–Im polyamides (A) and (B) had a maximum UV absorption at 310 nm (data not shown). Therefore, the UV detection wavelength at 310 nm was measured. Chromatograms of blank plasma and plasma spiked with Py–Im polyamides (A) and (B) (5 μg/ml) are shown in Fig. 2. Py–Im polyamides (A) and (B) were well separated from co-extracted material under the described chromatographic conditions at approximate retention times of 9.7 and 10.5 min, respectively. The peak shapes were satisfactory and completely resolved from one another. No interference with constituents from the plasma matrix was observed.

3.2. Linearity of calibration curves

Calibration curves for Py–Im polyamides (A) and (B) were linear over the concentration range of 1–200 μg/ml in rat plasma. The mean (±S.D.) regression equation from three replicate calibration curves on different days for Py–Im polyamide (A) was $Y = 24{,}206\ (\pm 1413)X - 7715(\pm 7112)$ and for Py–Im polyamide (B) was $Y = 32{,}876(\pm 924)X - 8753(\pm 12{,}146)$, where Y is

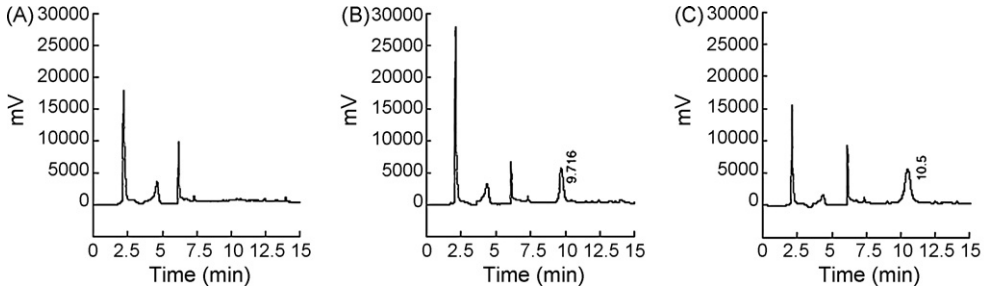

Fig. 2. Representative chromatograms of (A) blank rat plasma, (B) blank rat plasma spiked with Py–Im polyamide (A) (5 μg/ml), and (C) blank rat plasma spiked with Py–Im polyamide (B) (5 μg/ml). Approximate retention times: Py–Im polyamide (A) (5 μg/ml) = 9.7 min; Py–Im polyamide (B) (5 μg/ml) = 10.5 min.

Table 2
Accuracy and precision of the HPLC method for determining

Theoretical concentration (μg/ml)	Intra-day			Inter-day		
	Observed concentration (mean ± S.D.; μg/ml)	Accuracy (%)	CV (%)	Observed concentration (mean ± S.D.; μg/ml)	Accuracy (%)	CV (%)
Py–Im polyamide (A) concentration in plasma samples ($n = 3$)						
1	1.0 ± 0.1	102.2	5.3	1.1 ± 0.2	106.7	14.4
5	5.6 ± 0.1	111.8	1.6	5.3 ± 0.3	106.3	6.4
20	20.3 ± 0.3	101.4	1.4	18.3 ± 1.8	91.3	9.7
100	107.7 ± 4.0	107.7	3.7	103.6 ± 3.7	103.6	3.5
Py–Im polyamide (B) concentration in plasma samples ($n = 3$)						
1	1.0 ± 0.1	102.8	10.0	1.0 ± 0.2	102.2	15.0
5	5.0 ± 0.2	100.8	3.5	5.2 ± 0.2	104.0	3.1
20	19.5 ± 0.1	97.5	0.6	18.2 ± 1.4	90.8	7.9
100	103.7 ± 2.7	103.7	2.6	103.2 ± 3.3	103.2	3.2

peak area and X is the concentration of the analyte. R^2 of Py–Im polyamide (A) was 0.9997(±0.0003) and R^2 of Py–Im polyamide (B) was 0.9983(±0.0018).

3.3. Recovery

The efficiencies of the extraction procedure for the two analytes at QC levels (1, 5, 20, and 100 μg/ml) are presented in Table 1. The recovery ranged between 83.7 and 103.5% for Py–Im polyamide (A) and 87.3 and 109.0% for Py–Im polyamide (B).

3.4. Precision, accuracy and sensitivity

Table 2 shows the intra- and inter-day precision and accuracy of Py–Im polyamides (A) and (B). The intra- and inter-day accuracies (% deviation) were within ±20% for the LLOQ and ±15% for the other QC samples. The intra- and inter-day assay precisions (CV) were also within the acceptable range of 20% for LLOQ and 15% for the other QC samples. The LLOQ was determined as 1 μg/ml for both Py–Im polyamides (A) and (B).

3.5. Application

The plasma concentrations of Py–Im polyamides (A) and (B) were determined at 0, 10, 30, 60, 90 and 120 min after injection. The plasma concentration time profile after intravenous administration (2.0 mg/kg) of Py–Im polyamides (A) and (B) in the rat are shown in Fig. 3. The retention time of Py–Im polyamide (A) extracted from plasma (4.5 μg/ml) and water (5.5 μg/ml) were the same time at 9.8 min. The retention time of Py–Im polyamide (B) extracted from plasma (2.5 μg/ml) and water (5.6 μg/ml) were the same at 10.5 min. The respective retention time of Py–Im polyamides extracted from plasma and water were consistent.

In conclusion, the newly developed HPLC method for the determination of plasma Py–Im polyamides in rats is simple, sensitive and specific, and the method can be used for the analysis of large numbers of plasma samples in other species. The assay was validated to apply the requirements of pharmacokinetic studies.

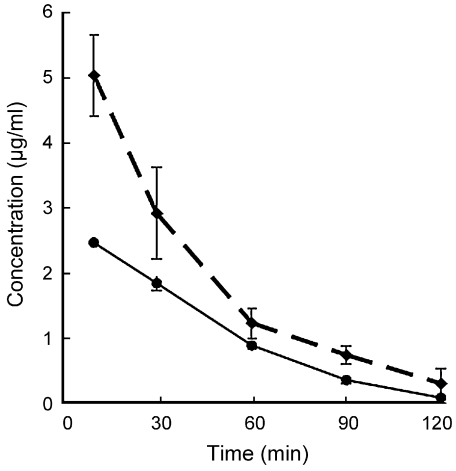

Fig. 3. Plasma concentration time profile after intravenous administration (2.0 mg/kg) of Py–Im polyamides (A) (♦) and (B) (●). The data was shown as the mean ± S.D. ($n = 3$).

Acknowledgments

This work was supported in part by a grant from "Academic Frontier" Project for Private Universities from the Ministry of Education, Culture, Sports, Science and Technology of Japan (2006–2010).

References

[1] J.W. Trauger, E.E. Baird, P.B. Dervan, Nature 382 (1996) 559.
[2] T. Bando, A. Narita, I. Saito, H. Sugiyama, Chem. Eur. J. 20 (2002) 4781.
[3] Y.M. Lai, N. Fukuda, T. Ueno, H. Matsuda, S. Saito, K. Matsumoto, H. Ayame, T. Bando, H. Sugiyama, H. Mugishima, K. Serie, J. Pharmacol. Exp. Ther. 315 (2) (2005) 571.
[4] S. White, E.E. Baird, P.B. Dervan, Chem. Biol. 4 (8) (1997) 569.
[5] M.S. Murty, H. Sugiyama, Biol. Pharm. Bull. 27 (4) (2004) 468.
[6] H. Matsuda, N. Fukuda, T. Ueno, Y. Tahira, H. Ayame, W. Zhang, T. Bando, H. Sugiyama, S. Saito, K. Matsumoto, H. Mugishima, K. Serie, J. Am. Soc. Nephrol. 17 (2) (2006) 422.
[7] M.E. Wieser, Pure Appl. Chem. 78 (11) (2006) 2051.

TGF-β_1 mRNA に対するDNA-RNA キメラ型リボザイムによる被嚢性腹膜硬化症の遺伝子治療の開発

丸山範晃　福田　昇　岡田一義　松本紘一

Development of gene therapy for encapsulating peritoneal sclerosis by a chimeric DNA-RNA hammerhead ribozyme targeting TGF-β_1 mRNA

Noriaki MARUYAMA , Noboru FUKUDA , Kazuyoshi OKADA , and Koichi MATSUMOTO

Department ot Medicine, Division of Nephrology and Endocrinology,
Advanced Research Institute of Science and Humanities, Life Science Program,
Nihon University, Tokyo, Japan

日本腎臓学会誌　第49巻 第2号　別刷
(平成19年2月25日発行)

日腎会誌 2007；49(2)：113-120.

原　著

TGF-β_1 mRNA に対する DNA-RNA キメラ型リボザイムによる被嚢性腹膜硬化症の遺伝子治療の開発

丸山範晃*　福田　昇**　岡田一義*　松本絃一

Development of gene therapy for encapsulating peritoneal sclerosis by a chimeric DNA-RNA hammerhead ribozyme targeting TGF-β_1 mRNA

Noriaki MARUYAMA*, Noboru FUKUDA**, Kazuyoshi OKADA*, and Koichi MATSUMOTO

*Department ot Medicine, Division of Nephrology and Endocrinology,
**Advanced Research Institute of Science and Humanities, Life Science Program,
Nihon University, Tokyo, Japan

要　旨

被嚢性腹膜硬化症は腹膜透析患者に発症する，稀ではあるが致死的な合併症として知られている。被嚢性腹膜硬化症の発症および進展に関与するサイトカインのなかで，transforming growth factor-β_1(TGF-β_1)は中心的な役割を果たしていると考えられている。われわれはTGF-β_1 mRNAを特異的に認識して切断するDNA-RNAキメラ型リボザイムを開発してきた。今回われわれは，腹膜硬化症モデルラットを作製し，TGF-β_1に対するキメラ型リボザイムをモデルラットの腹腔内へ投与した結果，腹膜の肥厚および硬化が有意に抑制され，また，腹膜組織中のTGF-β_1 mRNAおよびfibronectin mRNAの発現が有意に抑制された。

以上の結果より，TGF-β_1に対するキメラ型リボザイムは腹膜の線維化，硬化を強力に抑制し，被嚢性腹膜硬化症に対する新規の遺伝子治療薬として有用であると考えられた。

Background：Encapsulating peritoneal sclerosis(EPS) is a rare and devastating fibrotic complication in patients treated with peritoneal dialysis. Transforming growth factor-β_1(TGF-β_1) has been reported to be a pivotal factor in the induction of EPS. Ribozymes are RNA molecules that enzymatically cleave the target mRNAs and are expected to be utilized as a novel nucleic acid-based therapy. We examined the effects of the chimeric DNA-RNA hammerhead ribozyme targeting TGF-β_1 mRNA on a peritoneal sclerosis rat model to develop a possible gene therapy for EPS.

Methods：To create an animal model of peritoneal sclerosis, rats were given a daily intraperitoneal injection of chlorhexidine gluconate and ethanol dissolved in saline(CHX) for 14 days. On day 4, the chimeric ribozyme or mismatch ribozyme was intraperitoneally injected. On day 15, samples of peritoneum were obtained from the rats, and expression of TGF-β_1 mRNA and fibronectin mRNA in peritoneal tissues were evaluated by quantitative real-time PCR analysis.

Results：Injections of CHX significantly increased the submesothelial thickness, and increased the expression of TGF-β_1 and fibronectin mRNA in the rat peritoneum. Treatment with the chimeric ribozyme significantly reduced the CHX-induced peritoneal thickness, and expression of TGF-β_1 and fibronectin mRNA in peritoneal tissues.

Conclusions：These results indicate that the chimeric DNA-RNA hammerhead ribozyme targeting TGF-

* 日本大学医学部内科学講座腎臓内分泌内科部門，** 同 大学院総合科学研究科生命科学専攻

(平成18年10月27日受理)

β_1 mRNA has the potential for use as a gene therapy agent for EPS.

Jpn J Nephrol 2007；49：113-120.

Key words：encapsulating peritoneal sclerosis, transforming growth factor-β_1, ribozyme, gene therapy

はじめに

日本における慢性腎不全患者は25万人を超え，尿毒症に対し血液透析療法または持続性腹膜透析療法(continuous ambulatory peritoneal dialysis：CAPD)を受けている。CAPDは在宅でできる透析療法であるが，感染症の合併や血液透析の普及によりCAPDを受けている患者はここ10年間1万人を超えていない。また被嚢性腹膜硬化症(encapsulating peritoneal sclerosis：EPS)は腹膜透析に合併する稀な疾患であるが，発症すると重篤化しやすく死亡率も高い疾患であり，いまだ有効な治療法が確立しておらず，この合併症の存在が腹膜透析の普及を妨げている要因の一つとなっている。EPSの病態は，腹膜透析の継続によって生じる腹膜の肥厚および硬化といった慢性の腹膜劣化状態に細菌性腹膜炎などの炎症が加わることが契機となって，腹膜表面にフィブリンに代表される炎症性産物が多量に堆積して被膜が形成され，腸管同士が癒着して腸閉塞状態をきたすものであると考えられている[1]。また，EPSの発症，進展にはさまざまな原因が関与しており，多因性であると考えられているが[2]，腹膜硬化症はほぼすべてのEPSに合併する基礎的な病態である。この腹膜硬化に関与するサイトカインとしてtransforming growth factor-β_1 (TGF-β_1)，connective tissue growth factor, vascular endothelial growth factorなどが知られている[3,4]。なかでもTGF-β_1はfibronectinやcollagenなどの細胞外マトリックス蛋白の産生を増加させることが知られており[5]，細胞外基質の増生や線維化の進展において中心的な役割を果たすサイトカインであると考えられている。

遺伝子治療は，遺伝子欠損もしくは遺伝子異常に伴う疾患に遺伝子そのものを補う方法と，遺伝子の過剰発現によりもたらされる疾患に対し遺伝子発現を抑制する方法に分かれるが，後者にはリボザイム，アンチセンスDNAなどの核酸による遺伝子制御法がある。リボザイムはRNAを酵素的に切断するRNA核酸であり，人工的に設計，作製することによりアンチセンスDNAと同様，遺伝子発現を抑制できる。リボザイムはアンチセンスDNAと違い細胞内での非特異的作用がなく，ターゲット遺伝子への特異性が高く，癌やAIDSなど各種難治性疾患への新しい遺伝子治療法として開発が進められている。

しかしリボザイムはRNA構造であるため，単独では生体内で速やかに分解されてしまうという欠点がある。われわれはラットのTGF-β_1 mRNAの二次構造を解析して標的部位を選択し，ラットTGF-β_1 mRNAに対するハンマーヘッド型リボザイムを分子設計した。このリボザイムは生体内においてより安定して作用するように，DNA-RNAキメラ型のリボザイムに合成され核酸医薬として開発されてきた[6-9]。

今回われわれは，EPSに対するリボザイムによる遺伝子治療法の開発を目的として，EPSの進展においてTGF-β_1が中心的な役割を果たしていると想定し[10-12]，腹膜硬化症モデルラットを作製し，その腹腔内へTGF-β_1に対するリボザイムを投与してTGF-β_1の発現を抑制することを試み，腹膜の肥厚と硬化への影響を観察して生体レベルにおけるリボザイムの効果を検証した。

材料および方法

1．ラットTGF-β_1 mRNAに対するリボザイムの合成

われわれはラットTGF-β_1 mRNAの二次構造を解析して，mRNAがループ構造をとり，その切断により立体構造が大きく変化すると考えられる部位にあるGUC配列を特定し，その領域を認識して切断する38塩基から成るDNA-RNAキメラ型ハンマーヘッド型リボザイムを合成した(Fig. 1A)。このリボザイムは切断酵素活性を持った保存配列(Fig. 1Aの下線)のみRNA構造で，他の塩基をDNA構造として核酸合成機で合成し，さらにRNA分解酵素に耐性を持たせるために3'末端から2塩基間をphosphorothioate型(Fig. 1Aの＊)に化学修飾した。またリボザイムのコントロールとして，リボザイムの切断活性部位の塩基配列を1塩基のみ置換した(AからCに)ミスマッチリボザイムを合成した(Fig. 1B)。

2．腹膜硬化症モデルラットの作製

すべての動物実験は1980年の学術会議決議による実験動物取り扱い指針に基づいて行われた。

既報の方法に基づき[13]，7週齢雄性，体重約200 gのSprague-Dawleyラット(SDラット，日本クレア，東京)に対して，0.1％グルコン酸クロルヘキシジン，15％エタノール，生理食塩水混合液(以下，CHX)を1日1回，3

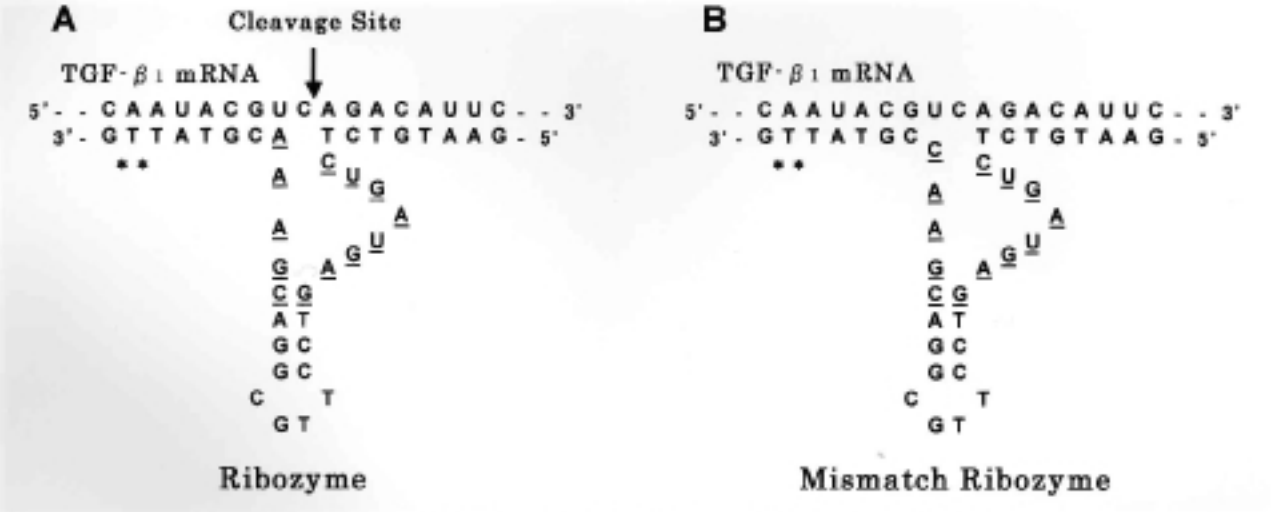

Fig. 1.　Structures of the chimeric DNA-RNA hammerhead ribozyme

A：Ribozyme specific to rat TGF-β_1 mRNA

B：Mismatch ribozyme. Mismatch ribozyme contains a single altered base (A to C) in the catalytic loop region.

mL ずつ腹腔内へ14日間連日投与して腹膜硬化症モデルラットを作製した。

3．腹膜組織へのリボザイムの移行性の検討

CHX を3日間腹腔内へ投与し，第4日目にラットTGF-β_1 mRNA をターゲットとした fluorescein-isothiocyanate (FITC) ラベルしたキメラ型リボザイム 20 μg を，3.6 μL の polyethylenimine (ExGen 500 *in vivo*, fermentas) をデリバリー試薬に使い，製品プロトコールに沿って調整後，腹腔内へ投与した。投与12時間後に解剖し腹膜組織を摘出，新鮮凍結切片を作製して腹膜組織へのリボザイムの取り込みを蛍光顕微鏡 (Nikon, TE2000-U) 下に組織学的に検討した。

4．腹膜硬化症モデルラットへのリボザイムの投与

以下の4実験群を設けた。

1）生理食塩水 (normal saline：NS) 3 mL を腹腔内へ連日14日間投与する群，6匹

2）CHX 溶液 3 mL を連日14日間腹腔内へ投与する群，6匹

3）CHX 溶液 3 mL を連日14日間腹腔内へ投与し，実験開始4日目にミスマッチリボザイム 200 μg を単回腹腔内へ投与する群，6匹

4）CHX 溶液 3 mL を連日14日間腹腔内へ投与し，実験開始4日目に TGF-β_1 mRNA に対するリボザイム 200 μg を単回腹腔内へ投与する群，6匹

なお，ラット TGF-β_1 mRNA をターゲットとしたリボザイムまたはミスマッチリボザイム 200 μg は，36 μL の polyethylenimine をデリバリー試薬に使い腹腔内へ投与した。

5．腹膜組織摘出

実験開始第15日目にラットを安楽死させ，壁側腹膜を腹直筋と一括して摘出，直ちに一部は RNA 抽出用に−80°C に保存し，残りの腹直筋については4%リン酸緩衝パラホルムアルデヒド溶液 (Wako Chemicals, Osaka, Japan) にて固定後，パラフィン切片を作製した。

6．組織学的検討

各個体の組織切片は Masson's trichrome 染色を行い，光学顕微鏡にて腹膜組織の形態変化を観察した。

7．腹膜肥厚度の計測

各標本について，Masson's trichrome 染色において青色に染まる線維化部位を腹膜表面から腹直筋表層まで垂直にランダムに10カ所計測して平均値を計算し，各群間の腹膜肥厚度を統計学的に検討した。

8．組織からの RNA 抽出

凍結した腹直筋の腹膜表面を 5×5 mm の大きさに統一して腹直筋も含めて切り出し (重量約 75 mg)，RNA 抽出試薬 TRIzol® (Gibco Life Technologies, Gaithersburg, MD, USA) を 1 mL 加え，メス刃にて細かく断片化してから組織をホモジナイズし，その後 AGPC 法[11] にて RNA を抽出した。抽出した RNA は滅菌水を加えて最終濃度 1 μg/μL の RNA 溶液とした。

9．cDNA 作製

抽出した RNA 1 μg に対して逆転写酵素 AMV Reverse Transcriptase XL (TaKaRa Biochemicals, Osaka, Japan) 5単位，ランダムプライマー (9 mers 50 μM, TaKaRa) 1.0 μL，10×RNA-PCR バッファー (TaKaRa) 2.0 μL，25

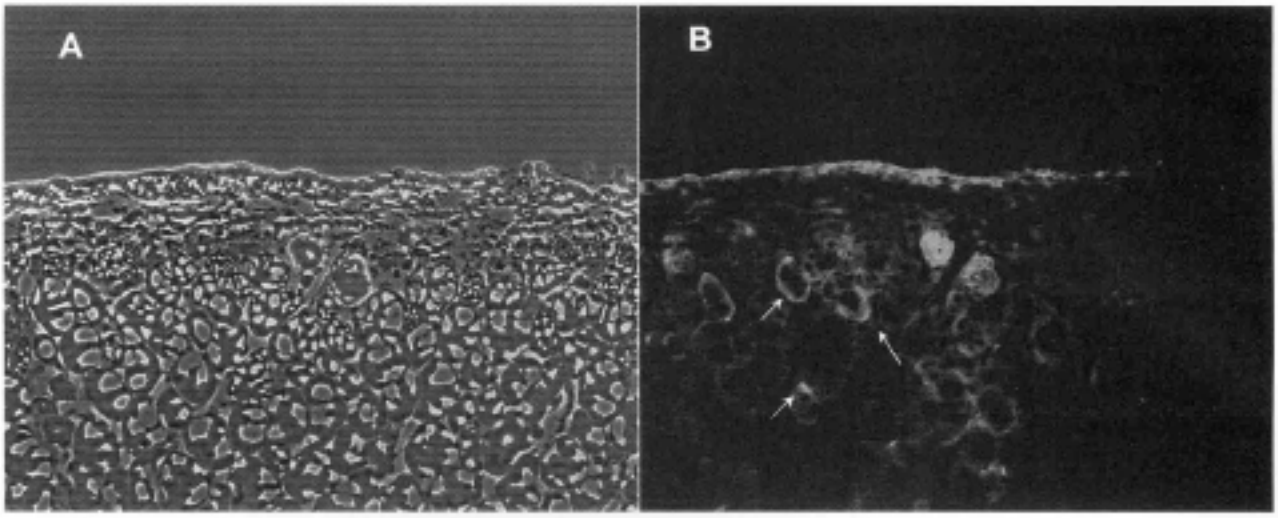

Fig. 2. Distribution of fluorescein-isothiocyanate (FITC)-labeled chimeric DNA-RNA hammerhead ribozyme targeting TGF-β_1 mRNA into the rat anterior abdominal wall

A : A fresh frozen section image of the anterior abdominal wall. Control bright field (Magnification, ×200)

B : A tissue section image with a fluorescence microscope. (White arrows indicate the distribution of FITC-labeled ribozymes in muscle cells) (Magnification, ×200)

mM $MgCl_2$ 4.0 μL, 10 mM dNTP Mix (TaKaRa) 2.0 μL, 0.1 M RNase inhibitor (TaKaRa) 0.5 μL および精製水を加えて総量 20 μL として，サーマルサイクラーにて 1st strand cDNA を作製した。

10. Real-time PCR 測定

腹膜組織に発現している TGF-β_1 mRNA，fibronectin mRNA を定量する目的にて，ABI PRISM 7000 Sequence Detection System (Applied Biosystems, Foster City, CA, USA) を使用して定量 real-time PCR を施行した。定量にあたっては，ラット TGF-β_1，ラット fibronectin，ラット GAPDH に対するプライマー・プローブ混合液 (TaqMan® Gene Expression Assays, TGF-β_1：Rn00572010-m1, TaqMan® Gene Expression Assays, fibronectin 1：Rn00569575-m1, TaqMan® Rodent GAPDH control reagents, Applied Biosystems) を使用した。1 ウェル当たりの反応液の組成は，作製したサンプル cDNA 4 μL，TaqMan® Universal Master Mix (Applied Biosystems) 12.5 μL，TaqMan® Gene Expression Assays (Applied Biosystems) 1.25 μL および精製水を加えて総量 25 μL として TaqMan™ PCR 法にて測定した。測定した TGF-β_1 の値は内在性コントロールである GAPDH にて補正後，Comparative Threshold Cycle (Ct) 法 (User Bulletin ♯2, ABI PRISM 7700 Sequence Detection System, December 11, 1997) を用いて定量測定を行った。

11. 統計処理

上記の 4 実験群に対して，多群間解析を Kruskal-Wallis 検定および Scheffe 検定にて行った。$p<0.05$ を有意とし，統計解析は StatView 5.0 (SAS Institute Inc., San Francisco, CA, USA) を使用した。

結　果

1．腹膜組織へのリボザイムの取り込み

腹腔内へ投与された FITC ラベルをしたキメラ型リボザイムが腹直筋表層の腹膜組織層に取り込まれていることが蛍光顕微鏡下の観察にて確認された (Fig. 2)。また，腹直筋においても筋細胞内へのリボザイムの取り込みが観察された (Fig. 2B の矢印)。

2．腹膜構造の変化

生理食塩水のみを投与した群においては (Fig. 3A)，腹膜中皮細胞は 1 層のままであり，腹膜肥厚の所見は見られなかった。CHX のみ投与した群 (Fig. 3B)，CHX およびミスマッチリボザイムを投与した群 (Fig. 3C) では腹膜中皮細胞下から筋層の間の組織成分が著明に増加し，新規血管形成も著明に生じ，全体として明らかな腹膜の肥厚を形成した。一方，CHX およびリボザイム投与群 (Fig. 3D) においては腹膜中皮細胞下から筋層までの間の組織成分の増加は目立たず，膠原線維の増生および新規血管形成も抑制されており，間質の浮腫様所見が観察された。また，表層

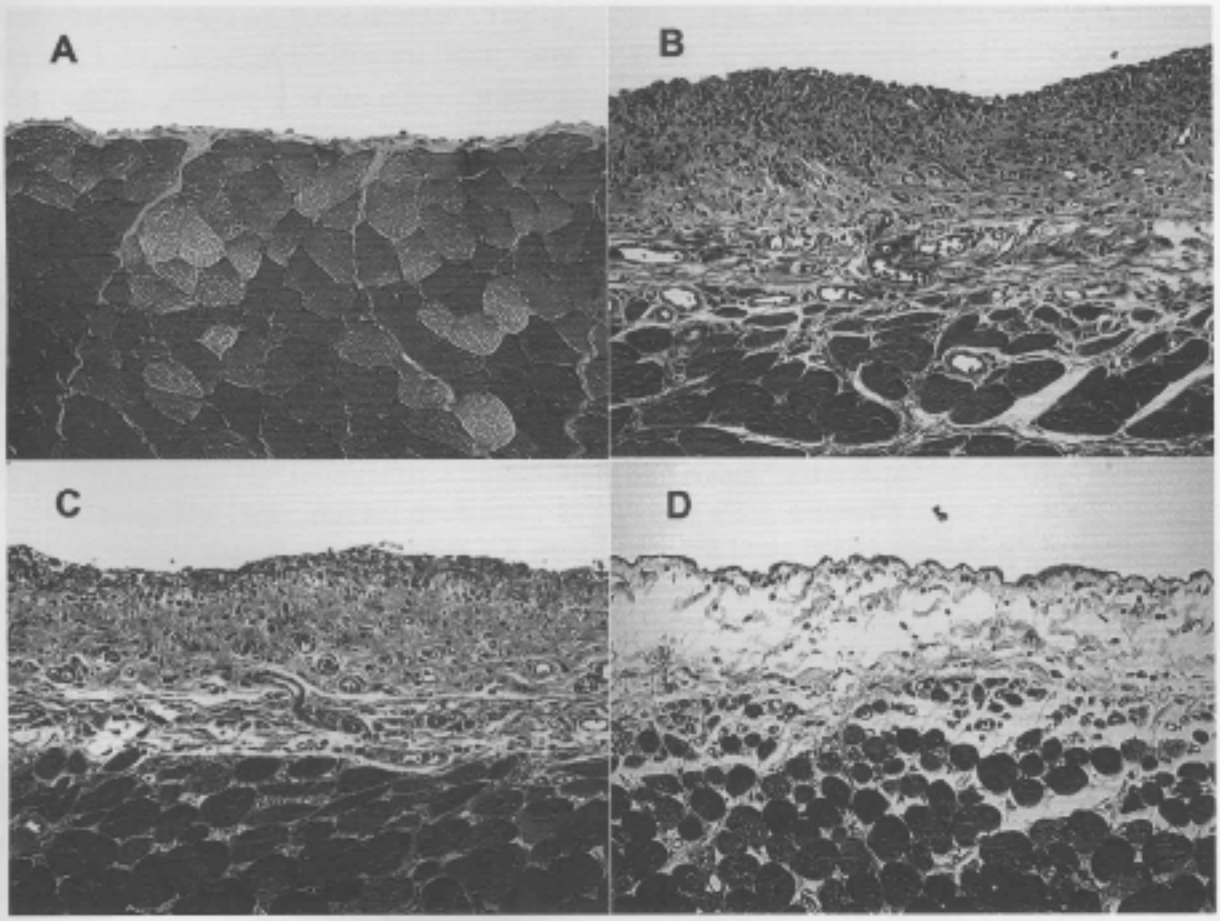

Fig. 3.　Histological assessment of the rat anterior abdominal wall

A : Treated with NS for 14 days
B : Treated with CHX for 14 days
C : Treated with CHX for 14 days and mismatch ribozyme on day 4
D : Treated with CHX for 14 days and the ribozyme specific to TGF-β_1 mRNA on day 4
All sections were stained with Masson's trichrome. (Magnification, ×200)

の腹直筋細胞には変性および萎縮の所見が他群よりも強く観察された。

3．腹膜肥厚度

Fig. 4 に腹膜肥厚度の定量比較を示す。CHX およびリボザイム投与群の腹膜肥厚は，CHX 単独投与群に比べて有意に($p<0.001$)抑制され，また CHX およびミスマッチリボザイム投与群に比べても有意に($p<0.01$)抑制されていた。

4．リボザイムの TGF-β_1 mRNA 発現への作用

Fig. 5 に TGF-β_1 に対する DNA-RNA キメラ型リボザイムの TGF-β_1 mRNA 発現に対する効果を示す。CHX およびリボザイム投与群では CHX 単独投与群に比べて有意に($p<0.01$) TGF-β_1 mRNA の発現が抑制され，また CHX およびミスマッチリボザイム投与群に比べても有意に($p<0.05$) TGF-β_1 mRNA の発現が抑制されていた。

5．リボザイムの fibronectin mRNA 発現への作用

Fig. 6 に TGF-β_1 に対する DNA-RNA キメラ型リボザイムの fibronectin mRNA 発現に対する効果を示す。CHX およびリボザイム投与群では CHX 単独投与群に比べて有意に($p<0.05$) fibronectin mRNA の発現が抑制された。

考　察

今回われわれは，TGF-β_1 の発現を特異的に阻害する DNA-RNA キメラ型リボザイムを腹膜硬化症モデルラットの腹腔内に投与して，腹膜の組織学的な変化および TGF-β_1 mRNA と fibronectin mRNA の発現量の変化を

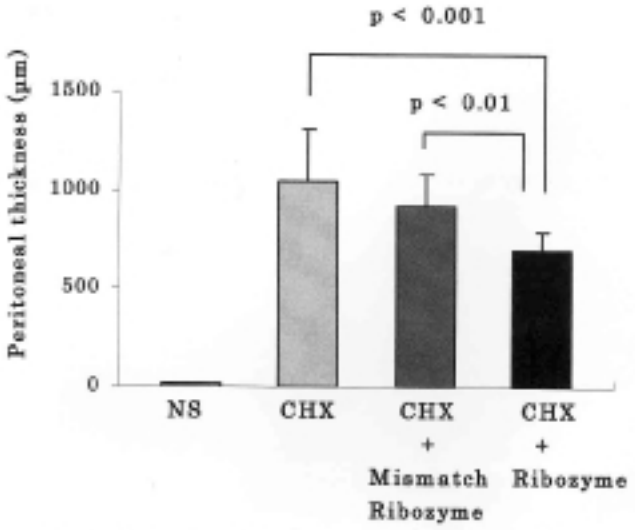

Fig. 4. Effects of the ribozyme specific to TGF-β_1 mRNA on submesothelial thickness in rats injected with CHX

Data are mean±SD.
$p<0.001$, CHX with ribozyme vs. CHX alone.
$p<0.01$, CHX with ribozyme vs. CHX with mismatch ribozyme

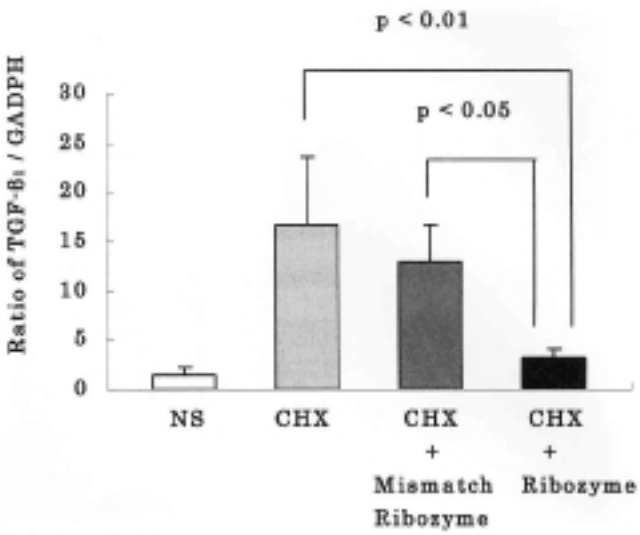

Fig. 5. Effects of the ribozyme specific to TGF-β_1 mRNA on the expression of TGF-β_1 mRNA in anterior abdominal wall tissues in rats injected with CHX

The amount of mRNA expression was determined by quantitative real-time PCR analysis.
Data are mean±SD.
$p<0.01$, CHX with ribozyme vs. CHX alone.
$p<0.05$, CHX with ribozyme vs. CHX with mismatch ribozyme

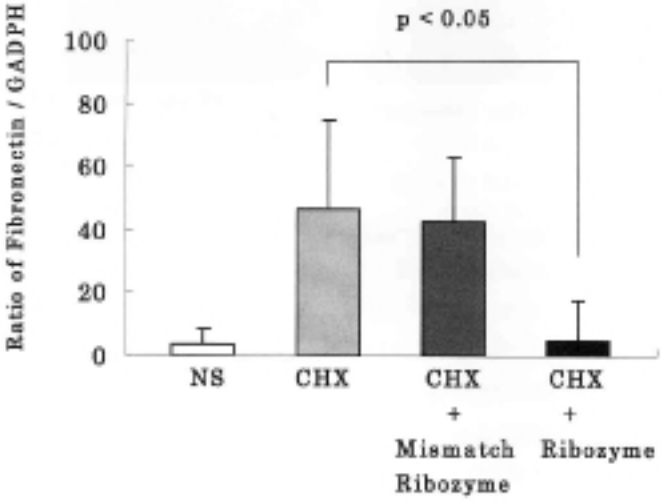

Fig. 6. Effects of the ribozyme specific to TGF-β_1 mRNA on the expression of fibronectin mRNA in anterior abdominal wall tissues in rats injected with CHX

The amount of mRNA expression was determined by quantitative real-time PCR analysis.
Data are mean±SD.
$p<0.05$, CHX with ribozyme vs. CHX alone.

検討した。その結果，リボザイムを投与した群の腹膜組織では腹膜の肥厚，線維化，硬化が著明に抑制されていた。また，リボザイム投与群の腹膜組織中ではTGF-β_1 mRNAの発現が有意に抑制され，fibronectin mRNAの発現も有意に抑制されていた。この結果より，腹腔内に投与されたリボザイムがTGF-β_1の発現を抑制し，組織線維化の過程においてTGF-β_1の下流因子で細胞外マトリックス蛋白の一つであるfibronectinの発現も抑制していることが示され，組織線維化の一連の過程が上流に位置するTGF-β_1の発現抑制によって抑制されて，組織所見における腹膜の肥厚，線維化，硬化の抑制に至ったものと考えられた。Margettsら[15,16]，アデノウイルスをベクターとしてTGF-β_1遺伝子をラット腹腔内において過剰に発現させたところ，腹膜の肥厚と硬化が惹起されたことを報告している。今回のわれわれの結果およびMargettsらの報告などから，TGF-β_1の発現増加が腹膜肥厚や硬化において中心的な役割を果たし，著明な組織学的な変化を生じさせることが明らかになった。

また今回の実験において，CHXおよびリボザイム投与群の組織所見では，腹膜の線維化と硬化は抑制されたものの，表層の腹直筋細胞に変性および萎縮の所見が明らかに観察された。一方，CHX単独投与群，CHXおよびミスマッチリボザイム投与群では著明な腹膜肥厚および硬化が観察されたが，腹直筋細胞への細胞傷害の所見は少なかった。これは，リボザイム投与群の腹腔内において，CHX

による強力な細胞傷害作用の存在にも関わらず，TGF-β_1 の発現がリボザイムによって強力に抑制された結果，腹膜中皮細胞下の線維化が発達せず，CHX に対する防御反応が取れなかったために直接表層の腹直筋細胞へ傷害が及んだためと考えられた。

TGF-β_1 は創傷や組織傷害で発現が亢進し，傷害部位を修復するため細胞外基質を増生させ，過剰になると線維化や硬化性変化が起こってくる。今回の動物実験レベルにおける組織所見からは，腹膜の肥厚が有害な刺激から細胞を保護している可能性があることが示唆された。この実験所見より，腹膜透析患者に生じる腹膜硬化症も，生体非適合性の腹膜透析液に対する生理的な防御反応による組織変化であることが類推された。現在，腹膜硬化症の延長線上に EPS があるのではなく，この2つは別の病態であるという考えもあり[17]，腹膜硬化の抑制が腹膜透析患者にとって有利なことであるのか，また EPS の発症予防に役立つのか，などといった詳細についてはいまだ明らかになっていない。一方，EPS 発症後の病態においては，明らかに生理的防御反応を超えた過剰な細胞外基質の増生が生じるため，積極的な腹腔内の線維化や硬化の抑制が望ましいと考えられた。

現在，EPS 発症後の治療法として副腎皮質ステロイドの使用報告が多く集積されているが，川西ら[18]による本邦における EPS に対する多施設前向き調査の報告では，約半数にしか効果が認められなかった。ステロイドは，炎症反応全般を抑制することによって細胞外基質の過剰産生，析出状態を抑制し有効であると考えられるが，中山らは[19]，ステロイドは炎症を伴わない時期に進展する癒着に対する効果は期待できず，ステロイドとは別の線維化を抑制する治療手段が必要であると述べている。今後の EPS 治療の方向性として，EPS の発症および進展に関与するサイトカインを明らかにし，サイトカインレベルでの線維化の抑制が治療において有効になると考えられる。

リボザイムは RNA 核酸であるため，RNA 分解酵素によって分解されやすい欠点があり，核酸分解酵素に対する耐性を上げる課題がある。今回われわれが合成した DNA-RNA キメラ型リボザイムは，切断活性のある保存配列のみを RNA とし他の塩基配列を DNA に変更し，またリボザイムの3'末端を phosphorothioate 型に化学修飾して RNA 分解酵素に耐性を持たせるような工夫を行った。また，リボザイムを実際の医薬品として使用する場合，リボザイムの生体への投与方法をどうするかという課題がある。リボザイムを標的組織に特異的に作用させるためには組織への局所投与が望ましいが，実際の生体では困難であり，組織特異性を持つベクターなどの開発が今後の課題となる。核酸医薬のなかでリボザイムはターゲット遺伝子に対する特異性と副作用の少なさなどの利点があり，今後上記課題を解消できれば，実際の医薬品として登場すると考えられる。

今回われわれが開発した TGF-β_1 mRNA に対する DNA-RNA キメラ型リボザイムは生体内において失活せず強力に作用して，線維化の過程に関わる主要なサイトカインである TGF-β_1 の発現を抑制し，過剰な細胞外基質の産生を抑制することを確認した。今後はリボザイム投与のタイミング，投与量，安全性などについて検討を重ねていくことによって，EPS に対するリボザイムによる遺伝子治療法が開発できる可能性があると考えられた。

結　語

今回われわれが開発した TGF-β_1 mRNA に対する DNA-RNA キメラ型リボザイムは，EPS の主要な病態である細胞外基質の過剰な産生，堆積，線維化の過程において中心的に働く TGF-β_1 を生体内において特異的に抑制できることが明らかになった。このリボザイムの効果は，ステロイドなどを使用する従来の治療法に比べてより選択的に EPS の病因に対して加療することを可能とし，EPS の新規の有効な治療手段になり得ると考えられた。

本論分の要旨は第5回腎不全病態治療研究会(2004年東京)，第48回日本腎臓学会学術総会(2005年横浜)，第464回日大医学会例会(2005年東京)，第6回腎不全病態治療研究会(2005年東京)にて発表した。

文　献

1. 川西秀樹，被嚢性腹膜硬化症(EPS)の病態と治療．伊藤克己，遠藤　仁，御手洗哲也，東原英二，秋澤忠男(編)：Annual Review 腎臓 2005．東京：中外医学社，2005：138-144.
2. Pollock C. Pathogenesis of peritoneal sclerosis. Int J Artif Organs 2005；28(2)：90-96.
3. Nakamura S, Niwa T. Advanced glycation end-products and peritoneal sclerosis. Semin Nephrol 2004；24(5)：502-505.
4. Io H, Hamada C, Ro Y, Ito Y, Hirahara I, Tomino Y. Morphologic changes of peritoneum and expression of VEGF in encapsulated peritoneal sclerosis rat models. Kidney Int 2004；65(5)：1927-1936.
5. Ignotz RA, Massague J. Transforming growth factor-beta

stimulates the expression of fibronectin and collagen and their incorporation into the extracellular matrix. J Biol Chem 1986；261(9)：4337-4345.
6. Fukuda N. Therapeutic application of ribozymes for cardiovascular disease. In：Levon Michael Khachigian(eds) Synthetic Nucleic Acids as Inhibitors of Gene Expression. Florida：CRC Press LLC, 2004：1-17.
7. Teng J, Fukuda N, Hu WY, Nakayama M, Kishioka H, Kanmatsuse K. DNA-RNA chimeric hammerhead ribozyme to transforming growth factor-β_1 mRNA inhibits the exaggerated growth of vascular smooth muscle cells from spontaneously hypertensive rats. Cardiovasc Res 2000；48：138-147.
8. Ando H, Fukuda N, Kotani M, Yokoyama S, Kunimoto S, Matsumoto K, Saito S, Kanmatsuse K, Mugishima H. Chimeric DNA-RNA hammerhead ribozyme targeting transforming growth factor-β_1 mRNA inhibits neointima formation in rat carotid artery after balloon injury. Eur J Pharmacol 2004；483(2-3)：207-214.
9. Yusa J, Fukuda N, Sato S, Matsumoto K, Mugishima H, Kamoi K. Inhibition of growth of human gingival fibroblasts by chimeric DNA-RNA hammerhead ribozyme targeting transforming growth factor-β_1. J Periodontol 2005；76(8)：1265-1274.
10. Offner FA, Feichtinger H, Stadlmann S, Obrist P, Marth C, Klingler P, Grage B, Schmahl M, Knabbe C. Transforming growth factor-β synthesis by human peritoneal mesothelial cells. Induction by interleukin-1. Am J Pathol 1996；148(5)：1679-1688.
11. Medcalf JF, Walls J, Pawluczyk IZ, Harris KP. Effects of glucose dialysate on extracellular matrix production by human peritoneal mesothelial cells(HPMC)：the role of TGF-β. Nephrol Dial Transplant 2001；16(9)：1885-1892.
12. Oh KH, Margetts PJ. Cytokines and growth factors involved in peritoneal fibrosis of peritoneal dialysis patients. Int J Artif Organs 2005；28(2)：129-134.
13. Ishii Y, Sawada T, Shimizu A, Tojimbara T, Nakajima I, Fuchinoue S, Teraoka S. An experimental sclerosing encapsulating peritonitis model in mice. Nephrol Dial Transplant 2001；16(6)：1262-1266.
14. Chomczynski P, Sacchi N. Single-step method of RNA isolation by acid guanidinium thiocyanate-phenol-chloroform extraction. Anal Biochem 1987；162(1)：156-159.
15. Margetts PJ, Kolb M, Galt T, Hoff CM, Shockley TR, Gauldie J. Gene transfer of transforming growth factor-β_1 to the rat peritoneum：effects on membrane function. J Am Soc Nephrol 2001；12(10)：2029-2039.
16. Margetts PJ, Bonniaud P, Liu L, Hoff CM, Holmes CJ, West-Mays JA, Kelly MM. Transient overexpression of TGF-β_1 induces epithelial mesenchymal transition in the rodent peritoneum. J Am Soc Nephrol 2005；16(2)：425-436.
17. Garosi G. Different aspects of peritoneal sclerosis. Contrib Nephrol 2003；140：18-29.
18. Kawanishi H, Kawaguchi Y, Fukui H, Hara S, Imada A, Kubo H, Kin M, Nakamoto M, Ohira S, Shoji T. Encapsulating peritoneal sclerosis in Japan；prospective multicenter survey. Am J Kidney Dis 2004；44：729-737.
19. 中山昌明，長谷川俊男．被嚢性腹膜硬化症(EPS)に対する内科的治療―副腎皮質ステロイド薬と腹腔洗浄の効果―．腎と透析 57 別冊腹膜透析 2004；57：83-87.

Chimeric DNA–RNA hammerhead ribozyme targeting transforming growth factor-β1 mRNA ameliorates renal injury in hypertensive rats

Yoshiko Tahira[a], Noboru Fukuda[a,b,d], Morito Endo[c], Takahiro Ueno[a], Hiroyuki Matsuda[a], Satoshi Saito[a], Koichi Matsumoto[a] and Hideo Mugishima[d]

Objective **Transforming growth factor (TGF)-β is a critical factor in the progression of renal injury, regardless of the primary etiology. Such injury is characterized by glomerular sclerosis and tubulointerstitial fibrosis. To develop a ribozyme-based therapy for progressive renal diseases, we examined the effects of chimeric DNA–RNA hammerhead ribozyme targeting TGF-β1 mRNA on glomerulosclerosis in salt-loaded, stroke-prone spontaneously hypertensive rats (SHR-SP) and salt-sensitive Dahl (Dahl-S) rats.**

Methods **The chimeric DNA–RNA ribozyme to TGF-β1 was delivered by polyethylenimine to cultured mesangial cells from SHR-SP *in vitro* and to glomeruli in SHR-SP *in vivo*. The chimeric ribozyme reduced expression of TGF-β1 mRNA and protein, which was accompanied by inhibition of expression of extracellular matrix molecules such as fibronectin and collagen type I in mesangial cells from SHR-SP *in vitro*.**

Results **One intraperitoneal injection of 200 μg of chimeric DNA–RNA ribozyme to TGF-β1 *in vivo* markedly ameliorated thickening of capillary artery walls and glomerulosclerosis in salt-loaded SHR-SP and Dahl-S rats without a reduction in blood pressure. The chimeric ribozyme reduced expression of TGF-β1 and connective tissue growth factor (CTGF) mRNAs in renal cortex in salt-loaded Dahl-S rats. Chimeric ribozyme to TGF-β1 significantly reduced levels of protein in urine in the Dahl-S rats.**

Conclusion **These results suggest that chimeric DNA–RNA ribozyme to TGF-β1 may be useful as a gene therapy for progressive tissue injury in a wide variety of renal diseases, including hypertensive nephrosclerosis. *J Hypertens* 25:671–678 © 2007 Lippincott Williams & Wilkins.**

Journal of Hypertension 2007, **25**:671–678

Keywords: gene therapy, glomerulosclerosis, hypertension, ribozyme, transforming growth factor-β1

[a]Department of Medicine, Nihon University School of Medicine, Division of Nephrology and Endocrinology, Tokyo, [b]Advanced Research Institute for the Science and Humanities, Nihon University, Tokyo, [c]Hachinohe University, Faculty of Human Health Science and [d]Department of Advanced Medicine, Division of Cell Regeneration and Transplantation, Nihon University School of Medicine, Tokyo, Japan

Correspondence and requests for reprints to Noboru Fukuda, MD, PhD, Department of Medicine, Nihon University School of Medicine, Ooyaguchi-kami 30-1, Itabashi-ku, Tokyo 173-8610, Japan
Tel: +81 3 3972 8111; fax: +81 3 3972 8666;
e-mail: fukudan@med.nihon-u.ac.jp

Sponsorship: This work was supported in part by a Grant-in-Aid for the High-Tech Research Center from the Japanese Ministry of Education, Science, Sports, and Culture to Nihon University and from the Ministry of Education, Science, Sports, and Culture of Japan (15590863).

Conflict of interest: none.

Received 13 April 2006 **Revised** 4 October 2006
Accepted 18 October 2006

Introduction

A number of studies have identified transforming growth factor (TGF)-β as a critical factor in kidney diseases such as glomerulosclerosis [1] and mesangioproliferative glomerulonephritis [2,3]. TGF-β mRNA and protein are expressed strongly in various animal models of progressive renal diseases such as hypertensive renal sclerosis, diabetic nephropathy and focal renal sclerosis [4–6].

Because there are still no effective treatments for progressive renal diseases, gene therapy is now being considered as a strategy. Ribozymes are RNA molecules that catalytically cleave a phosphodiester bond in the appropriate target RNAs in a sequence-specific manner, thereby inhibiting the expression of specific gene products. Ribozymes have progressed from being objects of scientific study to potential therapeutic agents for treatment of both acquired and inherited diseases [7]. We have demonstrated that ribozyme to TGF-β1 inhibits growth of vascular smooth muscle cells *in vitro* [8,9] and neointima formation of arteries after angioplasty *in vivo* [10]. However, ribozyme therapy for progressive renal diseases has not yet been reported.

Experimental evidence supports the notion that the pathogenesis of glomerulosclerosis with nephrosclerosis involves glomerular hypertension, mesangial dysfunction, such as mesangiolysis, and increased mesangial matrix [11]. Glomerular hypertension results from systemic hypertension and leads to increased glomerular capillary pressure with subsequent glomerular endothelial damage and sclerosis [12,13]. Stroke-prone spontaneously hypertensive rats (SHR-SP) show severe cardiovascular organ damage such as stroke, ventricular hypertrophy and glomerulosclerosis associated with TGF-β [5]. Salt-sensitive Dahl (Dahl-S) rats also show

0263-6352

glomerulosclerosis, which is known to be associated with TGF-β [4].

In the current study, to develop ribozyme therapy for progressive renal diseases, we examined the in-vivo effects of chimeric DNA–RNA hammerhead ribozyme targeting TGF-β1 mRNA on glomerulosclerosis in SHR-SP and Dahl-S rats.

Methods

Our investigation conformed to standards of the *Guide for the Care and Use of Laboratory Animals* [14].

Synthetic chimeric DNA–RNA hammerhead ribozyme

The 38-base chimeric DNA–RNA hammerhead ribozyme, which contained deoxyribonucleotides instead of ribonucleotides at noncatalytic residues and two phosphorothioate linkages at the 3′ terminus, was designed to cleave the GUC sequence in the rat TGF-β1 mRNA [7]. The TGF-β1 specific ribozyme and a mismatch ribozyme with a single base change in the catalytic loop region were synthesized with the use of a DNA/RNA synthesizer (Model 394; Applied Biosystems Inc., Foster City, California, USA).

Isolation of glomeruli and culture of mesangial cells

Glomeruli were isolated from the kidneys of 4-week-old male SHR-SP/Izumo rats (SHR Corporation, Funabashi, Chiba, Japan). Glomeruli were isolated with a graded-sieve technique as described previously [15]. The renal cortex was excised and minced into small pieces under sterile conditions. The minced cortex was pressed through a 200-μm sieve and suspended in RPMI 1640 medium (Gibco Laboratories, Grand Island, New York, USA). The suspension was passed through a 120-μm sieve, and glomeruli were collected on the surface of the sieve and resuspended in RPMI 1640. Mesangial cells were isolated from explants of whole glomeruli according to the differential growth capacities of glomerular epithelial and mesangial cells [15].

Delivery of chimeric DNA–RNA ribozyme to TGF-β1 *in vitro* and *in vivo*

For in-vitro delivery, mesangial cells were transfected with 1.0 μmol/l fluorescein isothiocyanate (FITC)-labeled chimeric DNA–RNA ribozyme to TGF-β1 with polyethylenimine for 120 min. After 24 h, cells were fixed with acetone at 4°C for 10 min and examined via fluorescence microscopy. Total intracellular FITC signal, as well as distribution of signal to the cytoplasmic or nuclear compartment, were noted.

For in-vivo delivery, 500 μg/kg of FITC-labeled chimeric DNA–RNA ribozyme to TGF-β1 in polyethylenimine was injected into SHR-SP subcutaneously, intraperitoneally or intravenously. After 24 h, kidneys were removed from SHR-SP and fixed in 10% neutral buffered formalin in a dark environment and embedded in paraffin for light microscopy with eriochrome black T stain.

Reverse transcription–polymerase chain reaction

mRNA was extracted from cultured mesangial cells of SHR-SP and renal cortex from Dahl-S rats loaded with 1% salt water. Aliquots of mRNA were reverse transcribed into single-stranded cDNA by incubation with avian myeloblastoma virus reverse transcriptase (Takara Biochemicals, Otsu, Shiga, Japan). Diluted cDNA products were then subjected to polymerase chain reaction (PCR). The primers used for amplification were as follows:

(1) TGF-β1: forward 5′-GCCCTGGATACCAACTAC TGCT-3′, reverse 5′-AGGCTCCAAATGTAGGG GCAGG-3′, product 161 base-pair (bp);
(2) fibronectin: forward 5′-TGCCACTGTTCTCCTA CGTG-3′, reverse 5′-ATGCTTTGACCCTTACA CGG-3′, product 312 bp;
(3) collagen type I: forward 5′-GGTGCTAGATCAG GAGCAGG-3′, reverse 5′-ATGCCCACTCCCTAA CAGTG-3′, product 182 bp; and
(4) connective tissue growth factor (CTGF): forward 5′-ATCCCTGCGACCCACACAAG-3′, reverse 5′-TT ACGTCTGGCGTCGAAGGC-3′, product 145 bp;
(5) human 18S ribosomal RNA was used as an internal control, the primers were as follows: forward 5′-TCAAGAACGAAAGTCGGAGG-3′, reverse 5′-GG ACATCTAAGGGCATCACA-3′, product 312 bp.

PCR was performed in a DNA thermal cycler (Perkin-Elmer Cetus, Norwalk, Connecticut, USA), and products were separated by electrophoresis on 1.5% agarose gels, stained with ethidium bromide and visualized by ultraviolet illumination.

Western blot analysis

Mesangial cells of SHR-SP (10^5 cells/cm^2) and renal cortex from Dahl-S rats loaded with 1% salt were disrupted with lysis buffer [50 mmol/lTris–HCl (pH8.0), 150 mmol/l NaCl, 0.02% sodium azide, 100 μg/ml phenylmethylsulfonyl fluoride, 1 μg/ml aprotinin, 1% Triton X-100]. Total proteins were extracted and purified with 100 μl of chloroform and 400 μl of methanol. Protein samples were boiled for 3 min and subjected to electrophoresis on 8% polyacrylamide gels and then transblotted to nitrocellulose membranes (BioRad Laboratories, Hercules, California, USA). Blots were incubated with rabbit pan-specific polyclonal antibody for TGF-β (R & D Systems, Minneapolis, Minnesota, USA) or mouse monoclonal antibody specific for α-tubulin as a control (Sigma BioScience, St. Louis, Missouri, USA), diluted 1 : 500 in 5% nonfat milk in TBST solution (10 mmol/l Tris–HCl, pH 8.0, 150 mmol/l NaCl, and 0.05% Tween 20) for 3 h at room temperature. The membrane was incubated with goat anti-mouse IgG for 1 h at room temperature, then washed with TBST once for 15 min,

and four times for 5 min. Immune complexes on the membrane were detected by the enhanced chemiluminescence method (Amersham Pharmacia Biotech, Buckinghamshire, UK).

Experimental design

Twelve-week-old male SHR-SP or 7-week-old male Dahl-S rats of the Iwai substrain (Seac Yoshitomi Ltd, Fukuoka, Japan) were loaded with 1% salt water for 6 or 8 weeks, respectively. After 4 weeks of loading with salt water, the control group received an intraperitoneal injection of 1.5 ml of saline. The mismatch or ribozyme group received an intraperitoneal injection of mismatch ribozyme or chimeric DNA–RNA ribozyme to TGF-β1 (200 μg/body weight) with polyethylenimine (Fig. 1). Systolic blood pressure (SBP) was measured by the tail-cuff method.

Histological examination

Kidneys removed from SHR-SP or Dahl-S rats were fixed in 10% neutral buffered formalin and embedded in paraffin for light microscopic study. Sections (2 μm thick) were stained with Masson trichrome (MT) stain or hematoxylin–eosin (HE). Histological examination was done by a pathologist without any prior knowledge of the experimental groups. To semiquantify the glomerular matrix, 50 glomeruli were selected randomly. The percentage of each glomerulus occupied by mesangial matrix was estimated and given a score of 0, normal; 1, involvement of up to 25% of the glomerulus; 2, involvement of 25–50% of the glomerulus; 3, involvement of 50–75% of the glomerulus; or 4, involvement of 75–100% of the glomerulus. The glomerular injury score (GIS) was obtained by the following formula: $[(0 \times n_0) + (1 \times n_1) + (2 \times n_2) + (3 \times n_3) + (4 \times n_4)]/50$. To semiquantify the tubulointerstitial area, 20 areas of renal cortex were selected randomly. The percentage of each area that showed sclerofibrotic change was estimated and assigned a score of 0, normal; 1, involvement of less than 10% of the area; 2, involvement of 10–30% of the area; 3, involvement of 30–50% of the area; or 4, involvement of more than 50% of the area. The tubulointerstitial injury score (TIS) was calculated as $[(0 \times n_0) + (1 \times n_1) + (2 \times n_2) + (3 \times n_3) + (4 \times n_4)]/20$.

Fig. 1

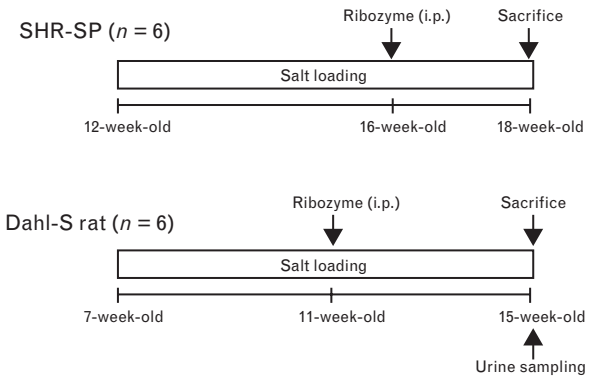

Experimental protocols for treatment of salt-loaded stroke-prone spontaneously hypertensive rats (SHR-SP) and salt-sensitive Dahl (Dahl-S) rats with chimeric DNA–RNA ribozyme targeting transforming growth factor (TGF)-β1 mRNA.

Statistical analysis

Results are given as the mean ± SEM. The significance of differences between mean values was evaluated by Student's *t*-test for unpaired data and by two-way analysis of variance (ANOVA) followed by Duncan's multiple range test.

Results

Delivery of chimeric DNA–RNA ribozyme to TGF-β1

FITC-labeled chimeric ribozyme was observed in the cytosol of cultured mesangial cells *in vitro*, and the transfection efficiency was approximately 20% (Fig. 2b).

FITC-labeled chimeric ribozyme was clearly visible in glomeruli from SHR-SP 24 h after subcutaneous, intraperitoneal or intravenous administration (Fig. 2c, e, f), but not visible in glomeruli 72 h after subcutaneous administration (Fig. 2d). FITC-labeled chimeric ribozyme was also visible in capillary arteries 24 h after subcutaneous administration (Fig. 2c). Intravenous and intraperitoneal administration were more effective than subcutaneous administration for delivery of the ribozyme.

Effects of chimeric DNA–RNA ribozyme to TGF-β1 on expression of TGF-β1, fibronectin, and collagen type I mRNAs and TGF-β1 protein in mesangial cells from SHR-SP

Levels of TGF-β1 mRNA were lower with chimeric DNA–RNA ribozyme to TGF-β1 (0.1 and 1.0 μmol/l) than with mismatch ribozyme in mesangial cells from SHR-SP. This reduction was dose dependent (Fig. 3a). Chimeric DNA–RNA ribozyme to TGF-β1 (1.0 μmol/l) also reduced levels of TGF-β1 protein (Fig. 3b). Ribozyme to TGF-β1 decreased levels of fibronectin mRNA at a concentration of 1.0 μmol/l and collagen type I mRNA at concentrations of 0.1 and 1.0 μmol/l in comparison to expression levels with mismatch ribozyme (Fig. 3a).

Effects of chimeric DNA–RNA ribozyme to TGF-β1 on expression of TGF-β1 and CTGF mRNAs and TGF-β1 protein in renal cortex from Dahl-S rats

Intraperitoneal administration of 200 μg of chimeric DNA–RNA ribozyme to TGF-β1 markedly reduced expression of TGF-β1 and CTGF mRNAs and TGF-β1 protein in renal cortex from salt-loaded Dahl-S rats (Fig. 4).

Fig. 2

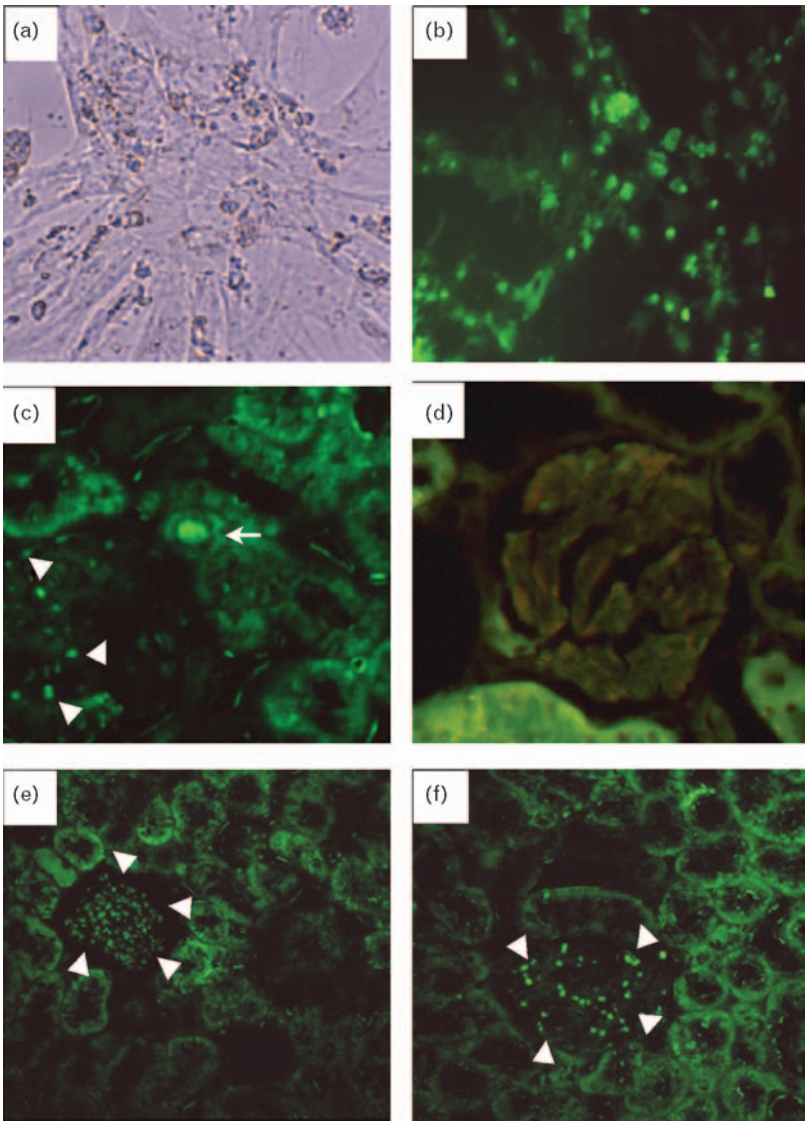

Delivery of chimeric DNA–RNA ribozyme to transforming growth factor (TGF)-β1 *in vitro* and *in vivo*. For in-vitro delivery, mesangial cells were transfected with 1.0 μmol/l fluorescein isothiocyanate (FITC)-labeled chimeric ribozyme with polyethylenimine for 120 min. Cells were fixed with acetone at 4°C for 10 min and examined via fluorescent microscopy without (a) or with (b) ultraviolet light. For in-vivo delivery, 200 μg of FITC-labeled chimeric DNA–RNA ribozyme to TGF-β1 polyethylenimine was injected into stroke-prone spontaneously hypertensive rats (SHR-SP) subcutaneously (c), intraperitoneally (d,e), or intravenously (f). After 24 h (c, e, f) or 72 h (d), kidneys were removed, fixed in 10% neutral-buffered formalin in the dark, and embedded in paraffin for light microscopy with eriochrome black T stain. Large arrows indicate the localization of labeled ribozyme in glomeruli and small arrows indicate capillary arteries.

Effects of chimeric DNA–RNA ribozyme to TGF-β1 on blood pressure and nephrosclerosis in SHR-SP and Dahl-S rats

The renal cortex of salt-loaded SHR-SP and of salt-loaded Dahl-S rats showed marked thickening of capillary artery walls and severe glomerulosclerosis with glomerular ischemia due to obstruction of the afferent artery. Intraperitoneal administration of 200 μg of chimeric DNA–RNA ribozyme to TGF-β1 or mismatch ribozyme had no effect on blood pressure in salt-loaded SHR-SP and Dahl-S rats with salt-loading (Table 1). Intraperitoneal administration of chimeric DNA–RNA ribozyme to TGF-β1 markedly ameliorated thickening of the capillary artery wall and glomerulosclerosis in kidneys of salt-loaded SHR-SP and Dahl-S rats. Administration of mismatch ribozyme had no effect on thickening or glomerulosclerosis (Fig. 5).

Intraperitoneal administration of chimeric DNA–RNA ribozyme to TGF-β1 significantly ($P < 0.05$) decreased the GIS and TIS in kidney from salt-loaded SHR-SP and Dahl-S rats. Mismatch ribozyme had no effect on GIS or

Fig. 3

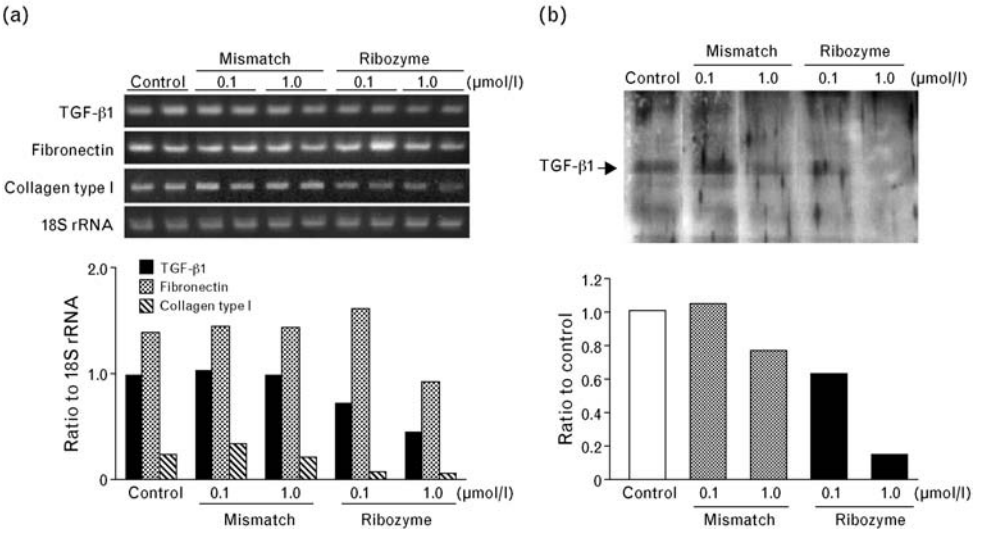

Effects of chimeric DNA–RNA ribozyme to transforming growth factor (TGF)-β1 on expression of TGF-β1, fibronectin and collagen type I mRNAs (a) and TGF-β1 protein (b) in cultured mesangial cells from stroke-prone spontaneously hypertensive rats (SHR-SP). Levels of TGF-β1, fibronectin and collagen type I mRNAs were evaluated by reverse transcription-polymerase chain reaction (RT-PCR). The ratio of the abundance of TGF-β1, fibronectin and collagen type I mRNAs to that of 18S rRNA was evaluated by densitometric analysis. Data are the means of experiments carried out in duplicate (a). Levels of TGF-β1 protein in renal cortex were evaluated by Western blot analysis. The abundance of TGF-β1 protein was evaluated by densitometric analysis. Data are the means of experiments carried out in duplicate (b).

Fig. 4

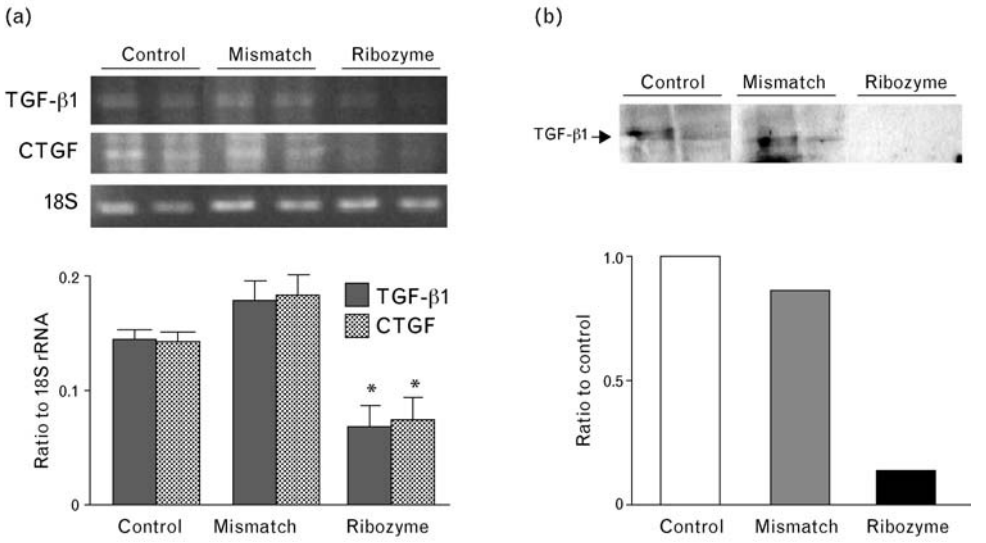

Effects of chimeric DNA–RNA ribozyme to transforming growth factor (TGF)-β1 on expression of TGF-β1 and connective tissue growth factor (CTGF) mRNAs and TGF-β1 protein in renal cortex of salt-loaded salt-sensitive Dahl (Dahl-S) rats. Seven-week-old male Dahl-S rats were given 1% salt water for 6 or 8 weeks. After 4 weeks of salt loading, the mismatch or ribozyme group received an intraperitoneal injection of mismatch ribozyme or chimeric DNA–RNA ribozyme to TGF-β1 (200 μg/body weight). Levels of TGF-β1 and CTGF mRNAs were evaluated by reverse transcription-polymerase chain reaction (RT-PCR). The ratio of the abundance of TGF-β1 and CTGF mRNAs to that of 18S rRNA was evaluated by densitometric analysis. Data are the mean ± SEM ($n = 4$). $^*P < 0.05$ versus mismatch ribozyme (a). Levels of TGF-β1 protein in renal cortex were evaluated by Western blot analysis. The abundance of TGF-β1 protein was evaluated by densitometric analysis. Data are the means of experiments carried out in duplicate (b).

Table 1 Systolic blood pressure in salt-loaded, stroke-prone spontaneously hypertensive rats (SHR-SP) and salt-sensitive Dahl (Dahl-S) rats treated without (control) or with mismatch ribozyme (mismatch) or chimeric DNA–RNA hammerhead ribozyme targeting transforming growth factor (TGF)-β1 mRNA (ribozyme)

	Systolic blood pressure (mmHg)	
	SHR-SP	Dahl-S
Control	272 ± 16	214 ± 28
Mismatch	275 ± 22	224 ± 36
Ribozyme	277 ± 10	205 ± 20

$n = 6$ in each group.

TIS in kidney from salt-loaded SHR-SP and Dahl-S rats (Table 2).

Table 2 Glomerular injury score (GIS) or tubulointerstitial injury score (TIS) in salt-loaded, stroke-prone spontaneously hypertensive rats (SHR-SP) and salt-sensitive Dahl (Dahl-S) rats treated without (control) or with mismatch ribozyme (mismatch) or chimeric DNA–RNA hammerhead ribozyme targeting transforming growth factor (TGF)-β1 mRNA (ribozyme)

Strain	Group	GIS	TIS
SHR-SP	Control	0.87 ± 0.01	0.67 ± 0.10
	Mismatch	0.84 ± 0.12	0.65 ± 0.18
	Ribozyme	0.68 ± 0.06*	0.50 ± 0.07*
Dahl-S	Control	1.01 ± 0.07	0.72 ± 0.18
	Mismatch	1.02 ± 0.14	0.78 ± 0.12
	Ribozyme	0.64 ± 0.09*	0.54 ± 0.26*

* $P < 0.05$ versus mismatch. $n = 4$ in each group.

Effects of chimeric DNA–RNA ribozyme to TGF-β1 on proteinuria in Dahl-S rats

Intraperitoneal administration of chimeric DNA–RNA ribozyme to TGF-β1 to salt-loaded Dahl-S rats decreased excretion of protein by 50% ($P < 0.05$). Administration of mismatch ribozyme had no effect on proteinuria (Fig. 6).

Discussion

In the present study, salt-loaded SHR-SP and Dahl-S rats experience significant thickening of the capillary arteries,

Fig. 5

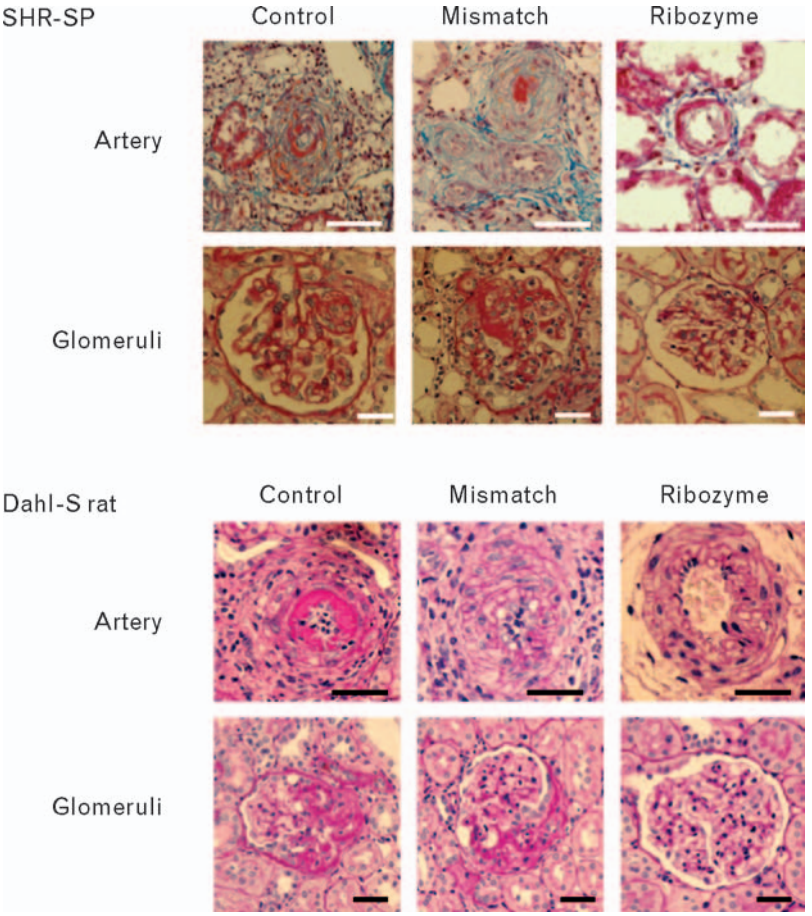

Histological findings in renal cortex of salt-loaded, stroke-prone spontaneously hypertensive rats (SHR-SP) and salt-sensitive Dahl (Dahl-S) rats treated with chimeric DNA–RNA ribozyme to transforming growth factor (TGF)-β1. Twelve-week-old male or 7-week-old male SHR-SP and Dahl-S rats were loaded with 1% salt water for 6 or 8 weeks, respectively. After 4 weeks of salt loading, the mismatch or ribozyme group received an intraperitoneal injection of mismatch ribozyme or chimeric DNA–RNA ribozyme to TGF-β1 (200 μg/body weight). Renal cortex was fixed and stained with Masson trichrome for SHR-SP or hematoxylin–eosin for Dahl-S rats. Bar = 20 μm.

Fig. 6

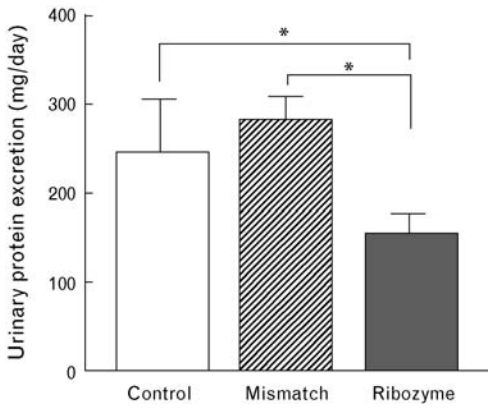

Effects of chimeric DNA–RNA ribozyme to transforming growth factor (TGF)-β1 on proteinuria in salt-loaded, salt-sensitive Dahl (Dahl-S) rats. Data are the mean ± SEM ($n = 4$). $^*P < 0.05$ versus mismatch ribozyme and control.

glomerulosclerosis, atrophic tubules and interstitial fibrosis in kidney in response to the development of hypertension. We have demonstrated previously that expression of TGF-β1 mRNA is higher in glomeruli and capillaries of renal cortex from SHR-SP than in those of normotensive Wistar–Kyoto rats [5]. In addition, Dahl-S rats also developed severe hypertension, glomerulosclerosis, thickening of capillary artery walls and interstitial fibrosis in response to salt loading [4].

TGF-β1 stimulates extracellular matrix formation [16,17]. TGF-β-induced production of extracellular matrix proteins in glomeruli causes renal damage in rats with thymidylate synthase complementing protein (Thy-1)-induced nephritis [18], diabetic nephropathy [19] and interstitial nephritis induced by obstructive nephropathy [20]. Moreover, TGF-β has recently been reported to induce epithelial–mesenchymal transformation in renal tissue, which plays a critical role in the pathogenesis of nephritis [21]. Thus, TGF-β may associate the nephrosclerosis and interstitial nephropathy by its effects on extracellular matrix formation and epithelial–mesenchymal transformation in kidney.

Ribozymes hybridize to and cleave a target RNA. Once the target RNA is cleaved, the ribozyme can dissociate from the cleaved products and repeat this process with another RNA molecule [22]. Thus, ribozyme does not require any cellular components and has high specificity for inhibiting expression of a target gene. One problem with ribozymes is rapid degradation in tissue, which diminishes the availability of the ribozyme and reduces their efficiency as a gene therapy. There are a number of modifications that can improve stability, specificity and efficacy of ribozymes. Our chimeric DNA–RNA hammerhead ribozyme to rat TGF-β1 mRNA contained deoxyribonucleotides instead of ribonucleotides at noncatalytic residues to enhance catalytic turnover and improve stability, as reported previously [23]. In addition, two deoxyribonucleotides at the 3′-terminus of the chimeric DNA–RNA ribozyme were modified with phosphorothioate linkages to improve resistance to nucleases [24]. Moreover, to increase uptake of the ribozyme, we delivered our ribozyme with polyethylenimine because liposome-complexed molecules are preferentially transported to the cytoplasm [25].

In the present study, the chimeric DNA–RNA ribozyme to TGF-β1 with polyethylenimine was transferred to cultured mesangial cells *in vitro* and to glomeruli in SHR-SP by subcutaneous, intraperitoneal or intravenous injection. The chimeric ribozyme reduced expression of TGF-β1 and inhibited expression of extracellular matrix proteins, such as fibronectin and collagen type I, in mesangial cells from SHR-SP *in vitro*, suggesting that ribozyme to TGF-β1 may inhibit extracellular matrix formation in glomeruli.

In the present experiments, a single injection of chimeric DNA–RNA ribozyme to TGF-β1 markedly ameliorated capillary artery hypertrophy and glomerulosclerosis in salt-loaded SHR-SP without any reduction in blood pressure. Because the effect of the ribozyme on glomerulosclerosis in SHR-SP was unexpectedly strong, to verify the efficiency we examined the effects of this ribozyme on glomerulosclerosis and proteinuria in salt-loaded Dahl-S rats. One injection of chimeric DNA–RNA ribozyme to TGF-β1 also markedly improved the capillary artery hypertrophy and glomerulosclerosis and significantly reduced proteinuria in salt-loaded Dahl-S rats without any reduction in blood pressure. These findings indicate that TGF-β contributes to both capillary artery hypertrophy and glomerulosclerosis in SHR-SP and Dahl-S rats, which were efficiently ameliorated by chimeric ribozyme independent of blood pressure. The chimeric ribozyme also reduced expression of TGF-β1 and CTGF mRNAs in renal cortex in salt-loaded Dahl-S rats. CTGF is a potent growth factor that stimulates growth of mesenchymal cells, including mesangial cells, and formation of extracellular matrix downstream of TGF-β1 [26]. These findings suggest that TGF-β1 causes glomerulosclerosis through induction of CTGF in Dahl-S rats. Ribozyme to TGF-β1 significantly decreased GIS and TIS of renal cortex in salt-loaded SHR-SP and Dahl-S rats, suggesting that TGF-β1 may also be involved in renal interstitial fibrosis due to extracellular matrix formation in these hypertensive rats. Dahly *et al.* [27] injected anti-TGF-β antibody every day for 2 weeks into salt-loaded Dahl-S rats and found that the antibody significantly reduced blood pressure, proteinuria and the degree of glomerulosclerosis and renal interstitial fibrosis. In the present study, the chimeric ribozyme to TGF-β1 ameliorated the renal injury

and proteinuria with only a single injection and without reduction of blood pressure in salt-loaded Dahl-S rats, suggesting that this ribozyme is an efficient strategy to ameliorate progressive renal injury.

Theoretically, nuclease-resistant ribozymes can be designed to cleave any target RNA. The recently completed sequencing of the human genome and of the genomes of several pathogenic species provide a large number of potential ribozyme targets that may benefit clinical medicine. These ribozymes can be chemically modified to prevent biological degradation, and thus, nuclease-resistant synthetic ribozymes are emerging as a new and broadly useful class of therapeutic agents. Gene therapy by nucleic acid-based therapeutics is currently in its infancy, but preliminary studies suggest that this type of therapy may be effective against diseases caused by genes encoding nontractable drug targets. We plan to develop chimeric DNA–RNA ribozyme targeting TGF-β1 mRNA as a clinical therapy for progressive renal diseases such as glomerulonephritis and hypertensive nephrosclerosis.

References

1 Gilbert RE, Wilkinson-Berka JL, Johnson DW, Cox A, Soulis T, Wu LL, *et al.* Renal expression of transforming growth factor-beta inducible gene-h3 (beta ig-h3) in normal and diabetic rats. *Kidney Int* 1998; **54**:1052–1062.

2 Yamamoto T, Noble NA, Cohen AH, Nast CC, Hishida A, Gold LI, Border WA. Expression of transforming growth factor-β isoforms in human glomerular diseases. *Kidney Int* 1996; **49**:461–469.

3 Iwano M, Akai Y, Fujii Y, Dohi Y, Matsumura N, Dohi K. Intraglomerular expression of transforming growth factor-β1 (TGF-β 1) mRNA in patients with glomerulonephritis: quantitative analysis by competitive polymerase chain reaction. *Clin Exp Immunol* 1994; **97**:309–314.

4 Tamaki K, Okuda S, Nakayama M, Yanagida T, Fujishima M. Transforming growth factor-beta 1 in hypertensive renal injury in Dahl salt-sensitive rats. *J Am Soc Nephrol* 1996; **7**:2578–2589.

5 Tahira Y, Fukuda N, Endo M, Suzuki R, Ikeda Y, Takagi H, Kanmatsuse K. Transforming growth factor-β expression in cardiovascular organs in stroke-prone spontaneously hypertensive rats with the development of hypertension. *Hypertens Res* 2002; **25**:911–918.

6 Wolf G, Ziyadeh FN. Molecular mechanisms of diabetic renal hypertrophy. *Kidney Int* 1999; **56**:393–405.

7 Rossi JJ. Therapeutic ribozymes, principles and applications. *Bio Drugs* 1998; **9**:1–10.

8 Teng J, Fukuda N, Hu WY, Nakayama M, Kishioka H, Kanmatsuse K. DNA–RNA chimeric hammerhead ribozyme to transforming growth factor-β1 mRNA inhibits the exaggerated growth of vascular smooth muscle cells from spontaneously hypertensive rats. *Cardiovasc Res* 2000; **48**:138–147.

9 Su J, Fukuda N, Hu Y, Kanmatsuse K. Ribozyme to human TGF-β1 mRNA inhibits the proliferation of human vascular smooth muscle cells. *Biochem Biophys Res Commun* 2000; **19**:401–407.

10 Ando H, Fukuda N, Kotani M, Kunimoto S, Matsumoto K, Kanmatsuse K, Saito S. Chimeric DNA–RNA hammerhead ribozyme targeting transforming growth factor-beta 1 mRNA inhibits neointima formation in rat carotid artery after balloon injury. *Eur J Pharmacol* 2004; **483**:207–214.

11 Ono H, Ono Y. Nephrosclerosis and hypertension. *Med Clin North Am* 1997; **81**:1273–1288.

12 Brenner BM. Nephron adaptation to renal injury or ablation. *Am J Physiol* 1985; **249**:F324–F337.

13 Bohle A, Mackensen-Haen S, von Gise H. Significance of tubulointerstitial changes in the renal cortex for the excretory function and concentration ability of the kidney: a morphometric contribution. *Am J Nephrol* 1987; **7**:421–433.

14 National Institutes of Health. *Guide for the care and use of laboratory animals* Bethesda, Maryland: US National Institutes of Health; revised 1996. NIH Publication No. 85-23.

15 Matsumoto K, Hatano M. Production of interleukin 1 in glomerular cell cultures from rats with nephrotoxic serum nephritis. *Clin Exp Immunol* 1989; **75**:123–128.

16 Sporn MB, Roberts AB, Wakefield LM, de Crombrugghe B. Some recent advances in the chemistry and biology of transforming growth factor-beta. *J Cell Biol* 1987; **105**:1039–1045.

17 Chen JK, Hoshi H, McKeehan WL. Transforming growth factor type beta specifically stimulates synthesis of proteoglycan in human adult smooth muscle cells. *Proc Natl Acad Sci U S A* 1987; **84**:5287–5291.

18 Kasuga H, Ito Y, Sakamoto S, Kawachi H, Shimizu F, Yuzawa Y, Matsuo S. Effects of anti-TGF-beta type II receptor antibody on experimental glomerulonephritis. *Kidney Int* 2001; **60**:1745–1755.

19 Yamamoto T, Nakamura T, Noble NA, Ruoslahti E, Border WA. Expression of transforming growth factor beta is elevated in human and experimental diabetic nephropathy. *Proc Natl Acad Sci U S A* 1993; **90**:1814–1818.

20 Klahr S, Morrissey J. Obstructive nephropathy and renal fibrosis: the role of bone morphogenic protein-7 and hepatocyte growth factor. *Kidney Int* 2003; **64 (suppl 87)**:S105–S112.

21 Zeisberg M, Hanai J, Sugimoto H, Mammoto T, Charytan D, Strutz F, Kalluri R. BMP-7 counteracts TGF-beta1-induced epithelial-to-mesenchymal transition and reverses chronic renal injury. *Nat Med* 2003; **9**:964–968.

22 Ohkawa J, Koguma T, Kohda T, Taira K. Ribozymes: from mechanistic studies to applications in vivo. *J Biochem (Tokyo)* 1995; **118**:251–258.

23 Taylor NR, Kaplan BE, Swiderski P. Chimeric DNA–RNA hammerhead ribozymes have enhanced in vitro catalytic efficiency and increased stability in vivo. *Nucleic Acids Res* 1992; **20**:4559–4565.

24 Shimayama T, Nishikawa F, Nishikawa S, Taira K. Nuclease-resistant chimeric ribozymes containing deoxyribonucleotides and phosphorothioate linkages. *Nucleic Acid Res* 1993; **21**:2605–2611.

25 Felgner PL, Gadek TR, Holm M, Roman R, Chan HW, Wenz M, *et al.* Lipofectin: highly efficient, lipid-mediated DNA-transfection procedure. *Proc Natl Acad Sci U S A* 1987; **84**:7413–7417.

26 Gupta S, Clarkson MR, Duggan J, Brady HR. Connective tissue growth factor: potential role in glomerulosclerosis and tubulointerstitial fibrosis. *Kidney Int* 2000; **58**:1389–1399.

27 Dahly AJ, Hoagland KM, Flasch AK, Jha S, Ledbetter SR, Roman RJ. Antihypertensive effects of chronic anti-TGF-beta antibody therapy in Dahl S rats. *Am J Physiol Regul Integr Comp Physiol* 2002; **283**:R757–R767.

Available online at www.sciencedirect.com
ScienceDirect
Biochemical and Biophysical Research Communications 353 (2007) 182–188
BBRC
www.elsevier.com/locate/ybbrc

A novel approach for myocardial regeneration with educated cord blood cells cocultured with cells from brown adipose tissue

Yoshihiro Yamada [a,*], Shin-ichiro Yokoyama [b], Noboru Fukuda [b], Hiroyasu Kidoya [a], Xiao-Yong Huang [a], Hisamichi Naitoh [a], Naoyuki Satoh [a], Nobuyuki Takakura [a,*]

[a] *Department of Signal Transduction, Research Institute for Microbial Diseases, Osaka University, 3-1 Yamadaoka, Suita-shi, 565-0871, Japan*
[b] *Second Department of Internal Medicine, Nihon University School of Medicine, Ooyaguchi-kami 30-1, Itabashi-ku, Tokyo 173-8610, Japan*

Received 22 November 2006
Available online 11 December 2006

Abstract

Umbilical cord blood (CB) is a promising source for regeneration therapy in humans. Recently, it was shown that CB was a source of mesenchymal stem cells as well as hematopoietic stem cells, and further that the mesenchymal stem cells could differentiate into a number of cells types of mesenchymal lineage, such as cardiomyocytes (CMs), osteocytes, chondrocytes, and fat cells. Previously, we reported that brown adipose tissue derived cells (BATDCs) differentiated into CMs and these CMs could adapt functionally to repair regions of myocardial infarction. In this study, we examined whether CB mononuclear cells (CBMNCs) could effectively differentiate into CMs by coculturing them with BATDCs and determined which population among CBMNCs differentiated into CMs. The results show that BATDCs effectively induced CBMNCs that were non-hematopoietic stem cells (HSCs) (educated CB cells: e-CBCs) into CMs in vitro. E-CBCs reconstituted infarcted myocardium more effectively than non-educated CBMNCs or CD34-positive HSCs. Moreover, we found that e-CBCs after 3 days coculturing with BATDCs induced the most effective regeneration for impaired CMs. This suggests that e-CBCs have a high potential to differentiate into CMs and that adequate timing of transplantation supports a high efficiency for CM regeneration. This strategy might be a promising therapy for human cardiac disease.

Keywords: Stem cell; Cord blood; Adipose tissue; Myocardial regeneration; Cell fusion

Myocardial regeneration is currently a popular topic in cardiac medicine, and research in regenerative medicine has advanced in an explosive manner. Many cell types such as bone marrow mesenchymal stem cells (BM-MSCs) [1–3], embryonic stem (ES) cells [4,5], and cardiac tissue stem cells [6,7] have been found to undergo myocardial differentiation and can be used as a source for cardiomyocytes (CMs). Additional cell types may also prove to have cardiac differentiation ability. With regard to human therapy, umbilical cord blood (CB) is a promising source because transplantation of CB has already been established for patients with blood diseases. Moreover, usage of CB overcomes considerable problems encountered with other sources of CMs, such as allergenic, ethical, and tumorigenic issues. Furthermore, CB contains both hematopoietic stem cells (HSCs) [8] and MSCs [9]. Also, stem cells are more abundant in CB than in adult human peripheral blood or bone marrow (BM) and stem cells in CB have a higher proliferative potential associated with an extended life span and longer telomeres [10–12].

Indeed, $CD34^+$ cells derived from human CB homed to infarcted hearts and reduced the size of the infarcted area; this was not through direct differentiation into CMs, but through enhancing neovascularization [13,14]. These studies showed no evidence of myocytes of human origin in the infracted myocardium; however, it was reported that unrestricted somatic stem cells (USSCs) from human CB could differentiate into CMs in vitro and in vivo [15]. Such

* Corresponding authors. Fax: +81 6 6879 8314.
E-mail addresses: yamaday@biken.osaka-u.ac.jp (Y. Yamada), ntakaku@biken.osaka-u.ac.jp (N. Takakura).

0006-291X/$ - see front matter © 2006 Elsevier Inc. All rights reserved.
doi:10.1016/j.bbrc.2006.12.017

USSCs are fibroblastic in appearance and negative for hematopoietic cell markers, such as c-kit, CD34, and CD45. USSCs injected into immunosuppressed pig model of myocardial infarction (MI) improved perfusion and wall motion, reduced infarct scar size, and enhanced cardiac function. USSCs seem to be a useful source for myocardial regeneration; however, they are a rare population, therefore, expansion of USSCs is required for application to clinical therapy. In spite of these challenges for the repair of CM, to date, no clinical studies of CB have been reported. Previously, we reported that brown adipose tissue derived cells (BATDCs) included cardiac progenitor cells and they effectively differentiated into CMs in vitro and in vivo [16]. This indicated that our culture system of BATDCs contained differentiation molecular cues for CMs. When BATDCs were injected into MI rats, they differentiated into CMs as well as endothelial cells (ECs) and smooth muscle cells (SMCs), supported the growth of resident cells and vascular cells, and restored cardiac function. This suggested a potential therapeutic use for BATDCs in human ischemic heart disease. However, in humans, BAT exists only in the embryonic stage and infants, therefore, it is difficult to obtain BATDCs to treat adult cardiac disease. In this study, we examined whether mononuclear cells from CB can differentiate into CMs upon coculturing with BATDCs. Moreover, usefulness of CB cells that were exposed to BATDCs for MI repair was evaluated.

Materials and methods

Cell preparation and flow cytometry. Brown adipose tissue (BAT) was dissected from postnatal day (P1) to P7 neonates of C57BL/6 mice. BAT was dissociated by DispaseII (Roche, Mannheim, Germany), drawn through a 23G needle and prepared as single cell suspension as previously reported [16]. Human CB mononuclear cells (CBMNCs) were purchased from Cambrex (Baltimore, MD). The cell-staining procedure for the flow cytometry was also as previously described [17]. The monoclonal antibodies (mAbs) used in immunofluorescence staining were anti-human CD45, -34, and -HLA–ABC mAbs (Pharmingen, SanDiego, CA). All mAbs were purified and conjugated with fluorescein isothiocyanate (FITC), PE (phycoerythrin), biotin or allophycocyanin (APC). Biotinylated antibodies were visualized with PE-conjugated streptavidin (Pharmingen) or APC-conjugated streptavidin (Pharmingen). Cells were incubated for 5 min on ice with CD16/32 (FcγIII/II Receptor) (1:100) (Fcblock™, Pharmingen) prior to staining with primary antibody. Cells were incubated in 5% fetal calf serum/phosphate-buffered saline (FCS/PBS; washing buffer) with primary antibody for 30 min on ice, and washed twice with washing buffer. Secondary antibody was added and the cells were incubated for 30 min on ice. After incubation, cells were washed twice with, and suspended in, the washing buffer for fluorescence-activated cell sorter (FACS) analysis. The stained cells were analyzed and sorted by EPICS Flowcytometer (BECKMAN COULTER, San Jose, CA). The sorted cells were added to 24-well dishes (Nunc, Roskilde, Denmark), precoated with 0.1% gelatin (Sigma, St. Louis, USA), and cultured in Dulbecco's modified Eagle's medium (DMEM; Sigma), supplemented with 10% FCS and 10^{-5}M 2-mercaptoethanol (2-ME), at 37 °C in a 5% CO_2 incubator.

Cell coculture. BATDCs were prepared as described above. When BATDCs and human (h) CBMNCs were cocultured in contact conditions, 1×10^5 BATDCs were plated per well of a 24-well plate and cultured for 7 days, and then, 1×10^5 CBMNCs, or 1×10^4 $CD34^+$ HSCs were cultured with BATDCs for 10 days. Staining was performed with anti-cardiac troponinT (Santa Cruz), -MEF-2C (Cell signaling) and -HLA ABC antibodies (Pharmingen).

Supplemental information reveals the Materials and methods for RT-PCR analysis, Immunohistochemistry, FISH staining, and procedure for mouse myocardial infarction (MI) model and echocardiography.

Results

Differentiaion of CBMNCs into CMs by coculturing with BATDCs in vitro

Previously, we reported that BATDCs differentiate into CMs spontaneously; this suggests that BATDCs produce molecules that induce self differentiation into CMs by an autocrine loop. Moreover, CBMNCs contained cells with a potential to differentiate into various cell types, such as osteoblasts, chondrocytes, and CMs. Therefore, to determine whether molecules produced from BATDCs induce CBMNCs to differentiate into CMs effectively, we cultured CBMNCs with BATDCs and observed the differentiation of CBMNCs into CMs. At first, dissociated BATDCs from P1 to P7 neonatal mice were cultured on 0.1% gelatin-coated dishes. After 1 week, human CBMNCs were added and cocultured with BATDCs. After coculturing CBMNCs with BATDCs for 14 days, among HLA-positive CBMNCs, nuclear located MEF2C positive and cardiac troponinT-positive cells (Fig. 1A and B), or cardiac troponinI-positive cells (Fig. 1C) were effectively produced. In contrast, sorted $CD34^+38^-$HSC population from CBMNCs, which was previously reported to differentiate into CMs [18], was differentiated into cardiac troponinT-positive CMs (Fig. 1E); however, the frequency of CM differentiation from HSC population was lower than that from total CBMNCs (Fig. 1I). CBMNCs alone did not differentiate into cardiac troponinT-positive or MEF2C-positive cells spontaneously under the same culture medium without coculturing with BATDCs (Fig. 1G, H, and I).

The expression of CM-specific genes in CBMNCs educated by culturing with BATDCs

Next, we evaluated the length of time required for CBMNCs to become committed CM lineage cells when cocultured with BATDCs. For this purpose, we attempted to coculture CBMNCs with BATDCs for 1 to 7 days and $HLA^+CD45^-CD34^-$ non-hematopoietic cells [we termed them educated CB cells (e-CBCs)] were then sorted and mRNA was extracted from the cells as indicated in Fig. 2A. Because mature hematopoietic cells from cocultured CBMNCs did not differentiate into CMs (data not shown) and HSC population barely differentiated into CMs (Fig. 1), we deduced that cardiac stem/progenitor cells were more abundant in non-hematopoietic cells and were therefore $CD45^-CD34^-$. We analyzed the expression of CM-specific genes on days 0, 3, and 7 as indicated in Fig. 2B and confirmed that cardiac actin, myosin light chain 2v, and specific transcriptional factor, such as

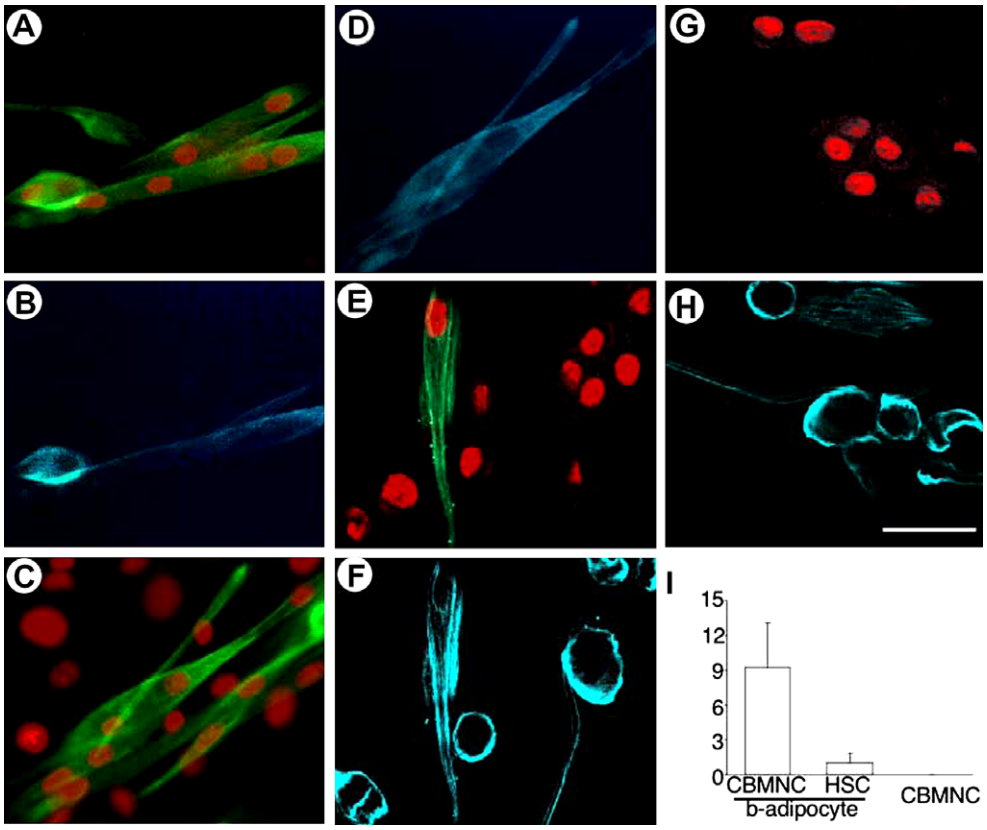

Fig. 1. CBMNCs can differentiate into CMs upon coculturing with BATDCs. Immunocytochemical analysis of human CBMNCs (A–D), and $CD34^{+}CD38^{-}$HSCs (E, F) cocultured with BATDCs from wild type mice, or CBMNCs (G, H) cultured without BATDCs for 14 days. (A) Expression of cardiac troponinT (green) and MEF2C (red). (B) Human HLA expression (blue) in the same field as (A). (C, E, and G) Expression of cardiac troponinI (green) and nuclear staining with PI (red). (D, F, and H) Human HLA expression (blue) in the same fields as (C, E, and G), respectively. Scale bar in (H) indicates 5 μm. (I) Quantitative evaluation of differentiated cardiac troponinT and MEF2C-positive CMs among adhering HLA-positive CB-derived cells. Data for CBMNC, and $CD34^{+}CD38^{-}$HSCs cocultured with BATDCs (b-adipocyte) and CBMNCs cultured without BATDCs are displayed. Results represent means ± SD of five independent experiments.

GATA-4 and Nkx2.5 were expressed on day 3 of coculture (Fig. 2B). MHC alpha and beta mRNAs were not expressed on day 3; however, they started to be expressed around day 7.

Educated CBMNCs in non-hematopoietic lineage contributed to myocardial regeneration

As indicated in Fig. 2, 3 days of coculturing with BATDCs was enough for commitment of CBMNCs into CM lineage. Next, in order to determine whether e-CBCs could effectively contribute to the regeneration of the heart, we injected the e-CBCs into the hearts of nude rats after the induction of an acute MI as indicated in Fig. 3A. At first, we cocultured CBMNCs with BATDCs for 3 days, purified $HLA^{+}CD45^{-}CD34^{-}$ cells (e-CBCs) by FACS and injected the cells into the hearts of experimental MI nude rats at each of five sites at the border of the infarcted tissue. As a control, infarcted hearts were injected with either equal volumes and numbers of CBMNCs that were not exposed to BATDCs (non-e-CBCs), or $CD34^{+}38^{-}$HSCs directly sorted from freshly isolated CBMNCs. Upon injection of e-CBCs, donor-derived human HLA- and SA-positive cells were detected abundantly in the infarct border zone (Fig. 3B, a, b, and c; 23.4 ± 3.1% of total cardiomyocytes in one field), but the contribution to CMs by the injection with non-e-CBCs and $CD34^{+}38^{-}$HSCs in the MI was 20- (Fig. 3B, d, e, and f; 1.1 ± 0.3%) and 15-fold (Fig. 3B, g, h, and i; 1.5 ± 0.3%), respectively, less than that of e-CBCs. e-CBC-derived SA-positive CMs also expressed connexin 43 (Fig. 3Bc), indicating that transplanted e-CBC-derived CMs formed gap junctions with host CMs. Moreover, the assessment of cardiac function by echocardiography revealed that the hearts injected with e-CBCs showed improved contractions of movement of the infarcted anterior walls and reduced left ventricular remodeling compared with the hearts injected with non-e-CBCs or $CD34^{+}38^{-}$HSCs (Fig. 4).

To clarify the origin of CMs in recipient tissue, donor-derived human chromosomes and host-derived rat chromosomes were simultaneously detected by using species-specific chromosome probes using fluorescent in situ hybridization (FISH) analysis. In this analysis, we used centromere probes, because 5 μm thick slices may not always include sex chromosomes in the nuclei as previously described [18]. Result showed that

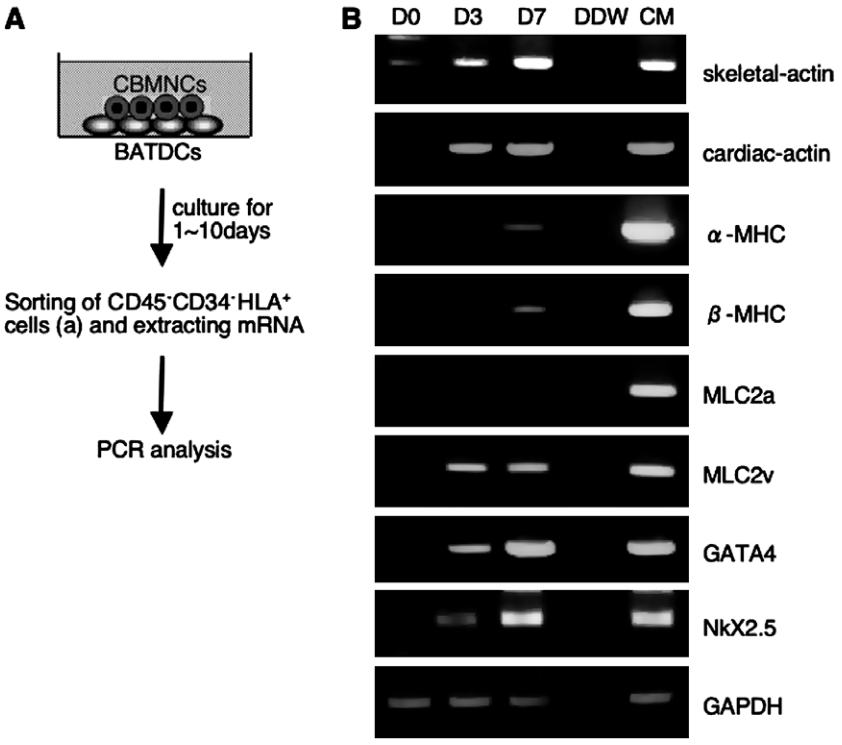

Fig. 2. Expression of CM-specific genes in e-CBCs. (A) Design of experiment for the isolation of human e-CBCs. CBMNCs were cocultured with BATDCs for 1 to 10 days, and then $CD45^{-}CD34^{-}$ human HLA^{+} cells were sorted and total RNA was extracted. (B) PCR analysis was performed with CM-specific primers in e-CBCs after coculturing with BATDCs for 0 day (D0; freshly isolated CBCs without exposure to BATDCs), 3 days (D3) and 7 days (D7). Distilled water (DDW) and CMs from embryos (CM) were used as a negative and a positive control, respectively. GAPDH was used as an internal control.

implanted e-CBCs of human origin transferred into female nude rats formed CMs that stained only with probes specific for human chromosomes (Fig. 3C, a and b). We also checked the serial confocal imaging to exclude the possibility that they arose from cell overlay as previously reported [18], but could not observe any superimposed cells (data not shown). This indicated that in vivo cardiac differentiation of e-CBCs was not induced by the fusion mechanism. In contrast, when $CD34^{+}CD38^{-}$HSCs were implanted into MI induced nude rats, human HLA-positive CMs were stained with both human and rat chromosome probes (data not shown). This indicated that generation of CM-derived HSCs was due to the fusion mechanism between donor-derived cells and host CMs as previously reported [18,19].

Discussion

So far, various kinds of sources for CMs, such as adult BM HSCs [19,20], MSCs [1–3], and ES cells [4,5] have been reported; however, there is some controversy regarding the efficiency of cardiomyoplasty. In terms of the myocardial regeneration therapy for human, human CB cells seem to be a safe and useful source compared to other sources, because these cells have already been utilized in CB transplantation for managing patients with blood disease. However, no clinical trials using CB cells to treat heart disease have been reported.

In this study, we raised two important points. The first is that e-CBCs of non-hematopoietic origin were more effectively differentiated into CMs compared with $CD34^{+}CD38^{-}$HSCs in vitro. Moreover, we showed that e-CBCs differentiation into CMs was not through the cell fusion mechanism. On the other hand, CMs derived from $CD34^{+}CD38^{-}$HSCs were generated through cell fusion with host CMs in vivo. Previously, it was reported that MSCs but not HSCs from BM could migrate into the heart and differentiate into CMs in mouse MI model [21]. This suggested that MSCs were the predominant source for myocardial regeneration. Our report is the first to show that non-hematopoietic cells can be used as CM source and how these compare with HSCs in human cord blood cells.

The second is the new strategy for myocardial regeneration using CB cells and BATDCs. Using the coculturing method described here, CB cells were effectively induced to differentiate into CMs in vitro. Moreover, e-CBCs were effectively differentiated into CMs in immunodeficient rat MI model and improved the cardiac function. Furthermore, we found that an adequate duration of coculturing of CB cells with BATDCs was critical for CM regeneration. In the present method, three days of coculturing was the most effective to produce CMs from e-CBCs and improve the CM function and this timing was consistent

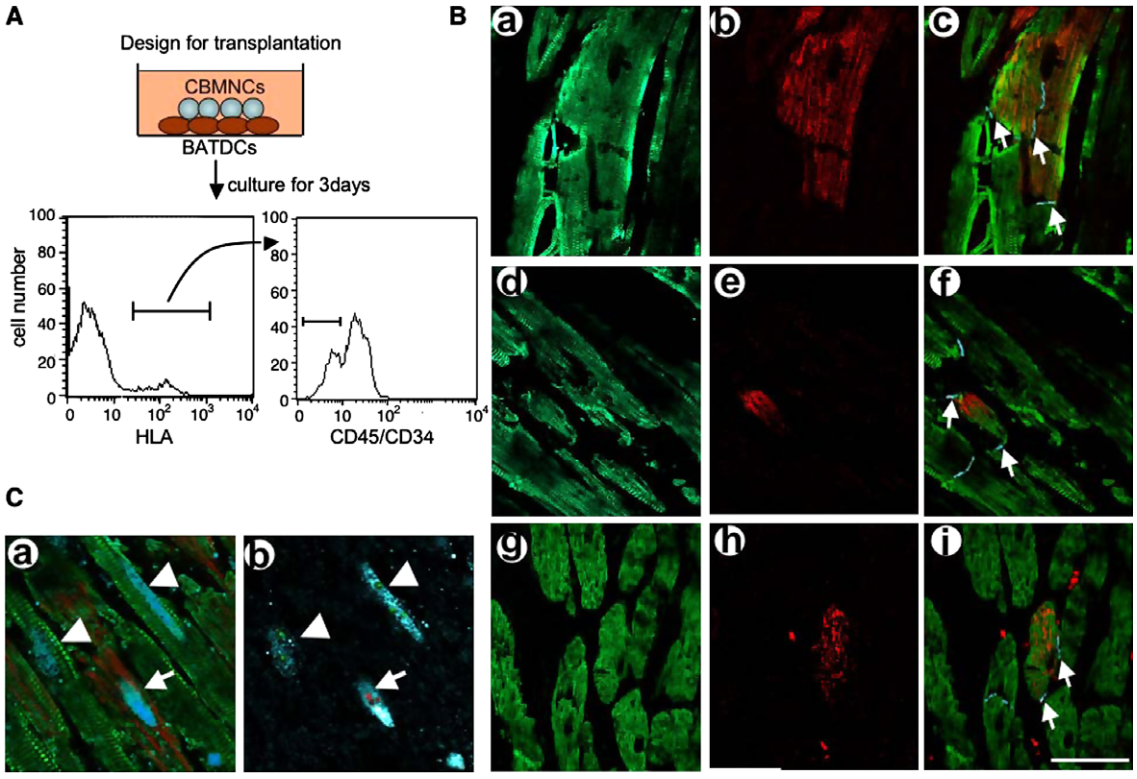

Fig. 3. CBMNCs cocultured with BATDCs contributed to cardiac regeneration. (A) Strategy for transplantation. After human CBMNCs were cocultured for 3 days with BATDCs from mice, human $HLA^{+}CD45^{-}CD34^{-}$ cells (e-CBCs) were sorted by FACS and injected into the border zone of ischemia induced nude rats. As a control, CBMNCs that were not cocltured (non-e-CBCs) and freshly isolated $CD34^{+}CD38^{-}$HSCs were used. (B) CM development from injected e-CBCs (a–c), non-e-CBCs (d–f), and $CD34^{+}CD38^{-}$HSCs in MI induced heart. (a, d, and g) Expression of SA (green). (b, e, and h) human HLA (red). (c, f, and i) are merged image of (a and b), (d and e), and (g and h), respectively, and stained with anti-connexin 43 antibody (blue). Arrows in (c, f, and i) indicate the regions in which human CB-derived connexin positive CMs make tight junction with resident host CMs. Scale bar in (i) indicates 20 μm. (C) (a) Expression of human HLA (red) and SA (green) in the site of implantation of e-CBCs in MI induced heart. Nuclei were counter stained with TOPRO3 (blue). (b) FISH staining in a serial section of (a). Green colors indicate rat chromosome, and red color indicates human chromosome. Nuclear staining was performed with TOPRO3 (blue). Cells expressing human chromosome (red) in the nuclei indicate that these cells were derived from e-CBCs and did not fuse with host CM expressing only rat chromosome (green). Arrowheads indicate nuclei from host CMs and arrow indicates human nuclei in e-CBCs (a, b). Scale bar indicates 5 μm.

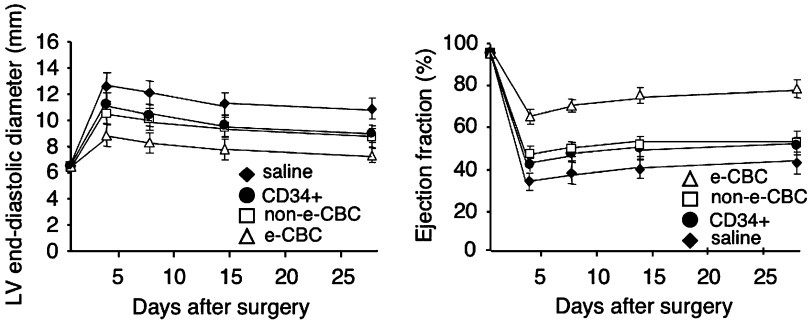

Fig. 4. e-CBCs transplantation improved cardiac function. LV diameter (LV end-diastolic diameter) and function (Ejection fraction) were assessed by echocardiography at 0, 3, 7, 14, and 28 days following myocardial infarction and injection of saline, e-CBCs, non-e-CBCs, and HSCs (CD34+). Note that in case of injection of e-CBCs, enlargement of LV diameter was reduced and LV function was significantly improved compared with injection of saline, non-e-CBCs, and HSCs. Each data point is the mean of five determinations; bars denote ±SD.

with the expression of Nkx2.5 and GATA-4 on CBMNCs (Fig. 2). In order to determine how e-CBCs differentiated into CMs, we tested a number of growth and survival factors and found that Akt activation seemed to play a role in the differentiation of CBMNCs into CMs (Supplemental data 1). Akt, a serine threonine kinase, transduces powerful survival signals in many systems [22,23]. Recently, it was reported that overexpression of Akt1 in MSCs increased the post-transplantation viability of these cells and enhanced their therapeutic efficiency [24]. In fact, intramyocardial injection of MSCs that had been transfected with a retroviral vector containing the Akt gene resulted in the

differentiation of MSCs into CMs and led to the prevention of ventricular remodeling and to the restoration of cardiac function after MI. In order to examine the survival signals in e-CBCs in each culture day as indicated, we checked the phosphorylation level of Akt (p-Akt) in e-CBCs on days 0, 3, and 7. Before extraction of cell lysate, e-CBCs were exposed to hypoxic condition for 24 h. The p-Akt level of e-CBCs on day 3 was 10-fold higher than that on day 7 and it was higher (1.7×) than that on day 0 before coculturing with BATDCs (Supplement data 1). The resistance of cell to apoptosis induced by hypoxic stimuli was proportional to the level of p-Akt in e-CBCs, i.e., it was higher on day 3 compared to day 0 and day 7. This anti-apoptotic effect might contribute to the high incidence of CMs derived from e-CBCs and to prevention of cardiac remodeling caused by conditions such as hypoxia, inflammation, and mechanical stress, and many endogenous factors such as angiotensin II, endothelin-1, and norepinephrine [25] in MI model.

We have as yet not clarified the precise mechanism whereby CB cells expressed high levels of p-Akt in hypoxic conditions after short-term coculturing with BATDCs. BATDCs were derived from adipose tissue, which possessed many beneficial factors, such as vascular endothelial growth factor (VEGF), hepatocyte growth factor (HGF), angiopoietin-1, and so on [16]. Therefore, these factors might support the high level of p-Akt in e-CBCs. Identification of such factors may enable effective myocardial regeneration. Use of CBCs together with such factors for protection against cell apoptosis may enable the application of the strategy described here to the clinic for managing patients of ischemic disease.

Acknowledgments

We thank Miss M. Sato for technical support. This study was supported in part by a grant from the Ministry of Education, Culture, Sports, Science, and Technology of Japan.

Appendix A. Supplementary data

Supplementary data associated with this article can be found, in the online version, at doi:10.1016/j.bbrc.2006.12.017.

References

[1] S. Makino, K. Fukuda, S. Miyoshi, F. Konishi, H. Kodama, J. Pan, M. Sano, T. Takahashi, S. Hori, H. Abe, J. Hata, A. Umezawa, S. Ogawa, Cardiomyocytes can be generated from marrow stromal cells in vitro, J. Clin. Invest. 103 (1999) 697–705.

[2] C. Toma, M.F. Pittenger, K.S. Cahill, B.J. Byrne, P.D. Kesseler, Human mesencymal stem cells differentiate to a cardiomyocyte phenotype in adult murine heart, Circulation 105 (2002) 93–98.

[3] S. Tomita, R.K. Li, R.D. Weise, D.A. Mickle, E.J. Kim, T. Sakai, Z.Q. Jia, Autologous transplantation of bone marrow cells improves damaged heart function, Circulation 100 (1999) 247–256.

[4] I. Kehat, D. Kenyagin-Karsenti, M. Snir, M. Segev, M. Amit, A. Gepstein, E. Livne, O. Binah, J. Itskovitz-Eldor, L. Gepstein, Human embryonic stem cells can differentiate into myocytes with structural and functional properties of cardiomyocytes, J. Clin. Invest. 108 (2001) 407–414.

[5] I. Kehat, A. Gepstein, A. Spira, J. Itskovitz-Eldor, L. Gepstein, High-resolution electrophysiological assessment of human embryonic stem cell-derived cardiomyocytes: a novel in vitro model for the study of conduction, Circ. Res. 91 (2002) 659–661.

[6] A.P. Beltrami, L. Barlucchi, D. Torella, M. Baker, F. Limana, S. Chimenti, H. Kasahara, M. Rota, E. Musso, K. Urbanek, A. Leri, J. Kajstura, B. Nadal-Ginard, P. Anversa, Adult cardiac stem cells are multipotent and support myocardial regeneration, Cell 114 (2003) 763–776.

[7] H. Oh, S.B. Bradfute, T.D. Gallardo, T. Nakamura, V. Gaussin, Y. Mishina, J. Pocius, L.H. Michael, R.R. Behringer, D.J. Garry, M.L. Entman, M.D. Schneider, Cardiac progenitor cells from adult myocardium: homing, differentiation, and fusion after infarction, Proc. Natl. Acad. Sci. USA 100 (2003) 12313–12318.

[8] H. Mayani, P.M. Lansdorp, Biology of human umbilical cord blood derived hematopoietic stem/progenitor cells, Stem Cells 16 (1998) 153–165.

[9] A. Erices, P. Congnet, J.J. Minguell, Mesenchymal progenitor cells in human umbilical cord blood, Br. J. Haemotol. 109 (2000) 235–242.

[10] S.J. Szilvassy, T.E. Meyerrose, P.L. Ragland, B. Grimes, Differentioal homing and engraftment properties of hematopoietic progenitor cells from murine bone marrow, mobilized peripheral blood, and fetal liver, Blood 98 (2001) 2108–2115.

[11] H. Vaziri, W. Dragowska, R.C. Allsopp, T.E. Thomas, C.B. Harley, P.M. Lansdorp, Evidence for a mitotic clock in human hematopoietic stem cells: loss of telomeric DNA with age, Proc. Natl. Acad. Sci. USA 91 (1994) 9857–9860.

[12] E.D. Zanjani, J.L. Ascensao, M. Tavassoli, Liver derived feta hematopoietic stem cells selectively and preferentially home to the fetal bone marrow, Blood 81 (1993) 399–404.

[13] N. Ma, Y. Ladilov, J.M. Moebius, L. Ong, C. Piechaczek, A. David, A. Kaminski, Y.H. Choi, W. Li, D. Egger, C. Stamm, G. Steinhoff, Intramyocardial delivery of human CD133+ cells in a SCID mouse cryoinjury model: bone marrow vs. cord blood-derived cells, Cardiovasc. Res. 71 (2006) 158–169.

[14] Y. Hirata, M. Sata, N. Motomura, M. Takanashi, Y. Suematsu, M. Ono, S. Takamoto, Human umbilical cord blood cells improve cardiac function after myocardial infarction, Biochem. Biophys. Res. Commun. 327 (2005) 609–614.

[15] G. Kogler, S. Sensken, J.A. Airey, T. Trapp, M. Muschen, N. Feldhahn, S. Liedtke, R.V. Sorg, J. Fischer, C. Rosenbaum, S. Greschat, A. Knipper, J. Bender, O. Degistirici, J. Gao, A.I. Caplan, E.J. Colletti, G. Almeida-Porada, H.W. Muller, E. Zanjani, P. Wernet, A new human somatic stem cell from placental cord blood with intrinsic pluripotent differentiation potential, J. Exp. Med. 200 (2004) 123–135.

[16] Y. Yamada, X.D. Wang, S.-I. Yokoyama, N. Fukuda, N. Takakura, Cardiac Progenitor cells in brown adipose tissue repaired damaged myocardium, Biochem. Biophys. Res.Commun. 343 (2006) 662–670.

[17] Y. Yamada, N. Takakura, H. Yasue, H. Ogawa, H. Fujisawa, T. Suda, Exogenous clustered neuropilin 1 enhances vasculogenesis and angiogenesis, Blood 97 (2001) 1671–1678.

[18] F. Ishikawa, H. Shimazu, L.D. Shultz, M. Fukata, R. Nakamura, B. Lyons, K. Shimoda, S. Shimoda, T. Kanemaru, K. Nakamura, H. Ito, Y. Kaji, A.C. Perry, M. Harada, Purified human hematopoietic stem cells contribute to the generation of cardiomyocytes through cell fusion, FASEB J. 20 (2006) 950–952.

[19] M. Alvarez-Dolado, R. Pardal, J.M. Garcia-Verdugo, J.R. Fike, H.O. Lee, K. Pfeffer, C. Lois, S.J. Morrison, A. Alvarez-Buylla, Fusion of bone-marrow-derived cells with Purkinje neurons, cardiomyocytes and hepatocytes, Nature 425 (2003) 968–973.

[20] D. Orlic, J. Kajstura, S. Chimenti, I. Jakoniuk, S.M. Anderson, B. Li, J. Pickel, R. Mckay, B. Nadal-Ginard, D.M. Bodine, A. Leri, P.

Anversa, Bone marrow cells regenerate infarcted myocardium, Nature 410 (2001) 701–705.
[21] H. Kawada, J. Fujita, K. Kinjo, Y. Matsuzaki, M. Tsuma, H. Miyatake, Y. Muguruma, K. Tsuboi, Y. Itabashi, Y. Ikeda, S. Ogawa, H. Okano, T. Hotta, K. Ando, K. Fukuda, Nonhematopoietic mesenchymal stem cells can be mobilized and differentiate into cardiomyocytes after myocardial infarction, Blood 104 (2004) 3581–3587.
[22] T.F. Franke, D.R. Kaplan, L.C. Cantley, PI3K: downstream AKTion blocks apoptosis, Cell 88 (1997) 435–437.
[23] S.R. Datta, A. Brunet, M.E. Greenberg, Cellular survival: a play in three Akts, Genes Dev. 13 (1999) 2905–2927.
[24] A.A. Mangi, N. Noiseux, D. Kong, H. He, M. Rezvani, J.S. Ingwall, V.J. Dzau, Mesenchymal stem cells modified with Akt prevent remodeling and restore performance of infarcted hearts, Nat. Med. 9 (2003) 1195–1201.
[25] H. Takano, Y. Qin, H. Hasegawa, K. Ueda, Y. Niitsuma, M. Ohtsuka, I. Komuro, Effects of G-CSF on left ventricular remodeling and heart failure after acute myocardial infarction, J. Mol. Med. 84 (2006) 185–193.

Available online at www.sciencedirect.com
ScienceDirect
European Journal of Pharmacology 549 (2006) 98–106
www.elsevier.com/locate/ejphar

Effects of G-CSF on cardiac remodeling and arterial hyperplasia in rats

Yuxin Li [a], Noboru Fukuda [a,b,*], Shin-Ichiro Yokoyama [a], Yoshiaki Kusumi [c], Kazuhiro Hagikura [a], Taro Kawano [a], Tadateru Takayama [a], Taro Matsumoto [d], Aya Satomi [d], Junko Honye [a], Hideo Mugishima [d], Masako Mitsumata [c], Satoshi Saito [a,d]

[a] *Department of Internal Medicine, Nihon University School of Medicine, Tokyo 173-8610, Japan*
[b] *Advanced Research Institute for the Sciences and Humanities, Nihon University, Tokyo 102-8275, Japan*
[c] *Department of Pathology, Nihon University School of Medicine, Tokyo 173-8610, Japan*
[d] *Department of Advanced Medicine, Nihon University School of Medicine, Tokyo 173-8610, Japan*

Received 16 March 2006; received in revised form 26 July 2006; accepted 2 August 2006
Available online 15 August 2006

Abstract

Although granulocyte colony-stimulating factor (G-CSF) has been shown to prevent cardiac remodeling after acute myocardial infarction, the mechanism and safety of G-CSF treatment acute myocardial infarction remain controversial. The purpose of the present study was to investigate in a rat model the mechanisms underlying the beneficial effect of G-CSF in acute myocardial infarction and to determine whether G-CSF treatment aggravates vascular remodeling of injured artery after acute myocardial infarction. Sprague–Dawley rats received transplanted bone marrow cells from green fluorescent protein (GFP) transgenic rats. Acute myocardial infarction was induced by ligation of the left coronary artery. After 24 h, the right carotid artery was injured with a balloon catheter. G-CSF (100 μg/kg/day) or saline was injected subcutaneously for 5 consecutive days after induction of acute myocardial infarction. G-CSF treatment significantly improved left ventricle function and reduced infarct size in rats with acute myocardial infarction. Expression of mRNA for the angiogenic cytokines was significantly higher in the infarction border area in the G-CSF group than in the control group. The surviving cardiomyocytes in infarction area were more in the G-CSF group. GFP-positive cells were gathered in the infarction border area in both groups; G-CSF did not increase cardiac homing of GFP-positive bone marrow cells in contrast to control group. Most GFP-positive cells were CD68-positive (macrophages). It was difficult to find bone marrow-derived cardiomyocytes in the infarcted area. G-CSF treatment inhibited neointima formation and increased reendothelialization of the injured artery. GFP-positive cells were identified most in the adventitia of the injured artery. A few cells in the neointima and reendothelialization were GFP positive. In conclusion, administration of G-CSF appears to be effective for treatment of left ventricular remodeling after acute myocardial infarction and does not aggravate vascular remodeling. The effect of G-CSF on cardiac and vascular remodeling may occur mainly through a direct action on the heart and arteries.

Keywords: Cytokine; Coronary disease; Infarction; Stem cell; Restenosis

1. Introduction

Myocardial infarction is a common cause of cardiac morbidity and mortality, and left ventricular remodeling after myocardial infarction is critical for progression to heart failure. Several cytokines, including granulocyte colony-stimulating factor (G-CSF), erythropoietin, and leukemia inhibitory factor, have been reported to reduce cardiac remodeling after myocardial infarction (Moon et al., 2003; Orlic et al., 2001; Zou et al., 2003). G-CSF improves cardiac function and reduces mortality after myocardial infarction in animal model (Adachi et al., 2004; Kawada et al., 2004; Minatoguchi et al., 2004; Ohtsuka et al., 2004; Orlic et al., 2001). G-CSF has various effects, for example, on proliferation, survival, and differentiation of hematopoietic cells and on mobilization of bone marrow cells (Avalos, 1996; Berliner et al., 1995). Mobilization of bone marrow cells, including stem and progenitor cells, to the myocardium and transdifferentiation of these cells into heart cells has been considered a main mechanism to improve cardiac remodeling after myocardial infarction (Adachi et al., 2004; Kawada et al., 2004; Minatoguchi et al., 2004; Orlic

* Corresponding author. Department of Internal Medicine, Nihon University School of Medicine, 30-1 Oyaguchi-Kamimachi, Itabashi-ku, Tokyo 173-8610, Japan. Tel.: +81 3 3972 8111; fax: +81 3 3972 8666.
E-mail address: fukudan@med.nihon-u.ac.jp (N. Fukuda).

0014-2999/$ - see front matter © 2006 Elsevier B.V. All rights reserved.
doi:10.1016/j.ejphar.2006.08.006

Table 1
RT-PCR primers used in the study

Primer name	Nucleotide sequence	PCR product length (bp)
VEGF	Sense: 5′-ACTGGACCCTGGCTTTACTG-3′ Antisense: 5′-ACGCACTCCAGGGCTTCATC-3′	256
Flt-1	Sense: 5′-AGGAGAGGACCTGAAACTGTCTT-3′ Antisense: 5′-ATTCCTGGGCTCTGCAGGCATAG-3′	214
Angiopoietin-1	Sense: 5′-GTGGCTGGAAAAACTTGAGA-3′ Antisense: 5′-TGGATTTCAAGACGGGATGT-3′	201
Angiopoietin-2	Sense: 5′-GACCAGTGGGCATCGCTACG-3′ Antisense: 5′-CTGGTTGGCTGATGCTACTG-3′	170
Tie-1	Sense: 5′-TGCGAGCCCAGTCCAAGAGA-3′ Antisense: 5′-ACAGGGTAACTCAAAGGCTC-3′	270
Tie-2	Sense: 5′-TGCCACCATCACTCAATACC-3′ Antisense: 5′-AAACGCCAATAGCACGGTGA-3′	217
Basic-FGF	Sense: 5′-AAGCGGCTCTACTGCAAG-3′ Antisense: 5′-AGCCAGACATTGGAAGAAACA-3′	372
TGFβ	Sense: 5′-ACCCTTCCAGGTGAGGTCT-3′ Antisense: 5′-CCACCTCTACATCGAACCT-3′	161

VEGF, vascular endothelial growth factor; basic-FGF, basic fibroblast growth factor; TGFβ, transforming growth factor β.

et al., 2001). However, recent studies (Harada et al., 2005; Ohtsuka et al., 2004) have shown that G-CSF acts directly on cardiomyocytes to reduce apoptotic cell death and protect the infarcted heart via activation of the Stat3 pathway. Thus, G-CSF may inhibit cardiac remodeling by several mechanisms.

However, administration of G-CSF may have negative effects in patients with acute myocardial infarction. G-CSF induced mobilization of progenitors from bone marrow may lead to transdifferentiation into vascular smooth muscle cells, which may aggravate restenosis (Shoji et al., 2004; Simper et al., 2002). Thus, G-CSF may worsen plaque formation and restenosis in coronary arteries. The administration of G-CSF to patients with acute myocardial infarction undergoing percutaneous coronary intervention remains controversial (Hill et al., 2005; Kang et al., 2004; Petzsch et al., 2004; Ripa et al., 2004; Valgimigli et al., 2005).

The purpose of the present study was to investigate in a rat model the mechanisms underlying the beneficial effect of G-CSF in acute myocardial infarction and to determine whether G-CSF treatment aggravates vascular remodeling of injured artery after myocardial infarction.

2. Materials and methods

All animal care and handling were performed in accordance with the guidelines specified by the National Institutes of Health Guide for the Care and Use of Laboratory Animals and were approved by Institutional Animal Care and Use Committee.

2.1. Rat myocardial infarction model and G-CSF administration

Eight-week-old male Sprague–Dawley (SD) rats were used in this study. Myocardial infarction was induced by permanent ligation of the left coronary artery with 6–0 polypropylene suture as described previously (Adachi et al., 2004; Orlic et al., 2001). Rats were randomly assigned to one of two groups: 100 μg/kg/day G-CSF (Kirin-Amgen Inc., G-CSF group) or the same volume of normal saline (control group) was injected subcutaneously immediately after induction of myocardial infarction and was continued daily for additional consecutive 4 days.

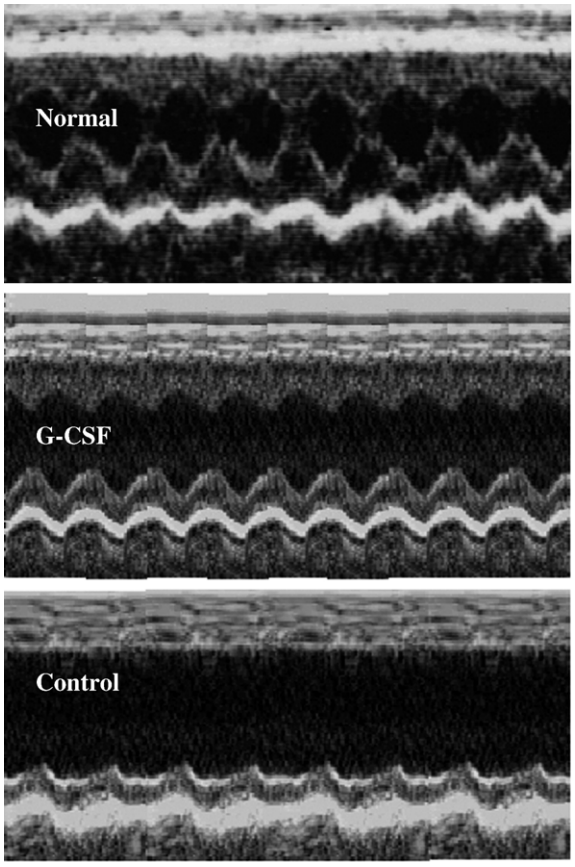

Fig. 1. Representative M-mode echocardiograms in normal rats (Normal, left ventricular ejection fraction: 93%, left ventricular internal diameter at end-diastole: 5.52 mm) and in rats with myocardial infarction (MI) with G-CSF (left ventricular ejection fraction: 60%, left ventricular internal diameter at end-diastole: 8.80 mm) or without G-CSF (Control, left ventricular ejection fraction: 33%, left ventricular internal diameter at end-diastole: 11.02 mm) treatment. Two-dimensional images and M-mode tracing were recorded from the parasternal short axis view 28 days after induction of MI.

Table 2
Echocardiographic analyses before and after 28 days of MI

	Control			G-CSF			P
	Pre-MI	Post-MI	Change	Pre-MI	Post-MI	Change	
N	10	10		10	10		
Left ventricular internal diameter at end-diastole (mm)	5.83±0.08	10.50±0.66	4.67±0.64	5.53±0.24	9.43±0.42	3.90±0.54	0.140
Left ventricular internal diameter at end-systole (mm)	1.90±0.13	8.93±0.53	7.03±0.41	1.93±0.22	7.15±0.66	5.23±0.76	0.039
Left ventricular ejection fraction (%)	95.6±0.9	35.9±1.5	59.7±1.5	94.6±1.0	53.8±5.9	40.8±6.3	0.004
Fractional shortening (%)	66.8±2.4	15.2±0.7	51.7±2.4	64.4±2.9	24.6±3.5	39.9±5.2	0.032

Data are expressed as mean±S.E.M.

2.2. Rat carotid artery balloon injury model

Balloon injury was performed 24 h after induction of acute myocardial infarction. The right common carotid artery was exposed at the level of bifurcation through a midline neck incision, as described previously (Griese et al., 2003; Qian et al., 2002). A 2F Fogarty arterial embolectomy catheter (Baxter Healthcare Corp.) was inserted through the external carotid artery, inflated with 0.2 ml air, and pulled five times along the common carotid artery (area injured by the catheter ~3 cm in length).

2.3. Transplantation of bone marrow cells from green fluorescent protein transgenic rats to SD rats

To evaluate the distribution of bone marrow cells in the heart after myocardial infarction and in the injured carotid artery, bone marrow cells from green fluorescent protein (GFP) transgenic rats (SD TgN [act-EGFP] OsbCZ-004, Japan SLC, Inc.) were transplanted into four-week-old male SD rats. Recipient rats were irradiated with a lethal dose (1300 rad) of X-rays and were injected with 1.3×10^8 GFP bone marrow cells from tail vein. One month after transplantation, 300 μl bloods was collected from the tail vein and subjected to fluorescence-activated cell sorting (FACS) analysis to determine the bone marrow replacement rate. A greater than 90% bone marrow chimerism rate was considered successful replacement. After transplantation success, acute myocardial infarction and carotid artery balloon injury model were performed.

2.4. Echocardiography

Transthoracic echocardiography (ProSound SSD-5500SV, Aloka Co., Ltd) was performed with a 10 MHz imaging transducer. Before and 28 days after induction of myocardial infarction, two-dimensional images and M-mode tracing were recorded from the parasternal short axis view. Left ventricular internal diameter at end-diastole, left ventricular internal diameter at end-systole, left ventricular ejection fraction, and fractional shortening were evaluated by two investigators blinded to the groups.

2.5. Peripheral blood cell count

In separate experiments, three rats were injected subcutaneously with 100 μg/kg/day G-CSF for 5 consecutive days. Before and 1, 2, 3, 4, 6, 7, 8, 10, and 15 days after G-CSF administration, 200 μl peripheral blood was harvested from the tail vein for blood cell counting.

2.6. Angiogenic cytokine levels in peripheral blood

One, 3, 7, 14, and 28 days after induction of myocardial infarction, rats were killed and peripheral blood (10 ml) was collected to measure plasma levels of vascular endothelial growth factor (VEGF), basic fibroblast growth factor (basic-FGF), hepatocyte growth factor (HGF), and interleukin-8 by enzyme-linked immunosorbent assay (ELISA).

2.7. Expression of angiogenic cytokines in the myocardial infarction border area

One, 3, 7, 14, and 28 days after induction of myocardial infarction, rats were killed, coronary blood was washed out with saline, the infarction border area of the heart (100 mg) was removed and minced, and total RNA was extracted by the guanidinium thiocyanate-phenol chloroform method. Reverse transcription-polymerase chain reaction (RT-PCR) was performed to determine expression of the myocardial cytokines VEGF and receptor Flt-1, Angiopoietin-1 and -2 and receptors Tie-1 and -2, basic-FGF, and transforming growth factor β1 (TGFβ1). Aliquots of total RNA (1 μg/20 μl) were reverse-transcribed into single-stranded cDNA with 0.25 U/μl avian myeloblastoma virus reverse transcriptase (Life Sciences, Inc.) in

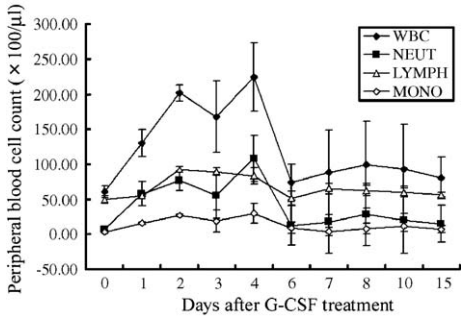

Fig. 2. Peripheral blood cell counts after G-CSF administration in rats. Three Sprague–Dawley rats were injected subcutaneously with 100 μg/kg/day G-CSF for 5 consecutive days. Before and 1, 2, 3, 4, 6, 7, 8, 10, and 15 days after G-CSF administration, 200 μl peripheral blood was harvested from the tail vein for blood cell counting. On day 4 after treatment, total white blood cells increased 3.7-fold, neutrophils increased 16-fold, monocytes increased 9.5-fold, and lymphocytes increased 0.9-fold. WBC, total leukocytes; NEUT, neutrocytes; LYMPH, lymphocytes; MONO, monocytes.

10 mM Tris–HCl (pH 8.3), 5 mM $MgCl_2$, 50 mM KCl, 1 mM deoxy-NTPs, and 2.5 μM random hexamers. Five microliters of the diluted cDNA product was mixed with 10 mM Tris–HCl (pH 8.3), 50 mM KCl, 4 mM $MgCl_2$, 0.025 U/ml Taq DNA polymerase (Takara BioInc.), and 0.2 μM of each primer in a total volume of 25 μl. The primers used in this study are listed in Table 1. To confirm noncontamination of genomic DNA, identical RT-PCR amplification reactions were performed in the absence of reverse transcriptase. PCR was performed with a DNA thermal cycler (PerkinElmer).

2.8. Morphometric analysis of infarct size and artery neointima formation

Twenty-eight days after induction of myocardial infarction, rats were killed by lethal injection of sodium pentobarbital (100 mg/kg body weight, i.p.) and then perfused with saline followed by 10% formalin at physiologic pressure. Six transverse segments of equivalent thickness from the base to the apex of the heart and five segments of equivalent thickness of the carotid artery were embedded in paraffin. From each segment, 4-μm-thick sections were cut and stained with hematoxylin–eosin and Masson trichrome stain. Scarred areas of the heart were stained blue with Masson trichrome stain. Infarct size measurements were performed as described previously (Grimm et al., 1998; Pfeffer et al., 1979). In brief; the lengths of the infarcted surfaces were measured and expressed as a percentage of the total circumference × 100. Final infarct size was calculated as the average of all segments from each heart.

For morphometric analysis of neointima formation, the carotid artery luminal area and internal elastic membrane were traced. The cross-sectional area between the lumen and the

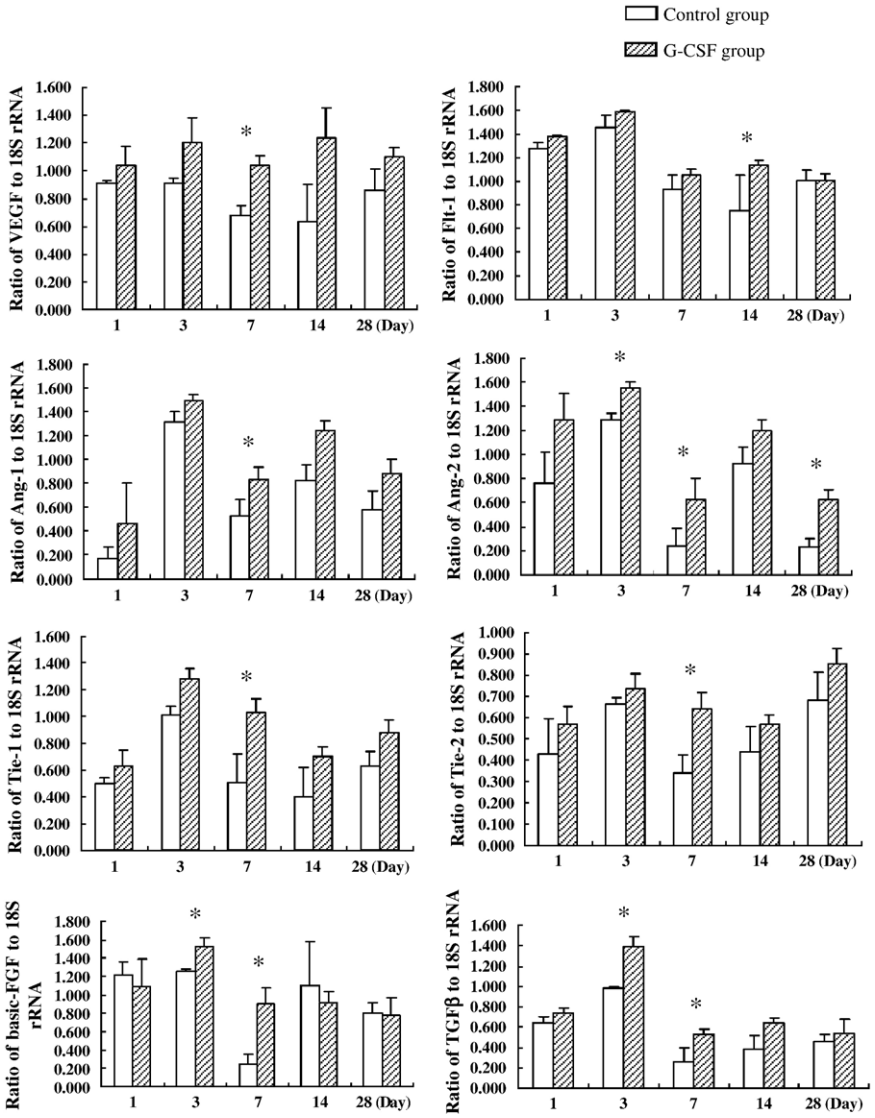

Fig. 3. RT-PCR analysis of angiogenic cytokine expression in the infarction border area. Sprague–Dawley rats with myocardial infarction (MI) were treated with G-CSF (G-CSF group) or saline (control group) for 5 consecutive days. Hearts were removed 1, 3, 7, 14, and 28 days after induction of MI. Rat 18S ribosomal RNA (rRNA) served as an internal control, the ratio of the abundance of cytokine mRNA to that of 18S rRNA was evaluated by densitometric analysis. Data are the means of experiments carried out in duplicate. G-CSF increased angiogenic cytokines expressions immediately after administration and the effect continued 7 to 28 days. *$P<0.05$ vs. control group. VEGF, vascular endothelial growth factor; Ang-1, angiopoietin-1; Ang-2, angiopoietin-2; basic-FGF, basic fibroblast growth factor; TGFâ, transforming growth factor β.

internal elastic membrane was hyperplastic neointimal area (Ohlstein et al., 2000). Restenosis rate was calculated as hyperplastic neointimal area/internal elastic membrane area.

2.9. Immunohistochemistry

Paraffin blocks of the third segment of heart and all segments of carotid artery were used for immunohistochemistry. Immunohistochemical evaluation of the heart focused on the infarction area and infarction border area. Endothelial cells were identified with antibody against von Willebrand factor (vWF, 1:100; DakoCytomation). Smooth muscle cells were identified with anti-smooth muscle actin antibody (1A4, 1:100; DakoCytomation). Inflammatory cells were identified with anti-CD68 antibody (1:50, Serotec). Cardiomyocytes were identified with anti-alpha-sarcomeric muscle actin antibody (αSr-1, 1:40; DakoCytomation). GFP cells were identified with anti-GFP antibody (1:200, MBL). For cell counting, digital photographs were taken at magnification ×400, and 10 random high power fields from each sample were chosen and quantified in a blinded manner.

2.10. Statistical analysis

Data are shown as mean±S.E.M. One-way analysis of variance (ANOVA) was performed for comparisons between groups at different time points. Between-group differences were analyzed by two-tailed Student's *t*-test. Probability values (*P*) less than 0.05 were considered statistically significant.

3. Results

3.1. Effect of G-CSF on hemodynamic changes

There were no significant differences in heart rate between the control and G-CSF groups before and after myocardial infarction. Representative M-mode echocardiograms after myocardial infarction are shown in Fig. 1. Changes in left ventricular internal diameter at end-diastole, left ventricular internal diameter at end-systole, left ventricular ejection fraction, and fractional shortening after myocardial infarction are shown in Table 2. After myocardial infarction, left ventricular internal diameter at end-diastole and left ventricular internal diameter at end-systole increased, left ventricular ejection fraction and fractional shortening decreased in both control and G-CSF-treated rats, whereas the increases in left ventricular internal diameter at end-systole and the decreases in left ventricular ejection fraction and fractional shortening were significantly less in the G-CSF group than in the control group.

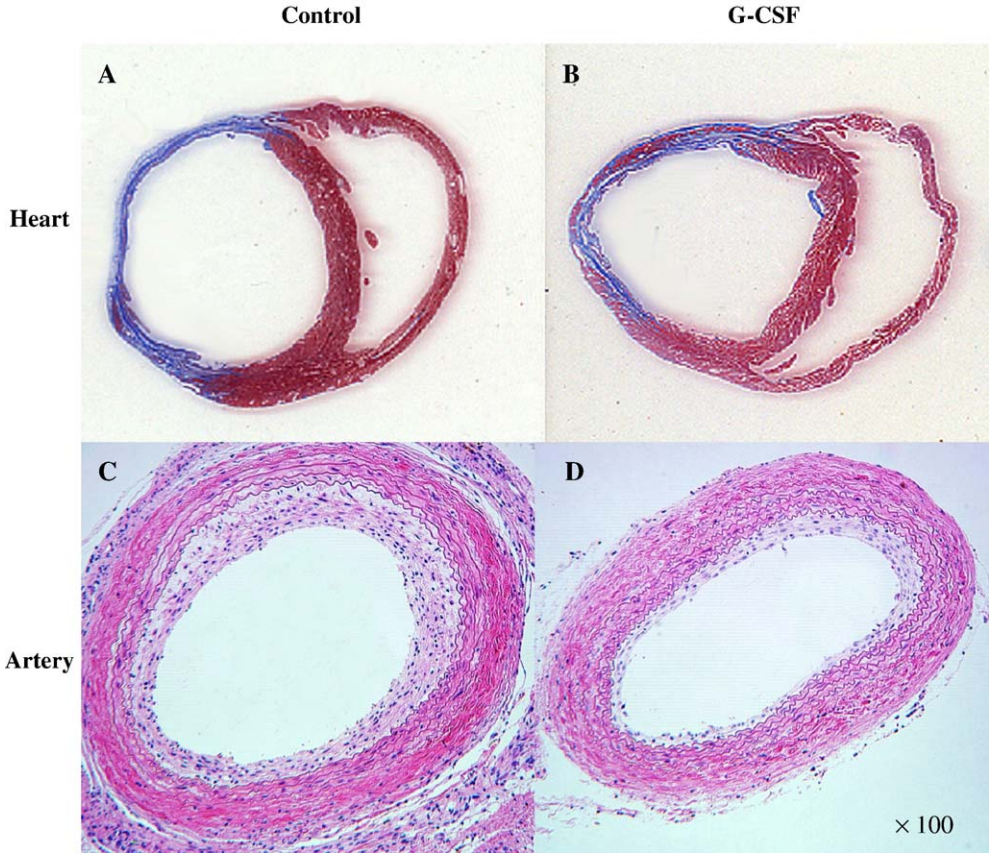

Fig. 4. Histologic analysis of heart and artery neointima formation. (A, B) Masson trichrome staining of heart 28 days after myocardial infarction. (A) Control group (n=10). (B) G-CSF group (n=10). Left ventricle free wall was thinner and the infarct area was replaced by fibrotic tissue in control group, while infarction wall thickness was maintained and surviving myocardium was observed in G-CSF group. (C, D) Effect of G-CSF on neointima formation in rat carotid artery 4 weeks after balloon injury. (C) Control group (n=10). (D) G-CSF group (n=10). G-CSF treatment reduced neointima formation in injured artery.

3.2. Effects of G-CSF on cell counts and angiogenic cytokines in peripheral blood

G-CSF treatment induced a significant transient increase in the number of white blood cells, which decreased immediately after termination of treatment. On day 4 after treatment, total white blood cells increased 3.7-fold, neutrophils increased 16-fold, monocytes increased 9.5-fold, and lymphocytes increased 0.9-fold (Fig. 2).

There were no differences in plasma levels of VEGF, basic-FGF, HGF, and interleukin-8 between control and G-CSF groups.

3.3. G-CSF increased expression of angiogenic cytokines in the infarction border area

G-CSF treatment increased the expression of most of the angiogenic cytokines analyzed in the infarction border area after myocardial infarction (Fig. 3). Expression increased immediately from 1 day after myocardial infarction and continued until 7 to 28 days after myocardial infarction.

3.4. Histologic analysis of heart and artery neointima formation

On day 28 after myocardial infarction, the left ventricle free wall was very thin in the control group (0.32±0.02 mm, $n=10$), showing complete transmural infarction with fibrosis (Fig. 4A), whereas G-CSF treatment preserved left ventricle wall thickness (0.85±0.06 mm, $n=10$, $P<0.05$ vs. control group) in the infarcted area (Fig. 4B). The size of the infarcted area was significantly larger in the control group (51.7±6.2%) than in the G-CSF group (34.1±2.7%, $P<0.05$ vs. control group).

The effect of G-CSF treatment on neointima formation in the carotid artery 4 weeks after myocardial infarction and balloon injury is shown in Fig. 4C–D. Morphometric analysis of five serial segments with equivalent thickness showed a 35% decrease

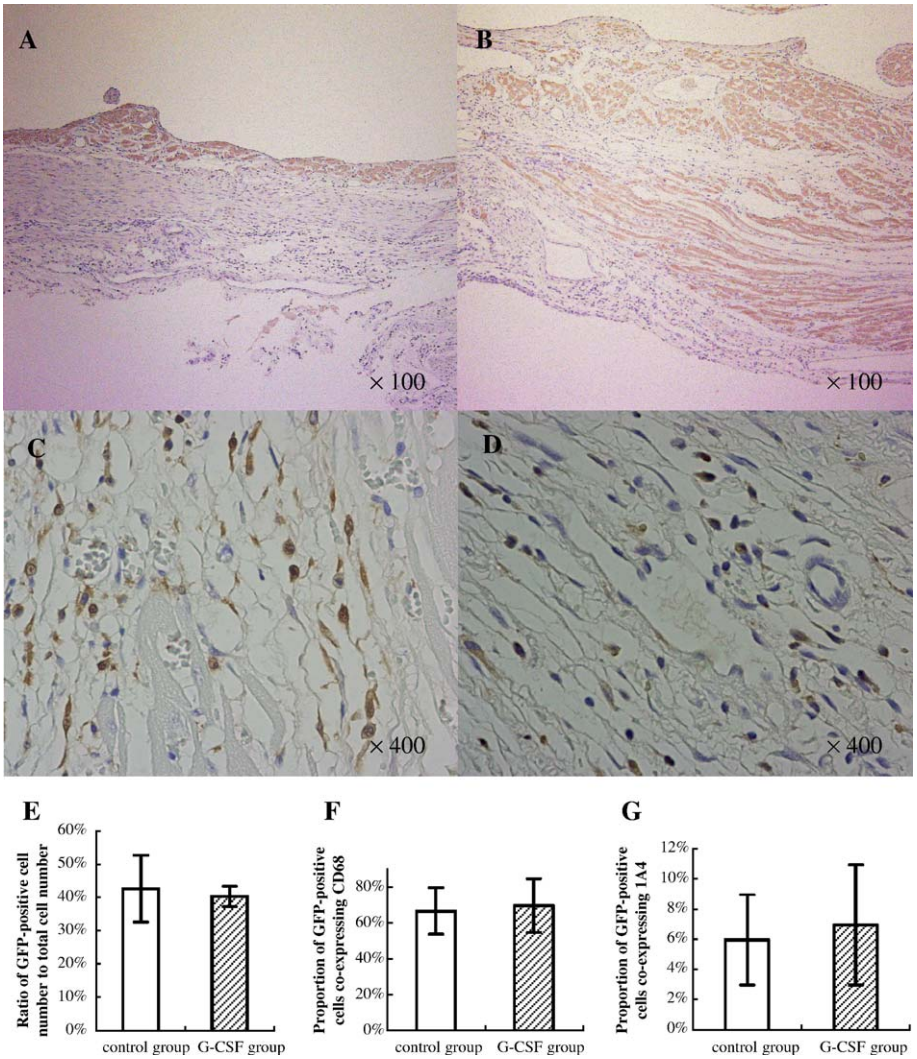

Fig. 5. Immunohistochemistry of infarction area and infarction border area. (A, B) Anti-alpha-sarcomeric muscle actin (αSr-1) staining of infarction area. (A) Control group. (B) G-CSF group. Surviving cardiomyocytes occupied the infarction area from the endocardium to the epicardium, preserving the wall thickness in the G-CSF group. (C, D) GFP-positive cells in infarction border area. (C) Control group. (D) G-CSF group. (E) The ratio of GFP-positive cell number to total cell number (43±10% vs. 41±3%, respectively, $P>0.05$). (F) Proportion of GFP-positive cells co-expressing CD68 (67±13% vs. 70±15%, respectively, $P>0.05$). (G) Proportion of GFP-positive cells co-expressing α1A4 (6±3% vs. 7±4%, respectively, $P>0.05$).

in neointimal area in the G-CSF group compared with that in the control group (43.9±6.2% vs. 28.6±4.7%, $P<0.05$).

3.5. Immunohistochemical evaluation of the heart after myocardial infarction

Immunohistochemical staining for αSr-1 was performed to detect surviving cardiomyocytes in the infarction area. The number of surviving cardiomyocytes was greatly reduced in the control group compared to those in the G-CSF group. Only a filmy layer of αSr-1-positive cells was identified on the endocardial side, and most of the infarction area was replaced by fibrotic tissue in the control group (Fig. 5A), whereas surviving cardiomyocytes occupied the infarction area from the endocardium to the epicardium, preserving the wall thickness in the G-CSF group (Fig. 5B).

G-CSF did not increase cardiac homing of GFP-positive bone marrow cells in the infarction border area. GFP-positive cells were gathered in the infarction border area in hearts from both the control and G-CSF groups (Fig. 5C, D, and E). Most GFP-positive cells were also CD68 positive (Fig. 5F), and some GFP-positive cells were also α1A4 positive (Fig. 5G). Few GFP-positive cells were αSr-1 positive (proportion of GFP-positive cells co-expressing αSr-1 was less than 1% in both groups).

3.6. Immunohistochemical evaluation of the carotid artery after balloon injury

The effect of G-CSF treatment on reendothelialization of the carotid artery was analyzed by vWF immunostaining 2 weeks after balloon injury. G-CSF treatment induced reendothelialization of the injured artery. A nearly complete and continuous lining of vWF-positive cells was observed along the lumen of the injured artery in the G-CSF group (Fig. 6B) compared with patchy and interrupted vWF-positive staining of the injured artery in the control group (Fig. 6A).

To confirm the source of new endothelial cells and neointimal cells, we analyzed GFP staining of injured carotid artery from rats transplanted with GFP bone marrow cells at different time points after balloon injury. One week after injury, the elastic membrane was extended by balloon inflation; some GFP-positive cells were gathered in the adventitia, clinging to the external elastic membrane (Fig. 6D). No GFP-positive cells were identified in normal artery without balloon injury (Fig. 6C). Two weeks after injury, GFP-positive cells were distributed in a patchy pattern near the adventitia in the media and neointima in injured artery in both the control and G-CSF groups (Fig. 6E–F). Four weeks after injury, neointima formation and GFP-positive

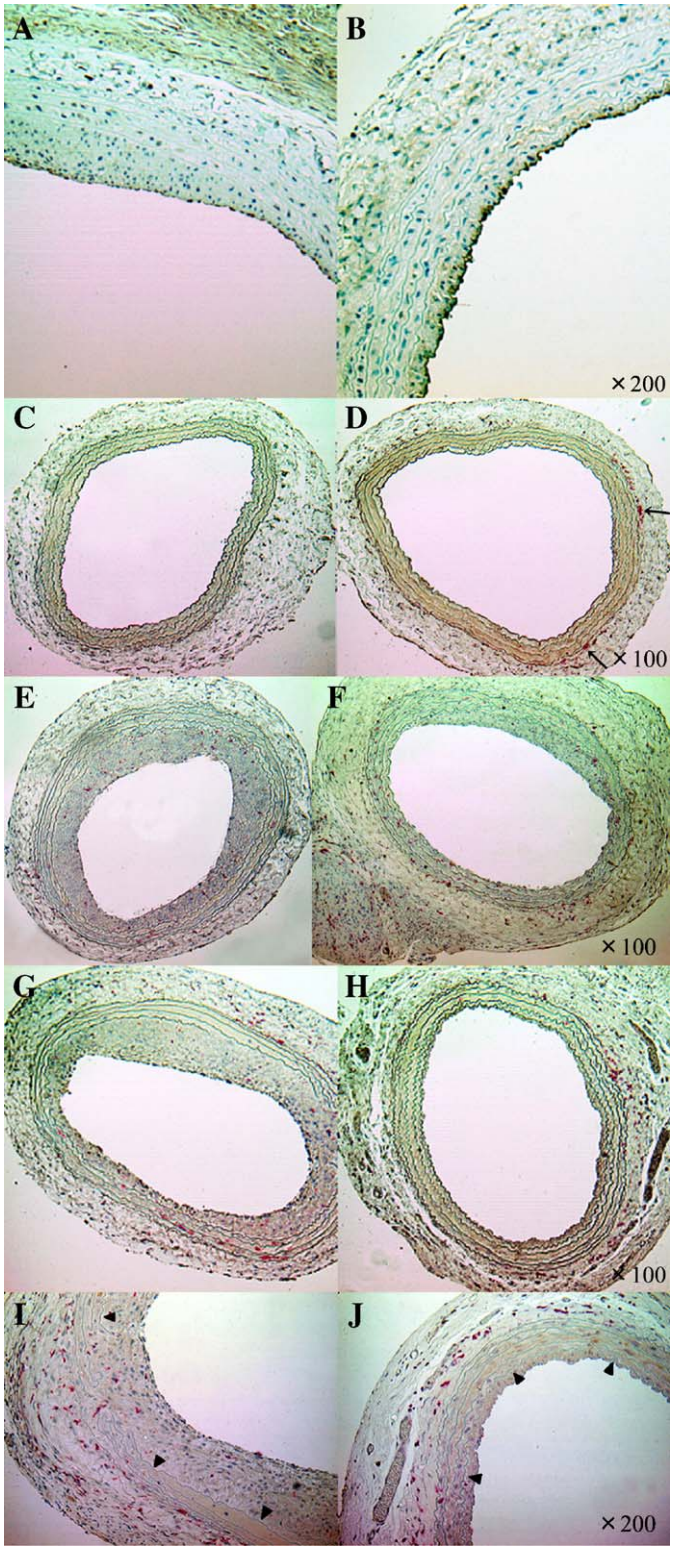

Fig. 6. Immunohistochemistry of carotid artery. (A, B) von Willebrand factor (vWF) staining 2 weeks after balloon injury. Interrupted vWF-positive cells were observed in the control group (A). Continuous lining of vWF-positive cells was observed along the lumen of the injured artery in the G-CSF group (B). (C, D) GFP staining 1 week after balloon injury with G-CSF treatment. No GFP-positive cells were identified in left normal carotid artery without balloon injury (C). Some GFP-positive cells were gathered in the adventitia (arrows) after balloon injury (D). (E, F) GFP staining 2 weeks after balloon injury. GFP-positive cells were distributed in a patchy pattern near the adventitia in the media and neointima in injured artery in both the control (E) and G-CSF groups (F). (G, H) GFP staining 4 weeks after balloon injury. (G) control group. (H) G-CSF group. Neointima formation and GFP-positive cell distribution were similar to those 2 weeks after injury. (I, J) GFP staining 4 weeks after balloon injury at higher magnification. (I) Control group. (J) G-CSF group. Arrows show the internal elastic lamina. Most GFP-positive cells were located in the adventitia of the artery, and a few neointimal cells and new endothelial cells were GFP positive.

cell distribution were similar to those 2 weeks after injury (Fig. 6G–H). Most GFP-positive cells were located in the adventitia of the artery, and a few neointimal cells and new endothelial cells were GFP positive (Fig. 6I–J).

4. Discussion

In the present study, G-CSF treatment in rats prevented cardiac remodeling and improved cardiac function after acute myocardial infarction by preserving the number of cardiomyocytes in the infarction area. G-CSF treatment also accelerated reendothelialization and inhibited neointima formation in rat carotid artery after balloon injury.

Since Orlic et al. first reported the beneficial effects of G-CSF on infarcted heart (Orlic et al., 2001), some studies have confirmed that G-CSF improves cardiac function after myocardial infarction (Adachi et al., 2004; Harada et al., 2005; Kawada et al., 2004; Minatoguchi et al., 2004; Ohtsuka et al., 2004). Most of these studies have shown that G-CSF improves cardiac function by mobilizing bone marrow cells to the myocardium and transdifferentiating these cells into heart cells. However, a recent study (Harada et al., 2005) and the results of the present study suggest that G-CSF acts directly on cardiomyocytes. Harada et al. (2005) showed that cardiomyocytes and cardiac fibroblasts express G-CSF receptor and that G-CSF exerts direct protective effects on cardiomyocytes via activation of the G-CSF receptor. In the present study, although G-CSF increased neutrophils in peripheral blood approximately 16-fold and increased total leukocytes approximately 4-fold, it did not increase blood cytokine levels and did not increase cardiac homing of bone marrow cells, suggesting that the increased cardiac expression of various angiogenic factors in the infarction border area may be the result of a direct effect of G-CSF on heart.

In our experiments, most bone marrow-derived cells in the infarcted area were CD68-positive (macrophages) or α1A4 positive (vascular smooth muscle cells, myofibroblasts, or bone marrow stromal cells). However, it was difficult to find bone marrow-derived cardiomyocytes in the infarcted area. Thus the transdifferentiation of bone marrow cells into cardiomyocytes remains to be confirmed; if it did occur, the number of transdifferentiated cardiomyocytes may be too low to explain G-CSF-induced amelioration of cardiac remodeling and improvement of function (Murry et al., 2004; Nadal-Ginard et al., 2003; Wagers et al., 2002). Most surviving cardiomyocytes in the infarcted area were not derived from bone marrow. Thus, these cardiomyocytes may be associated with the direct protective effect of G-CSF against cardiomyocytes death. Surviving cardiomyocytes in the infarction area may play an important role in preventing cardiac remodeling and in maintaining heart function.

Given previous reports that G-CSF mobilizes bone marrow cells to migrate to the infarcted heart (Kawada et al., 2004; Minatoguchi et al., 2004; Ohtsuka et al., 2004), it is possible that mobilized bone marrow progenitors transdifferentiate into vascular smooth muscle cells, potentially aggravating plaque formation and restenosis in percutaneous coronary intervention-treated vessels (Simper et al., 2002). There have been reports of clinical administration of G-CSF in patients with acute myocardial infarction who underwent percutaneous coronary intervention (Hill et al., 2005; Kang et al., 2004; Petzsch et al., 2004; Ripa et al., 2004; Valgimigli et al., 2005). The MAGIC trial reported an unexpectedly high rate of in-stent restenosis in infarct-related vessels after G-CSF treatment (Kang et al., 2004). Hill et al. (2005) reported potential adverse outcomes in some coronary artery disease patients after G-CSF administration. whereas other groups reported that G-CSF was safe and did not induce coronary artery restenosis in patients with acute myocardial infarction (Petzsch et al., 2004; Ripa et al., 2004; Valgimigli et al., 2005). To investigate the effect of post-acute myocardial infarction G-CSF administration on treated vessels remodeling, rat carotid arteries were injured by balloon catheter after acute myocardial infarction. G-CSF showed effect of inducing reendothelialization and inhibiting neointima formation in injured artery after acute myocardial infarction.

Vascular injury leads to pathologic repair and remodeling involving vascular smooth muscle cell migration and proliferation (Pauletto et al., 1994; Schwartz, 1998). Endothelial cell loss is a major contributing factor to the pathologic repair of injured vessels. The origin of neointimal vascular smooth muscle cells and new endothelial cells is controversial (Campbell et al., 2001; Han et al., 2001; Hu et al., 2002a,b; Kong et al., 2004; Shoji et al., 2004; Tanaka et al., 2003). Hu et al. (2002a) showed that smooth muscle cells in the neointima and atherosclerotic lesions in allografts are not derived from bone marrow, whereas, some studies (Campbell et al., 2001; Han et al., 2001) reported that bone marrow-derived cells are recruited as a complementary source of smooth muscle-like cells, and few resident smooth muscle cells are available to effect repair. In the present study, GFP-positive cells were localized most in the adventitia of the injured artery in both the control and G-CSF groups, in contrast to normal artery, in which no GFP-positive cells were identified. These results suggest that injury itself stimulates the migration of bone marrow cells to the injured region. Few neointimal smooth muscle cells or new endothelial cells were GFP positive. It is possible that bone marrow cells do not provide a main source of neointimal smooth muscle cells and new endothelial cells. Thus, most bone marrow cells may not differentiate into vascular smooth muscle cells and may not aggravate neointimal hyperplasia.

In conclusion, results of the present study suggest that G-CSF treatment in rat model is safe and effective for treatment of left ventricle remodeling after acute myocardial infarction and it does not aggravate vascular remodeling. Moreover, effects may be mediated by direct action of cardiomyocytes rather than regenerating myocardium.

References

Adachi, Y., Imagawa, J., Suzuki, Y., Yogo, K., Fukazawa, M., Kuromaru, O., Saito, Y., 2004. G-CSF treatment increases side population cell infiltration after myocardial infarction in mice. J. Mol. Cell. Cardiol. 36, 707–710.

Avalos, B.R., 1996. Molecular analysis of the granulocyte colony-stimulating factor receptor. Blood 88, 761–777.

Berliner, N., Hsing, A., Graubert, T., Sigurdsson, F., Zain, M., Bruno, E., Hoffman, R., 1995. Granulocyte colony-stimulating factor induction of normal human bone marrow progenitors results in neutrophil-specific gene expression. Blood 85, 799–803.

Campbell, J.H., Han, C.L., Campbell, G.R., 2001. Neointimal formation by circulating bone marrow cells. Ann. N. Y. Acad. Sci. 947, 18–24 (discussion 24–15).

Griese, D.P., Ehsan, A., Melo, L.G., Kong, D., Zhang, L., Mann, M.J., Pratt, R.E., Mulligan, R.C., Dzau, V.J., 2003. Isolation and transplantation of autologous circulating endothelial cells into denuded vessels and prosthetic grafts: implications for cell-based vascular therapy. Circulation 108, 2710–2715.

Grimm, D., Cameron, D., Griese, D.P., Riegger, G.A., Kromer, E.P., 1998. Differential effects of growth hormone on cardiomyocyte and extracellular matrix protein remodeling following experimental myocardial infarction. Cardiovasc. Res. 40, 297–306.

Han, C.I., Campbell, G.R., Campbell, J.H., 2001. Circulating bone marrow cells can contribute to neointimal formation. J. Vasc. Res. 38, 113–119.

Harada, M., Qin, Y., Takano, H., Minamino, T., Zou, Y., Toko, H., Ohtsuka, M., Matsuura, K., Sano, M., Nishi, J., Iwanaga, K., Akazawa, H., Kunieda, T., Zhu, W., Hasegawa, H., Kunisada, K., Nagai, T., Nakaya, H., Yamauchi-Takihara, K., Komuro, I., 2005. G-CSF prevents cardiac remodeling after myocardial infarction by activating the Jak-Stat pathway in cardiomyocytes. Nat. Med. 11, 305–311.

Hill, J.M., Syed, M.A., Arai, A.E., Powell, T.M., Paul, J.D., Zalos, G., Read, E.J., Khuu, H.M., Leitman, S.F., Horne, M., Csako, G., Dunbar, C.E., Waclawiw, M.A., Cannon III, R.O., 2005. Outcomes and risks of granulocyte colony-stimulating factor in patients with coronary artery disease. J. Am. Coll. Cardiol. 46, 1643–1648.

Hu, Y., Davison, F., Ludewig, B., Erdel, M., Mayr, M., Url, M., Dietrich, H., Xu, Q., 2002a. Smooth muscle cells in transplant atherosclerotic lesions are originated from recipients, but not bone marrow progenitor cells. Circulation 106, 1834–1839.

Hu, Y., Mayr, M., Metzler, B., Erdel, M., Davison, F., Xu, Q., 2002b. Both donor and recipient origins of smooth muscle cells in vein graft atherosclerotic lesions. Circ. Res. 91, e13–e20.

Kang, H.J., Kim, H.S., Zhang, S.Y., Park, K.W., Cho, H.J., Koo, B.K., Kim, Y.J., Soo Lee, D., Sohn, D.W., Han, K.S., Oh, B.H., Lee, M.M., Park, Y.B., 2004. Effects of intracoronary infusion of peripheral blood stem-cells mobilised with granulocyte-colony stimulating factor on left ventricular systolic function and restenosis after coronary stenting in myocardial infarction: the MAGIC cell randomised clinical trial. Lancet 363, 751–756.

Kawada, H., Fujita, J., Kinjo, K., Matsuzaki, Y., Tsuma, M., Miyatake, H., Muguruma, Y., Tsuboi, K., Itabashi, Y., Ikeda, Y., Ogawa, S., Okano, H., Hotta, T., Ando, K., Fukuda, K., 2004. Nonhematopoietic mesenchymal stem cells can be mobilized and differentiate into cardiomyocytes after myocardial infarction. Blood 104, 3581–3587.

Kong, D., Melo, L.G., Gnecchi, M., Zhang, L., Mostoslavsky, G., Liew, C.C., Pratt, R.E., Dzau, V.J., 2004. Cytokine-induced mobilization of circulating endothelial progenitor cells enhances repair of injured arteries. Circulation 110, 2039–2046.

Minatoguchi, S., Takemura, G., Chen, X.H., Wang, N., Uno, Y., Koda, M., Arai, M., Misao, Y., Lu, C., Suzuki, K., Goto, K., Komada, A., Takahashi, T., Kosai, K., Fujiwara, T., Fujiwara, H., 2004. Acceleration of the healing process and myocardial regeneration may be important as a mechanism of improvement of cardiac function and remodeling by postinfarction granulocyte colony-stimulating factor treatment. Circulation 109, 2572–2580.

Moon, C., Krawczyk, M., Ahn, D., Ahmet, I., Paik, D., Lakatta, E.G., Talan, M.I., 2003. Erythropoietin reduces myocardial infarction and left ventricular functional decline after coronary artery ligation in rats. Proc. Natl. Acad. Sci. U. S. A. 100, 11612–11617.

Murry, C.E., Soonpaa, M.H., Reinecke, H., Nakajima, H., Nakajima, H.O., Rubart, M., Pasumarthi, K.B., Virag, J.I., Bartelmez, S.H., Poppa, V., Bradford, G., Dowell, J.D., Williams, D.A., Field, L.J., 2004. Haematopoietic stem cells do not transdifferentiate into cardiac myocytes in myocardial infarcts. Nature 428, 664–668.

Nadal-Ginard, B., Kajstura, J., Leri, A., Anversa, P., 2003. Myocyte death, growth, and regeneration in cardiac hypertrophy and failure. Circ. Res. 92, 139–150.

Ohlstein, E.H., Romanic, A.M., Clark, L.V., Kapadia, R.D., Sarkar, S.K., Gagnon, R., Chandra, S., 2000. Application of in vivo and ex vivo magnetic resonance imaging for evaluation of tranilast on neointima formation following balloon angioplasty of the rat carotid artery. Cardiovasc. Res. 47, 759–768.

Ohtsuka, M., Takano, H., Zou, Y., Toko, H., Akazawa, H., Qin, Y., Suzuki, M., Hasegawa, H., Nakaya, H., Komuro, I., 2004. Cytokine therapy prevents left ventricular remodeling and dysfunction after myocardial infarction through neovascularization. FASEB J. 18, 851–853.

Orlic, D., Kajstura, J., Chimenti, S., Limana, F., Jakoniuk, I., Quaini, F., Nadal-Ginard, B., Bodine, D.M., Leri, A., Anversa, P., 2001. Mobilized bone marrow cells repair the infarcted heart, improving function and survival. Proc. Natl. Acad. Sci. U. S. A. 98, 10344–10349.

Pauletto, P., Sartore, S., Pessina, A.C., 1994. Smooth-muscle-cell proliferation and differentiation in neointima formation and vascular restenosis. Clin. Sci. (Lond) 87, 467–479.

Petzsch, M., Ince, H., Kleine, H., Schmidt, H., Rehders, T., Korber, T., Freund, M., Nienaber, C., 2004. No restenosis after G-CSF in acute myocardial infarction: insights from FIRSTLINE-AMI (front-integrated revascularization and stem cell liberation in evolving acute myocardial infarction by granulocyte colony-stimulating factor). Circulation Suppl. III 110 (III-238) (abstract).

Pfeffer, M.A., Pfeffer, J.M., Fishbein, M.C., Fletcher, P.J., Spadaro, J., Kloner, R.A., Braunwald, E., 1979. Myocardial infarct size and ventricular function in rats. Circ. Res. 44, 503–512.

Qian, J.Y., Haruno, A., Asada, Y., Nishida, T., Saito, Y., Matsuda, T., Ueno, H., 2002. Local expression of C-type natriuretic peptide suppresses inflammation, eliminates shear stress-induced thrombosis, and prevents neointima formation through enhanced nitric oxide production in rabbit injured carotid arteries. Circ. Res. 91, 1063–1069.

Ripa, R., Wang, Y., Jorgensen, E., Kastrup, J., 2004. Bone-marrow stem cell mobilization induced by granulocyte-colony stimulating factor in patients with a PCI-treated acute ST-elevation myocardial infarction is safe: results from a double-blind randomized study, the stem cells in myocardial infarction (STEMMI) trial. Circulation Suppl. III 110 (III-238) (abstract).

Schwartz, R.S., 1998. Pathophysiology of restenosis: interaction of thrombosis, hyperplasia, and/or remodeling. Am. J. Cardiol. 81, 14E–17E.

Shoji, M., Sata, M., Fukuda, D., Tanaka, K., Sato, T., Iso, Y., Shibata, M., Suzuki, H., Koba, S., Geshi, E., Katagiri, T., 2004. Temporal and spatial characterization of cellular constituents during neointimal hyperplasia after vascular injury: potential contribution of bone-marrow-derived progenitors to arterial remodeling. Cardiovasc. Pathol. 13, 306–312.

Simper, D., Stalboerger, P.G., Panetta, C.J., Wang, S., Caplice, N.M., 2002. Smooth muscle progenitor cells in human blood. Circulation 106, 1199–1204.

Tanaka, K., Sata, M., Hirata, Y., Nagai, R., 2003. Diverse contribution of bone marrow cells to neointimal hyperplasia after mechanical vascular injuries. Circ. Res. 93, 783–790.

Valgimigli, M., Rigolin, G.M., Cittanti, C., Malagutti, P., Curello, S., Percoco, G., Bugli, A.M., Della Porta, M., Bragotti, L.Z., Ansani, L., Mauro, E., Lanfranchi, A., Giganti, M., Feggi, L., Castoldi, G., Ferrari, R., 2005. Use of granulocyte-colony stimulating factor during acute myocardial infarction to enhance bone marrow stem cell mobilization in humans: clinical and angiographic safety profile. Eur. Heart J. 26, 1838–1845.

Wagers, A.J., Sherwood, R.I., Christensen, J.L., Weissman, I.L., 2002. Little evidence for developmental plasticity of adult hematopoietic stem cells. Science 297, 2256–2259.

Zou, Y., Takano, H., Mizukami, M., Akazawa, H., Qin, Y., Toko, H., Sakamoto, M., Minamino, T., Nagai, T., Komuro, I., 2003. Leukemia inhibitory factor enhances survival of cardiomyocytes and induces regeneration of myocardium after myocardial infarction. Circulation 108, 748–753.

Development of Gene Silencing Pyrrole-Imidazole Polyamide Targeting the TGF-β1 Promoter for Treatment of Progressive Renal Diseases

Hiroyuki Matsuda,* Noboru Fukuda,*†‡ Takahiro Ueno,* Yoshiko Tahira,* Hirohito Ayame,§ Wen Zhang,§ Toshikazu Bando,§ Hiroshi Sugiyama,§ Satoshi Saito,† Koichi Matsumoto,* Hideo Mugishima,† and Kazuo Serie‖

*Departments of *Internal Medicine and †Advanced Medicine and ‡Advanced Research Institute of the Sciences and Humanities, Nihon University, Tokyo Japan; §Department of Chemistry, Graduate School of Science, Kyoto University, Kyoto, Japan; and ‖Gentier Biosystems Incorporation, Tokyo, Japan*

Pyrrole-imidazole (Py-Im) polyamides are nuclease-resistant novel compounds that inhibit gene expression by binding to the minor groove of DNA. A Py-Im polyamide that targets rat TGF-β1 was designed as a gene-silencing agent for progressive renal diseases, and the distribution and the effects of this polyamide on renal injury were examined in Dahl-salt sensitive (Dahl-S) rats. For identification of transcription factor binding elements for activation of the rat TGF-β1 gene, recombinant TGF-β1 reporter plasmids were transfected into HEK-293 cells, and promoter activity was measured. Py-Im polyamide was designed to the activator protein-1 binding site of the rat TGF-β1 promoter. This Py-Im polyamide showed strong, fast, and specific binding to the target DNA in gel mobility shift and Biacore assays. Py-Im polyamide significantly inhibited TGF-β1 promoter activity and expression of TGF-β1 mRNA and protein in rat mesangial cells. Intravenously administered fluorescein-labeled polyamide distributed to the kidney of rats. Py-Im polyamide significantly inhibited expression of TGF-β1 mRNA and protein in the renal cortex of Dahl-S rats and reduced the increase in urinary protein and albumin in Dahl-S rats independent of changes in blood pressure. These results indicate that Py-Im polyamide that targets TGF-β1 will be a novel gene-silencing agent for the TGF-β1–associated diseases, including progressive renal diseases.

J Am Soc Nephrol 17: 422–432, 2006. doi: 10.1681/ASN.2005060650

The use of reverse genetics to inactive genes can aid in the elucidation of gene function and may also be helpful in the treatment of viral infections, cancer, and other diseases that involve aberrant gene expression. Gene function can be inactivated at the DNA level by homologous recombination and at the RNA level by antisense DNA, ribozymes, and siRNA. However, these compounds are degraded easily by nucleases. Therefore, suitable chemical modifications or drug-delivery systems are necessary for their therapeutic applications.

Pyrrole-imidazole (Py-Im) polyamides first were identified from duocarmycin A and distamycin A, which recognize and bind DNA with sequence specificities and are small synthetic molecules that are composed of the aromatic rings of N-methylpyrrole and N-methylimidazole amino acids (1–3). Synthetic Py-Im polyamides bind to specific nucleotide sequences in the minor groove of double-helical DNA with high affinity and block binding of specific proteins. Therefore, Py-Im polyamides may be useful tools in molecular biology medicine. Py-Im polyamides are resistant to nucleases and do not require particular delivery systems (4). Various types of sequence-specific DNA-binding Py-Im polyamides have been developed to regulate gene expression by targeting the promoter regions of enhancer and transcription factor binding elements (5). Binding of enhancers to the major and minor grooves of DNA can be inhibited by the minor groove-binding Py-Im polyamides (6). DNA recognition by Py-Im polyamides depends on a code of side-by-side pairing of Py and Im in the minor groove; pairing of Im opposite Py (Im/Py) targets a G-C base pair, and Py/Im targets a C-G base pair. Py/Py targets either a T-A or an A-T base pair (3). The binding constants and specificity of Py-Im polyamides are comparable to those of transcription factors. Dickinson *et al.* (7) reported the genes of the HIV were silenced by Py-Im polyamides to their regulatory sequences.

A number of studies have identified TGF-β1 as a critical factor in kidney diseases such as glomerulosclerosis (8) and mesangioproliferative glomerulonephritis (9,10). TGF-β1 stimulates the proliferation of mesangial cells and the production of extracellular matrix (11,12). TGF-β1 has been reported to induce Thy-1–associated nephritis (13), diabetic nephropathy (14), and interstitial nephritis associated with obstructive nephropathy (15) in rats. TGF-β1 was reported recently to induce epithelial-mesenchymal transformation in renal tissue, which

Received June 22, 2005. Accepted November 2, 2005.

Published online ahead of print. Publication date available at www.jasn.org.

Address correspondence to: Dr. Noboru Fukuda, Department of Internal Medicine, Nihon University School of Medicine, Ooyaguchi-kami 30-1, Itabashi-ku, Tokyo 173-8610, Japan. Phone: +81-3-3972-8111; Fax: +81-3-3972-8666; E-mail: fukudan@med.nihon-u.ac.jp

ISSN: 1046-6673/1702-0422

plays a critical role in the pathogenesis of nephritis (16). Thus, TGF-β1 induces nephrosclerosis and interstitial nephropathy by its effects on mesangial cell growth, extracellular matrix formation, and epithelial-mesenchymal transformation. TGF-β1 is expressed highly in various animal models of progressive renal disease such as hypertensive renal sclerosis, diabetic nephropathy, and focal renal sclerosis (17–20). Dahl salt-sensitive (Dahl-S) rats show glomerulosclerosis, which is known to be associated with TGF-β1 (17). To develop a novel gene-silencing agent for the treatment of progressive renal diseases, we designed and synthesized a Py-Im polyamide targeting TGF-β1 and examined its distribution and effects on TGF-β1 expression and renal injury in Dahl-S rats.

Materials and Methods

This study conformed to the standards of the *Guide for the Care and Use of Laboratory Animals* published by the National Institutes of Health (NIH Publication No. 85-23, revised 1996).

Synthesis of Polyamide Targeting Rat TGF-β1

Polyamide targeting rat TGF-β1 (polyamide) was designed to span the boundary of the activator protein-1 (AP-1) binding site (−2303 to −2297) of the TGF-β1 promoter (Figure 1A). Numbering refers to the start of the open reading frame as +1 (21). Mismatch polyamide (mismatch) was designed not to bind transcription binding sites of the promoter. Polyamides were synthesized according to previously described methods (22) (Figure 1B).

DNA Binding Assays

Fluorescein-labeled DNA corresponding to −2289 to −2310 including the AP-1 binding site and 2-bp mutated DNA were synthesized for gel mobility shift assays. One micromole of the DNA was incubated with 50 μM polyamide or mismatch for 1 h at 37°C. Moreover, fluorescein-labeled appropriate DNA was incubated with polyamide or mismatch, and then it was incubated with AP-1 extract (Promega, Madison, WI) again. Those resulting complexes were separated by electrophoresis and visualized by luminescent image analyzer LAS-3000 (Fujifilm, Tokyo, Japan).

Kinetics of binding of polyamide and mismatch to target sequence were assessed by surface plasmon resonance technique with a molecular interaction model. Biotin double-strand DNA was immobilized to streptavidin-functionalized sensorchip SA (Biacore, Uppsala, Sweden). Measurements of binding curves of polyamide or mismatch to the DNA and data processing were performed on a Biacore X (Biacore) according to recommended protocols.

Construction and Activity of Rat TGF-β1 Promoter Plasmid and Effect of Polyamide on Promoter Activity

Rat TGF-β1 promoter cloned into the KpnI site of the pGL3-basic vector was a gift from Dr. Kyoung Lim (Ajou University School of Medicine, Suwon, Korea). The promoter deletion mutant (−2676 to 72) was cleaved with KpnI and *Bpu*I102I and self-ligated to the promoter-pGL3-basic vector fragment with DNA blunting kit (TaKaRa; Otsu, Shiga, Japan). Other deletion mutants were generated by cleaving with KpnI and SacI, XhoI, *Pvu*II, *Van*91I, *Nsi*I, *Bst*PI, SacII, or *Bsu*36I to obtain promoter terminating at −2424, −2153, −1715, −1474, −1327, −1104, −742, and −513 to 72.

HEK-293 cells were seeded onto 24-well plates and grown in DMEM (Sigma-Aldrich, St. Louis, MO) with 20% calf serum. At 70 to 90% confluence, a mixture of reporter plasmid (1 μg/well) and phRG-TK vector (0.01 μg/well; Promega) as an internal control was used to transfect cells with Lipofectamine2000 (Invitrogen, Carlsbad, CA) as described previously (23) and then changed to flesh medium in the presence or absence 1.0 mM phorbol 12-myristate 13-acetate (PMA; Sigma-Aldrich). Cells were incubated for an additional 24 h and scraped into 100 μl of cold lysis buffer (PBS [pH 7.4] and 1 mM PMSF). Luciferase activity was measured with a Dual-luciferase reporter assay

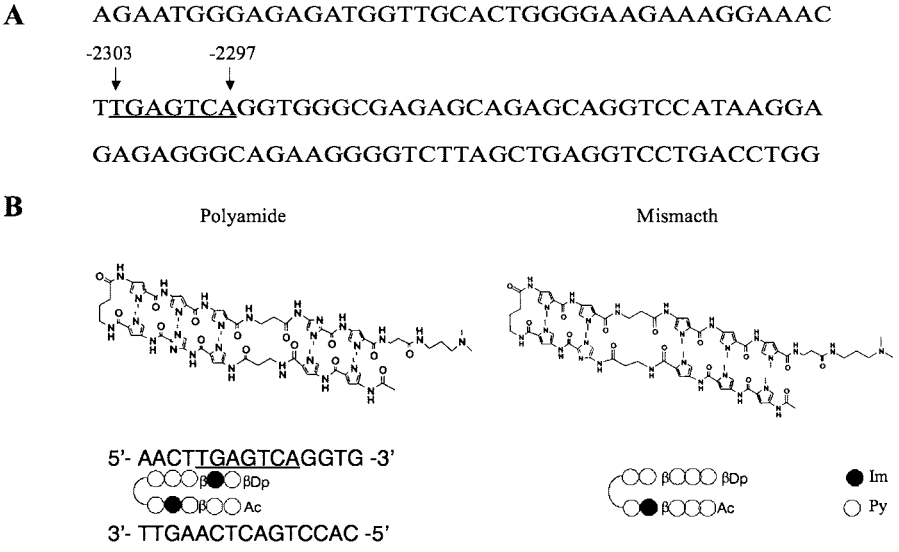

Figure 1. Target sequence and structure of the synthetic pyrrole-imidazole (Py-Im) polyamide that targets the rat TGF-β1 promoter. (A) The polyamide was designed to bind to the rat TGF-β1 promoter adjacent to the activator protein-1 (AP-1) binding site (−2303 to −2297) in the −2424 to −2153 region of the deletion mutant. (B) Structure of the rat TGF-β1–specific polyamide and mismatch polyamide (mismatch). Mismatch was designed not to bind transcription binding sites of the promoter. Polyamides were synthesized by solid-phase methods and were purified by HPLC (0.1% AcOH/CH_3CN 0 to 50% linear gradient, 0 to 40 min, 254 nm through a Chemcobond 5-ODS-H column).

system (Promega) and a TD-20/20 luminometer (Turner Designs, Sunnyvale, CA) (24).

For evaluation of the effect of polyamide on promoter activity, HEK-293 cells were transfected with rat TGF-β1 promoter plasmid and incubated with 0.1 or 1.0 μM polyamide or 1.0 μM mismatch in the presence of 1.0 μM PMA for 24 h. Luciferase activity then was measured.

Distribution of Fluorescein-Labeled Polyamide In Vitro *and* In Vivo

Glomeruli were isolated from the kidneys of 4-wk-old Wistar-Kyoto rats (SHR Corp., Funabashi, Chiba, Japan) by a graded-sieve technique as described previously (25). Mesangial cells were isolated from explants of whole glomeruli according to the differential growth capacities of glomerular epithelial and mesangial cells.

Mesangial cells were seeded onto plates and grown in RPMI-1640 medium (Sigma-Aldrich) with 10% FCS. After 24 h, cells were incubated with 2 μM fluorescein-labeled polyamide in RPMI-1640 medium for 2 h. Cells were washed, and fresh RPMI-1640 was added. After 22 h, cells were viewed at ×200 under live cell conditions and then fixed in 4% paraformaldehyde for 10 min. Nuclei were stained with Hoechst 33342 (Invitrogen) and viewed again.

Five milligrams of fluorescein-labeled polyamide was injected into Wistar rats (250 g body wt) *via* the tail vein. After 24 h, the kidneys, aorta, heart, and brain were removed, and frozen specimens were made and viewed at ×200. Subsequently, 50 to 100 mg of each tissue was homogenized in DMSO (Sigma-Aldrich). Each sample was centrifuged and freeze-dried. The precipitate was reconstituted with 50 μl of N,N-dimethylformamide (Sigma-Aldrich). Urine was also collected for 24 h in metabolic cages. Fluorescein-labeled polyamide in 20 μl of N,N-dimethylformamide and 20 μl of urinary samples were subjected to HPLC (0.01% CHO_2NH_4/CH_3CN 0 to 100% linear gradient from 0 to 30 min through a Chemcobond 5-ODS-H column [Chemco Scientific, Osaka, Japan]). Fluorescence was measured with a fluorescence detector (FP-2020 Plus; Nihon Bunko, Tokyo, Japan).

In Vivo *Experimental Design*

Seven-week-old male Dahl-S rats (CLEA Japan, Tokyo, Japan) were used in this study. Rats were divided into two groups and were fed 0.3% NaCl (low-salt [LS]) or 8% NaCl (high-salt [HS]) diet (both from Oriental Yeast, Tokyo, Japan) *ad libitum* for 2 wk. One milligram of polyamide or mismatch was dissolved in 100 μl of DMSO plus 100 μl of H_2O and injected *via* the tail veins of HS rats every 2 d for 2 wk (total 7 mg of polyamide per rat). Control rats received injections of 100 μl of DMSO plus 100 μl of H_2O (Figure 2). Systolic BP (SBP) was measured by the tail-cuff method. Urine was collected in metabolic cages for 24 h every week. Urinary protein and albumin excretion were determined with a Bio-Rad protein assay kit (Bio-Rad, Hercules, CA).

Determination of mRNA Expression

For *in vitro* experiments, mesangial cells were incubated with 0.1 or 1.0 μM polyamide or 1.0 μM mismatch in the presence of 1.0 μM PMA in RPMI-1640 medium with 0.5% FCS for 8 h. Total RNA was isolated and reverse-transcribed as described previously (18). For *in vivo* experiments, total RNA was isolated from 20 mg of renal cortical tissue from Dahl-S rats and reverse-transcribed.

Real-time quantitative PCR was performed with cDNA diluted four times and TaqMan Universal Master Mix and an ABI 7500 sequence detector (Applied Biosystems, Foster City, CA) according to the manufacturer's instructions. Assay-on-Demand primers and probes (TGF-β1, Rn00572010-m1; connective tissue growth factor [CTGF], Rn00573960-g1; collagen type 1 α1, Rn00801649-g1; fibronectin, Rn00569575-m1 and TaqMan Rodent GAPDH control reagents) were purchased from Applied Biosystems. Real-time PCR data were analyzed with a standard curve. Correlation coefficients for the standard curves all were >0.90.

Measurement of TGF-β1 Protein

TGF-β1 protein levels in urine and conditioned medium were determined by enzyme immunoassay (TGF-β1 Emax ImmunoAssay System; Promega) as described previously (26). Mesangial cells were treated with 0.1 or 1.0 μM polyamide or 1.0 μM mismatch in the presence of 1.0 μM PMA for 24 h. Conditioned medium was collected and diluted with TGF-β1 sample buffer. Because this assay detects only active TGF-β1 protein, each sample was acidified to convert latent TGF-β1 to the active form. Urine samples from Dahl-S rats that were fed an HS diet for 2 wk were collected for 24 h and diluted 1:1000 in sample buffer.

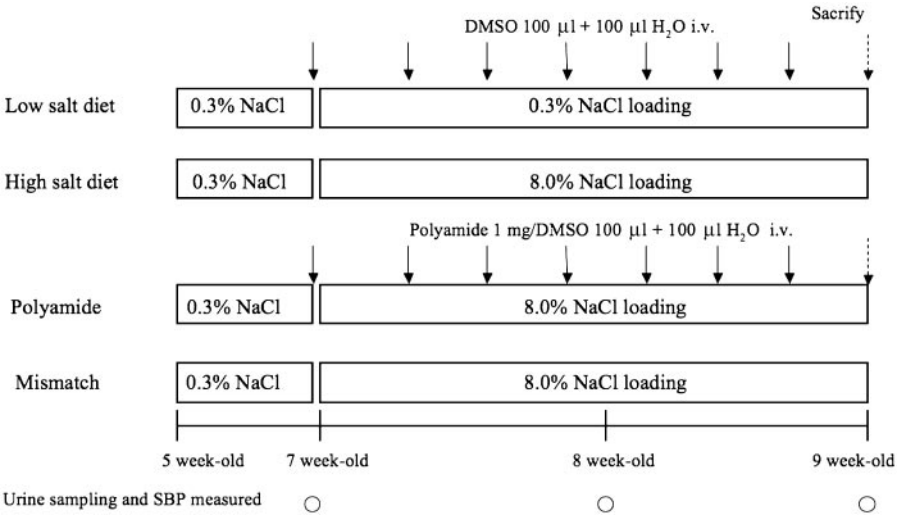

Figure 2. Experimental protocols for administration of Py-Im polyamide that targets TGF-β1 to Dahl-salt sensitive (Dahl-S) rats.

TGF-β1 Immunofluorescence

Unstained 3-μm-thick paraffin sections of renal cortex were deparaffinized, hydrated, and heated for antigen unmasking. Sections were blocked with Serum Blocking Reagent G (R&D Systems, Minneapolis, MN) for 15 min. The slides then were incubated with diluted primary antibody (mAb to TGF-β1; R&D Systems) for 3 h at room temperature, washed in PBS, and incubated with fluorescein-conjugated polyclonal goat anti-mouse antibody (Dako, Carpinteria, CA) for 30 min at room temperature. After being washed in PBS, sections were incubated with Hoechst 33342 and viewed at ×200.

Statistical Analyses

Values are reported as mean ± SEM. A *t* test was used for unpaired data. Two-way ANOVA and Duncan multiple range tests were also used. $P < 0.05$ was considered statistically significant.

Results

Rat TGF-β1 Promoter Analysis

For identification of transcription factor elements that are responsible for activation of the rat TGF-β1 gene, a rat TGF-β1 promoter-pGL3-basic luciferase reporter chimeric plasmid was created (Figure 3). The start site of the rat 2.5-kb TGF-β1 transcript (892 nucleotides upstream of ATG) (24) is at a position homologous to that of human TGF-β1 (858 and 852 nucleotides upstream of ATG) (27) and mouse (856 nucleotides upstream of ATG) (28). A comparison of this conserved region with that of other species revealed 91.4% overall identity with the mouse sequence and 81.7% identity with the human sequence (29).

Deletion of −742 markedly reduced promoter activity compared with deletion of −1104 in the presence or absence of PMA. Deletion of −2153 reduced promoter activity compared with deletion of −2424 in the presence of PMA. There was no significant difference in promoter activity between the deletion of −2153 and −2424 in the absence of PMA, and deletion of −2153 was not affected by PMA. These results suggest that the −1104 to −742 region contains the basal transcriptional regulatory element and the 2.5-kb transcription start site and that the −2424 to −2153 region contains a highly sensitive PMA response element.

We searched for transcription factor binding sites between −2424 and −2153 with TFSEACH (http://mbs.cbrc.jp/research/db/TFSEARCH.html) (30). This region contained an AP-1 binding site (−2303 to −2297). Polyamide was designed to bind to this region (Figure 1A).

Binding and Specificity of Polyamide to Double-Stranded DNA and Inhibition of AP-1 Complex Binding

Gel mobility shift and Biacore assays allow for the determination of the binding affinity and specificity of polyamides for target DNA. Polyamide bound the appropriate 21-bp double-stranded DNA but did not bind the 2-bp mutated DNA, whereas mismatch did not show binding to appropriate DNA (Figure 4A). As shown in Figure 4B, a single mobility band was observed when the DNA were incubated with AP-1 or treatment with mismatch. Polyamide inhibited AP-1 binding to target DNA.

Figure 4, C and D, shows kinetics of polyamide and mismatch bindings with target double-strand DNA obtained from fitting resulting sensorgrams (Biacore assay). Fast binding of polyamide to the target sequence occurred relative to that of mismatch to allow match binding to reach equilibrium at high

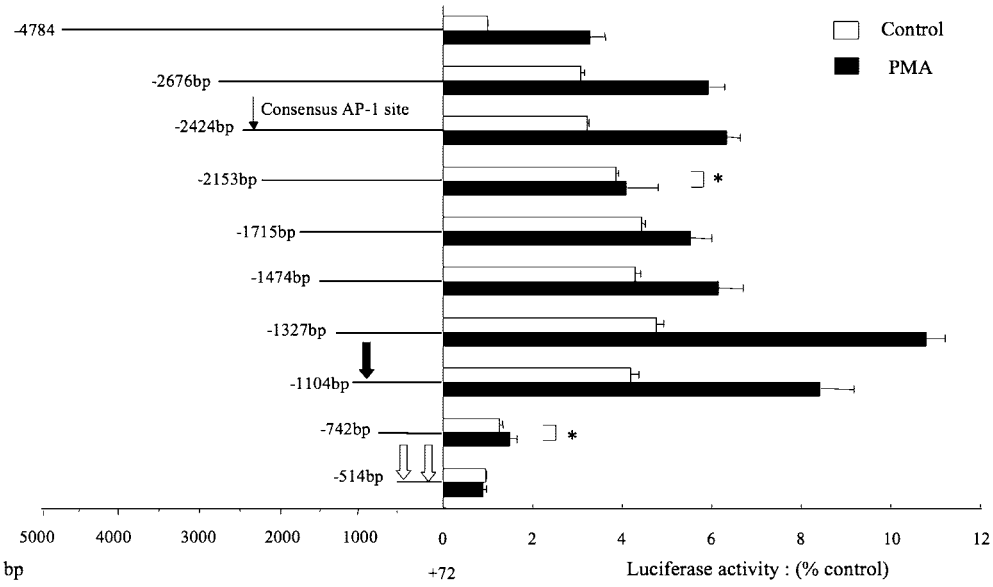

Figure 3. Deletion analysis of TGF-β1 promoter activity. Bars indicate the upstream region of the TGF-β1 gene. Bold arrow indicates the start site for the 2.5-kb transcript as identified previously in mice. Open arrows indicate the start sites for the 1.9-kb transcript and 1.4-kb transcript in rats. HEK-293 cells were transfected with recombinant plasmids and stimulated with 1.0 μM phorbol 12-myristate 13-acetate (PMA). The transcription factor binding sites between −2424 and −2153 were searched with TFSEACH. Narrow arrow indicates the consensus AP-1 binding site at −2303 to −2297 upstream of ATG. *NS *versus* control with PMA.

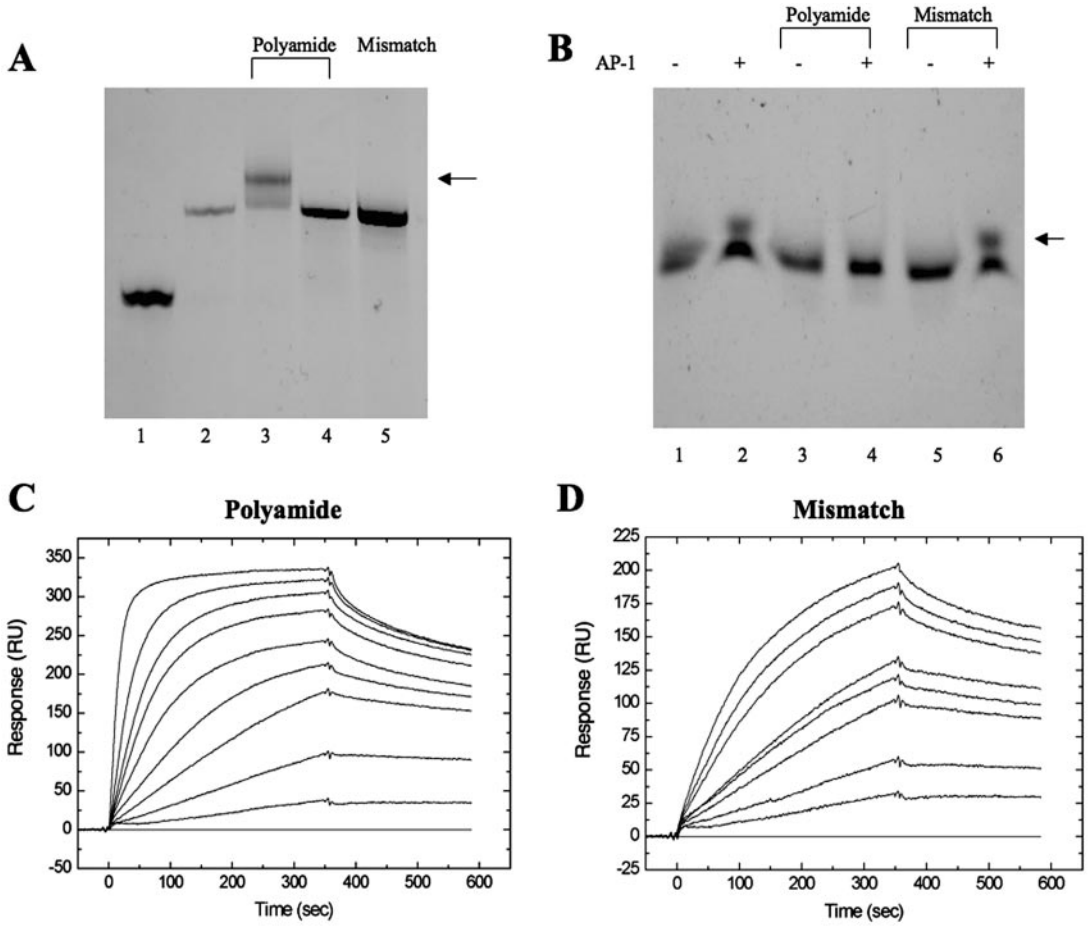

Figure 4. (A) Gel mobility shift assay. Fluorescein-labeled DNA corresponding to the AP-1 binding site (5′-GGAAACTTGAGT-CAGGTGGGC) and 2-bp mutated DNA (5′-GGAAAGGTGAGTCAGGTGGGC) were synthesized and incubated with Py-Im polyamides for 1 h at 37°C and loaded onto a 20% polyacrylamide gel. Lane 1, single-stranded DNA; lane 2, double-stranded DNA; lane 3, DNA with polyamide targeting TGF-β1 (polyamide); lane 4, 2-bp mutated DNA with polyamide; lane 5, DNA with mismatch polyamide (mismatch). (B) After the fluorescein-labeled appropriate DNA was incubated with polyamides, the resulting complexes were incubated with AP-1 extract for 30 min at 37°C and loaded onto a 4% polyacrylamide gel. Lane 1, double-stranded DNA; lane 2, DNA with AP-1; lane 3, DNA with polyamide; lane 4, DNA with polyamide and AP-1; lane 5, DNA with mismatch; lane 6, DNA with mismatch and AP-1. Arrows indicate shifted complex. (C and D) Typical surface plasmon resonance sensorgrams for the interaction of polyamide and mismatch with the DNA immobilized on the surface of a sensor chip SA (Biacore assays). The binding response in resonance units is changed with time. The data are fitted to Langmuir double molecular interaction model with mass transport. All experiments were done using the same DNA immobilization level sensor chips in HBS-EP buffer (0.01 M HEPES [pH 7.4], 0.15 M NaCl, 3 mM EDTA, and 0.005% surfactant P20) with 0.1% DMSO at 25°C. Concentrations for polyamide are 0, 1, 5, 10, 20, 30, 50, 75, 100, and 150 nM from lowest to top curves. Concentrations for mismatch are 0, 0.1, 0.2, 0.6, 0.8, 1, 5, 7.5, and 10 μM from lowest to top curves.

concentrations. Dissociation equilibrium constant (KD) was 1.43×10^{-9} and 9.76×10^{-7} M for the interaction of polyamide and mismatch with the DNA, respectively (Table 1).

Effect of Polyamide on TGF-β1 Promoter Activity and Expression of TGF-β1

Treatment with PMA significantly increased luciferase activity in HEK-293 cells that were transfected with rat TGF-β1 promoter plasmid. Polyamide was significantly and in a concentration-dependent manner decreased luciferase activity stimulated by PMA (Figure 5A). In mesangial cells, polyamide decreased expression of TGF-β1 mRNA (Figure 5B) and protein (Figure 5C) stimulated by PMA in a concentration-dependent manner. Mismatch did not affect luciferase activity or expression of TGF-β1 mRNA and protein in response to PMA.

Distribution of Polyamide In Vitro *and* In Vivo

The distribution of fluorescein-labeled polyamide in mesangial cells after a 24-h incubation is shown in Figure 6A. Fluorescein-labeled polyamide was present in all nuclei by 96 h (data not shown).

The *in vivo* distribution of fluorescein-labeled polyamide in the kidney, aorta, heart, and brain 24 h after intravenous injection is shown in Figure 6B. Fluorescein-labeled polyamide strongly localized in nuclei of nephrotubuli and glomeruli.

Table 1. Kinetic constants for polyamide binding and mismatch binding[a]

	KD (M)	k_a (1/Ms)	k_d (1/s)	Specificity
Polyamide binding	1.43×10^{-9}	5.97×10^{5}	8.54×10^{-4}	685
Mismatch binding	9.76×10^{-7}	7.68×10^{2}	7.49×10^{-4}	

[a]Kinetic constants were calculated from the surface plasmon resonance sensorgrams for the interaction of polyamide and mismatch with the DNA immobilized on the surface of a sensor chip SA (Biacore assays, Figure 4C). Polyamide, pyrrole-imidazole polyamide targeting rat TGF-β1 promoter; mismatch, mismatch polyamide; KD, dissociation equilibrium constant; k_a, association rate constant; k_d, dissociation rate constant. Specificity is defined as KA (polyamide binding)/KA (mismatch binding).

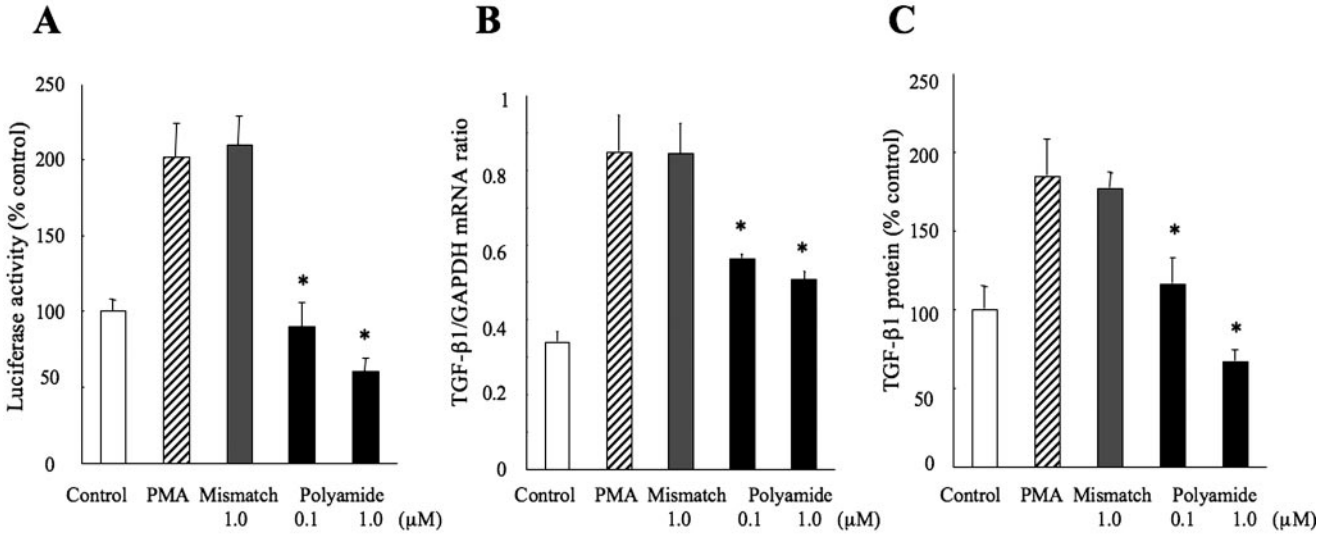

Figure 5. (A) Effect of polyamide targeting TGF-β1 on rat TGF-β1 promoter activity. Rat TGF-β1 promoter plasmid with luciferase was transfected into HEK-293 cells, and cells were incubated with polyamide in the absence or presence of 1.0 μM PMA for 24 h. Promoter activity was measured with a dual-luciferase reporter assay system. (B) Effect of polyamide on expression of TGF-β1 mRNA and protein in mesangial cells. Mesangial cells from Wistar-Kyoto rats were incubated with polyamide in the presence or absence of 1.0 μM PMA for 8 h. The abundance of TGF-β1 mRNA was determined by real-time PCR analysis. (C) Effect of polyamide on expression of TGF-β1 protein in mesangial cells. Mesangial cells were incubated with polyamide in the presence or absence of 1.0 μM PMA for 24 h. Conditioned medium was collected, and total (latent and active) TGF-β1 protein was measured by ELISA. Values are mean ± SEM ($n = 8$). *$P < 0.05$ *versus* treatment with PMA alone.

Fluorescein-labeled polyamide also localized in nuclei of aortic midlayer smooth muscle. Fluorescein-labeled polyamide did not distribute considerably in heart or brain.

HPLC analysis of fluorescein-labeled polyamide in urine, kidney, aorta, heart, and brain is shown in Figure 6C. Fluorescein-labeled polyamide was clearly detected in urine, kidney, and aorta but not in heart or brain.

Effect of Polyamide on Urinary Protein and TGF-β1 Expression in Dahl-S Rats

Intravenous administration of polyamide or mismatch did not affect the body weights of Dahl-S rats (Figure 7A). SBP was remarkably increased in HS rats compared with LS rats. Polyamide or mismatch did not affect SBP (Figure 7B). Both urinary protein and albumin were significantly increased in HS rats compared with levels in LS rats. Treatment with polyamide significantly reduced the increased urinary protein and albumin in HS rats. Mismatch did not affect urinary protein or albumin levels (Figure 7, C and D).

The effects of polyamide on the expression of TGF-β1, CTGF, collagen type 1 α1, and fibronectin mRNA in the renal cortex of Dahl-S rats are shown in Figure 8, A through D. Expression of these mRNA was significantly higher in HS rats than in LS rats. Treatment with polyamide significantly decreased expression of these mRNA in HS rats. Mismatch did not affect expression of these mRNA.

The effects of polyamide on urinary excretion of TGF-β1 protein in Dahl-S rats is shown in Figure 8E. Urinary excretion of TGF-β1 protein was significantly higher in HS rats than in LS rats. Treatment with polyamide significantly decreased urinary excretion of TGF-β1 protein in HS rats. Mismatch did not affect urinary excretion of TGF-β1 protein in HS rats.

Immunofluorescence of TGF-β1 in Renal Cortex

Immunofluorescence of TGF-β1 in the renal cortex of Dahl-S rats is shown in Figure 9. TGF-β1 staining in glomeruli and nephrotubuli in HS rats was stronger than that in LS rats.

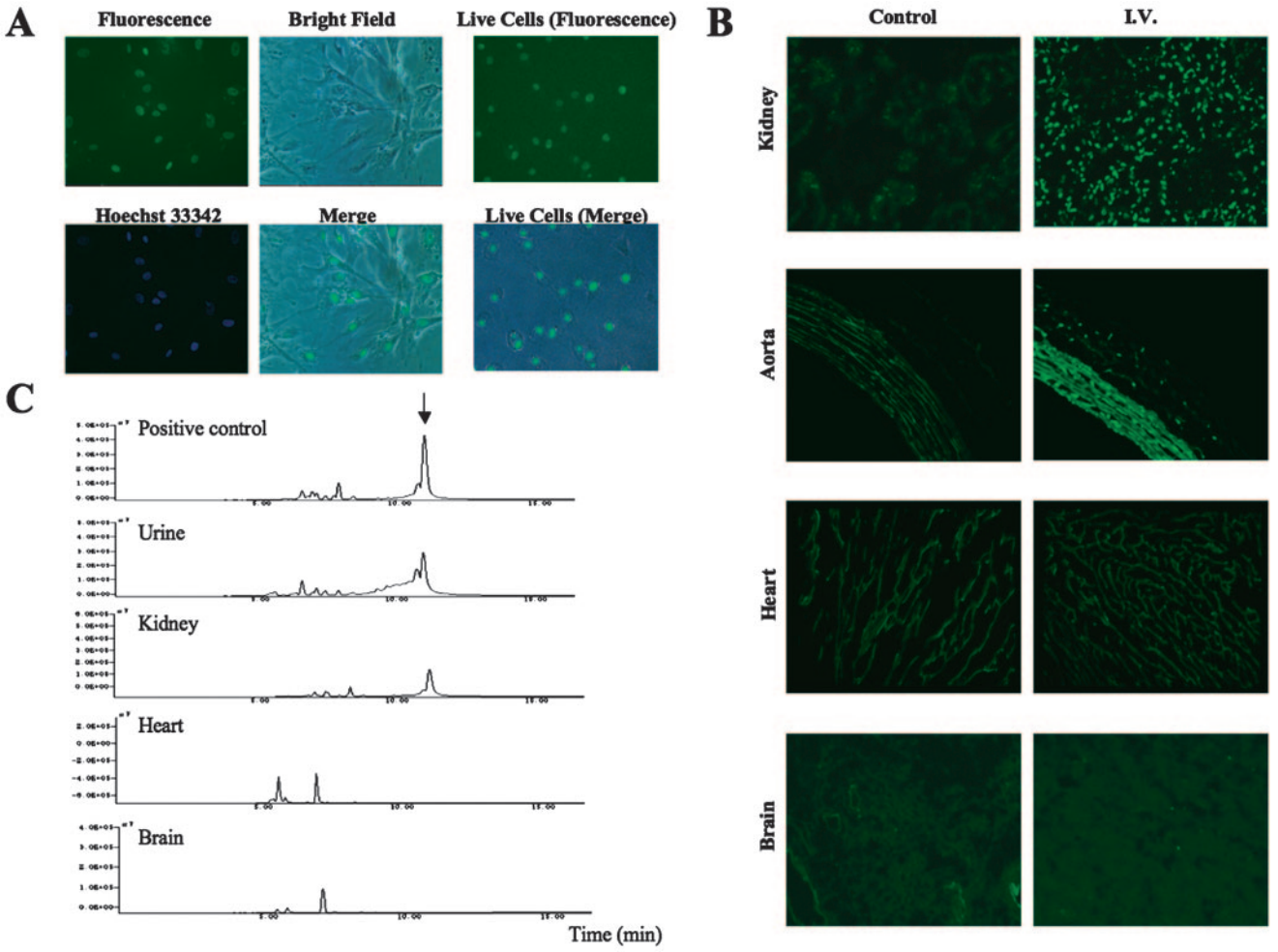

Figure 6. Distribution of fluorescein-labeled Py-Im polyamide *in vitro* and *in vivo*. (A) Mesangial cells from Wistar-Kyoto rats were incubated with fluorescein-labeled polyamide and examined by fluorescence microscopy under live cells condition and then fixed and viewed again. Nuclei were stained with Hoechst 33342 (blue). (B) Five milligrams of fluorescein-labeled polyamide was injected into Wistar rats intravenously. Twenty-four hours after injection, the kidneys, aorta, heart, and brain were removed, and frozen specimens were made. (C) HPLC analysis for the fluorescein-labeled polyamide in the urine, renal cortex, aorta, heart, and brain. Fluorescein-labeled polyamide was subjected into HPLC. Arrow indicates fluorescein-labeled polyamide positive control. Magnification, ×200 in A and B.

Treatment with polyamide considerably reduced TGF-β1 staining in glomeruli and nephrotubuli in HS rats. Mismatch did not affect TGF-β1 staining.

Discussion

Synthetic polyamides have been reported to bind target sites within nucleosomes and may influence chromatin structure (1,2). Because polyamides can be readily designed and synthesized to target any sequence of interest, they may be useful in studies of gene function and perhaps in gene therapy. Polyamides are removed from duplex DNA during transcription; therefore, inhibition of transcription of coding regions is difficult. Polyamides also can inhibit the formation of mRNA in mammalian cells by alkylation of coding regions (31,32). Extensive inhibition of gene expression by alkylating polyamides to a coding region may provide a powerful tool for the gene suppression therapy of viral infections and cancers. Inhibition of gene expression by nonalkylating polyamides that target regulatory sequences is more physiologically relevant than that by alkylating polyamides because this strategy suppresses the enhancing effect of transcription factors and preserves the baseline expression of the target gene. Thus, suppression of gene expression by nonalkylating polyamides may be more efficient in the treatment of chronic nonmalignant diseases. Studies of polyamides have recently focused on the structural characterization of transcription factor–DNA complexes within promoter sequences.

To design a polyamide that targets rat TGF-β1, we analyzed the rat TGF-β1 promoter structure and PMA-stimulated activity in promoter deletion mutants. Positive-regulatory elements that were stimulated by PMA were found at bases −2424 to −2153, which contain an AP-1 binding site. AP-1 elements respond to AP-1 transcription factors such as Jun homodimers or Fos/Jun heterodimers, PMA, angiotensin II, and v-Src. Stim-

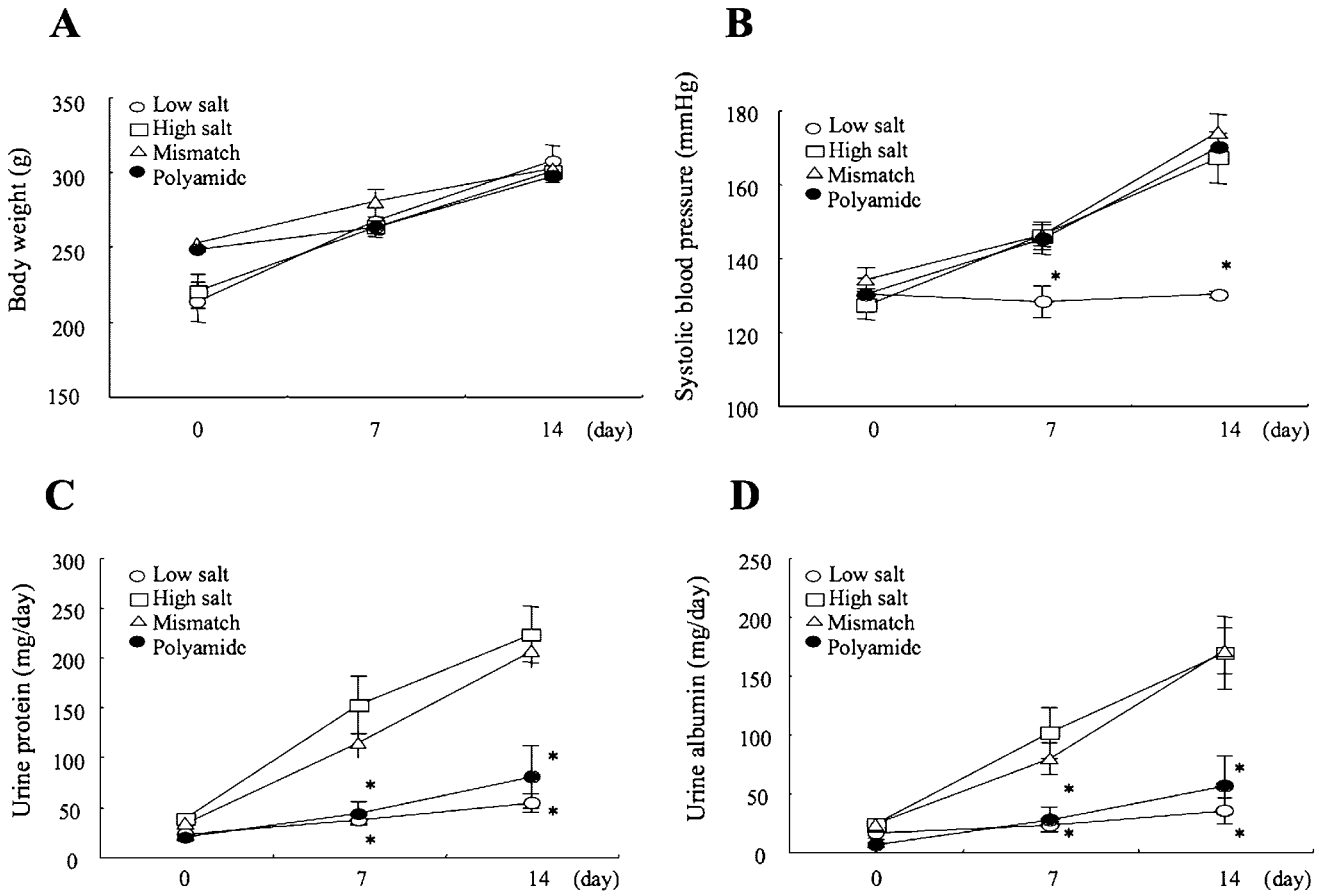

Figure 7. Changes in body weight (A), systolic BP (B), urinary protein (C), and urinary albumin (D) in Dahl-S rats before and after treatments with Py-Im polyamide targeting the TGF-β1 promoter (polyamide). Dahl-S rats were fed a 0.3% NaCl (low salt; ○) or 8% NaCl (high salt; □) diet. Dahl-S rats that were fed a high-salt diet also received an intravenous injection of 1 mg of polyamide (●) or mismatch polyamide (mismatch; △) every 2 d (total 7 mg) for 2 wk. *$P < 0.05$ *versus* Dahl-S rats that were fed a high-salt diet without polyamide.

ulation of TGF-β1 promoter activity occurs by binding to the AP-1 element (33,34). Polyamide targeting TGF-β1 was designed not to cover AP-1 consensus sequences but spans the boundary of AP-1 binding site with the intention of obtaining specificity to the promoter. This polyamide showed strong, fast, and specific binding to the target DNA in gel mobility shift and Biacore assays. Fluorescein-labeled polyamide distributed sufficiently in the kidney without any delivery systems and localized in the nuclei of cultured cells for long periods of time. Best *et al.* (35,36) reported that fluorescein-polyamide conjugates exhibit good nuclear uptake in a wide variety of cell lines. In our *in vivo* experiments, polyamide administered intravenously was delivered sufficiently to the kidney and aorta and was localized to nuclei. Thus, this polyamide bound to target DNA *in vitro* and *in vivo*. HPLC analysis also confirmed that the presence of polyamide administered intravenously was in the urine, kidney, aorta, liver, and lung. Polyamide was not delivered in heart and brain. It is possible that the differentiated cardiac tissue does not express TGF-β1 in normal heart, and this polyamide does not pass through the blood-brain barrier.

Nucleic acid medicines such as antisense DNA, ribozymes, and decoy have been developed as gene-silencing agents. Decoys, in particular, inhibit the binding of target transcription factors in a manner similar to polyamides. However, because these agents are degraded easily by nucleases, they require drug-delivery systems for sufficient distribution into organs. Because polyamides are completely resistant to nucleases and can be delivered into organs without delivery systems, polyamides will be more feasible gene-silencing medicines.

Dahl-S rats are useful models of human progressive renal disease. Dahl-S rats develop severe hypertension, glomerulosclerosis with thickening of capillary artery walls, and interstitial fibrosis in response to salt loading. Tamaki *et al.* (17) reported increased levels of TGF-β1, plasminogen activator inhibitor-1, fibronectin, and collagen type 1 in the renal cortex of Dahl-S rats. In these experiments, expression of TGF-β1 mRNA and protein was enhanced in the renal cortex of HS rats. Treatment with polyamide significantly inhibited this increased expression of TGF-β1 mRNA and protein. Expression of mRNA for CTGF, a potent growth factor that stimulates the proliferation of mesenchymal cells, including mesangial cells, and induces the production of extracellular matrix downstream of TGF-β1 signaling (37–39), was inhibited by polyamide. However, when cell cultures were treated with exogenous TGF-β1,

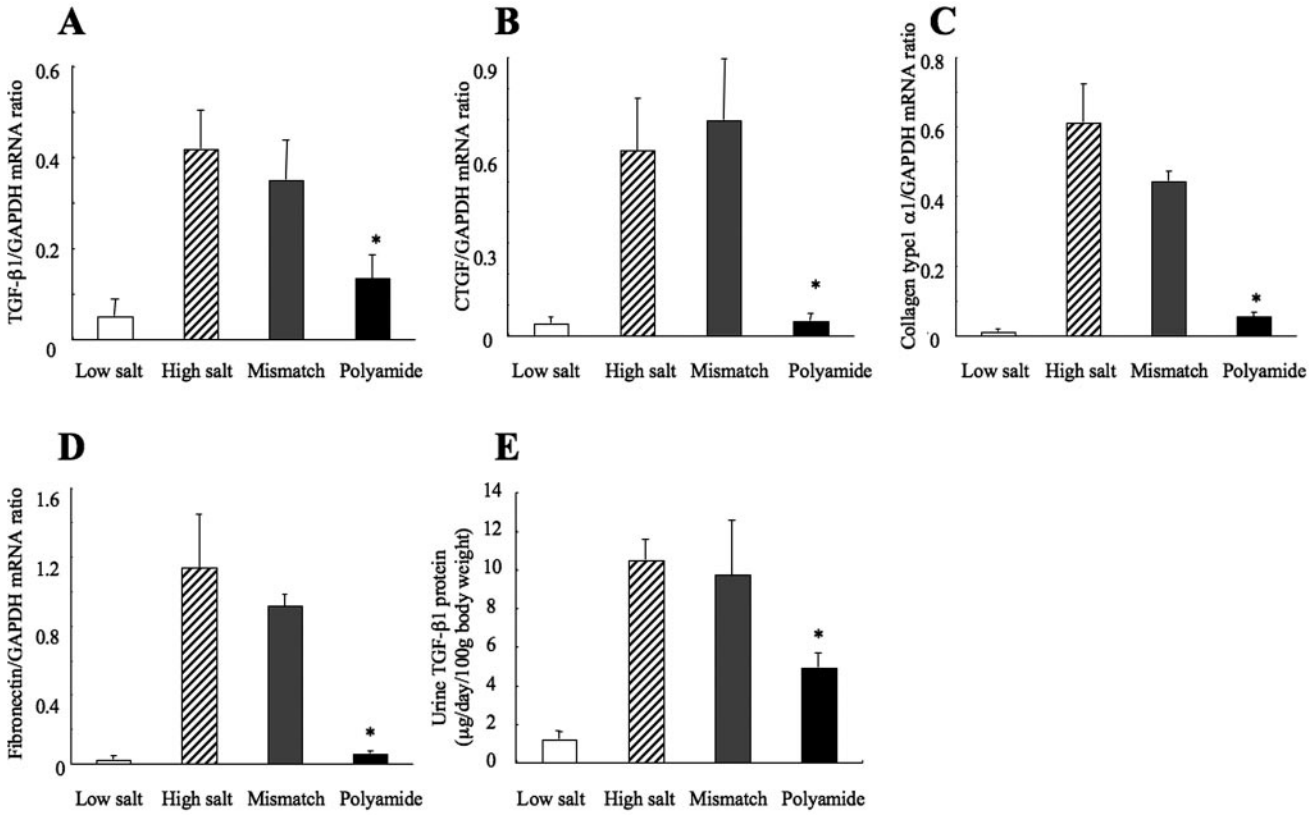

Figure 8. (A through D) Effect of Py-Im polyamide targeting the TGF-β1 promoter (polyamide) on the expression of TGF-β1, connective tissue growth factor (CTGF), collagen type 1 α1, and fibronectin mRNA in the renal cortex from Dahl-S rats. Dahl-S rats were fed a 0.3% NaCl (low salt) or 8% NaCl (high salt) diet. Dahl-S rats that were fed a high-salt diet also received an intravenous injection of 1 mg polyamide or mismatch every 2 d (total 7 mg) for 2 wk. Total RNA then was extracted from the renal cortex. The abundance of all mRNA was determined by real-time PCR. (B) Effect of polyamide on the urinary excretion TGF-β1 protein in Dahl-S rats. Two weeks after treatment with polyamide, urine was collected for 24 h. TGF-β1 protein levels were determined by ELISA. *$P < 0.05$ *versus* Dahl-S rats that were fed a high-salt diet without polyamide.

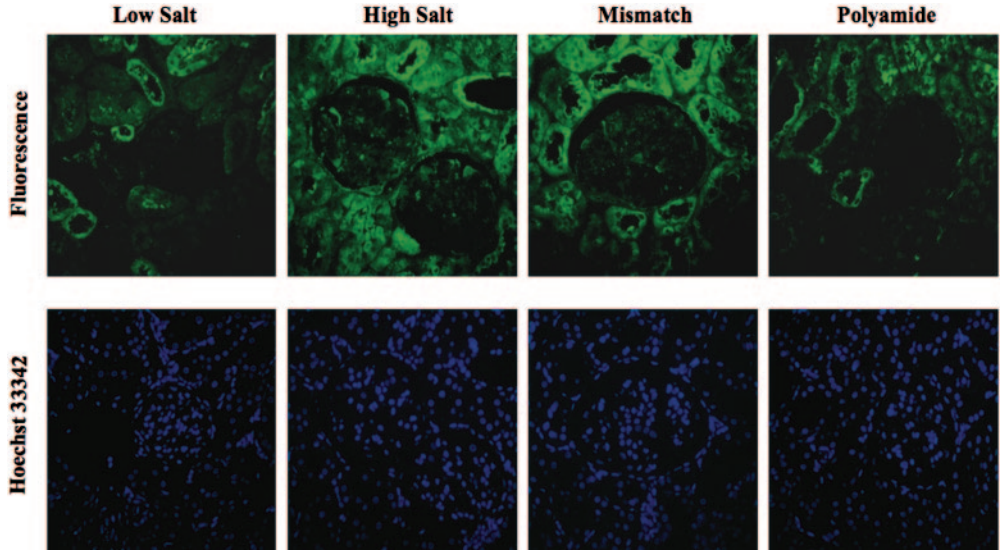

Figure 9. Immunofluorescence analysis of TGF-β1 in the renal cortex of Dahl-S rats that were treated with Py-Im polyamide targeting the TGF-β1 promoter (polyamide). Dahl-S rats were fed a 0.3% NaCl (low salt) or 8% NaCl (high salt) diet. Dahl-S rats that were fed a high-salt diet also received an intravenous injection of 1 mg polyamide or mismatch every 2 d (total 7 mg) for 2 wk. Sections were generated and incubated with an mAb to TGF-β1 and a fluorescein-conjugated polyclonal goat anti-mouse antibody. Nuclei were stained with Hoechst 33342 (blue). Magnification, $\times$200.

polyamide did not block CTGF production. Because the CTGF promoter also has an AP-1 site, this finding further supports the specificity of polyamide for the TGF-β1 promoter. Expression of downstream extracellular matrix components such as collagen type 1 and fibronectin were also increased in the renal cortex of HS rats. This, too, was suppressed significantly by treatment with polyamide. In addition, the increased urinary protein and albumin in HS rats was significantly decreased by treatment with polyamide without a reduction in BP. These findings suggest that the polyamide ameliorated the renal damages by inhibition of TGF-β1 in organs and extracellular matrix components in the renal cortex of Dahl-S rats.

In our study, although an HS diet did not induce considerable renal damage in Dahl-S rats during a 2-wk period, treatment with polyamide significantly suppressed TGF-β1 immunofluorescence in the glomeruli and nephrotubuli of HS rats. Dahly *et al.* (40) injected anti–TGF-β antibody into salt-loaded Dahl-S rats every day for 2 wk and found a significant decrease in BP, proteinuria, and degree of glomerulosclerosis and renal interstitial fibrosis. Polyamide completely inhibited the increases in proteinuria and albuminuria in salt-loaded Dahl-S rats, along with suppression of TGF-β1 staining in glomeruli and nephrotubuli. These findings suggest that polyamide may be feasible gene-silencing agent for the treatment of progressive renal diseases.

We believe that polyamides will be important gene-silencing agents in the postgenome era. Polyamides can be readily designed and synthesized to target any gene. In the future, control of gene expression by polyamides may ameliorate diseases that are not treatable with current medicines.

Acknowledgments

This work was supported in part by Grants-in-Aid from the Japanese Ministry of Education, Science, Sports, and Culture of Japan (15590863).

References

1. Dervan PB: Molecular recognition of DNA by small molecules. *Bioorg Med Chem* 9: 2215–2235, 2001
2. Trauger JW, Baird EE, Dervan PB: Recognition of DNA by designed ligands at subnanomolar concentrations. *Nature* 382: 559–561, 1996
3. White S, Baird EE, Dervan PB: On the pairing rules for recognition in the minor groove of DNA by pyrrole-imidazole polyamides. *Chem Biol* 4: 569–578, 1997
4. Fujimoto K, Iida H, Kawakami M, Bando T, Tao ZF, Sugiyama H: Sequence-specific protection of plasmid DNA from restriction endonuclease hydrolysis by pyrrole-imidazole-cyclopropapyrroloindole conjugates. *Nucleic Acids Res* 30: 3748–3753, 2002
5. Murty MS, Sugiyama H: Biology of N-methylpyrrole-N-methylimidazole hairpin polyamide. *Biol Pharm Bull* 27: 468–474, 2004
6. Nguyen-Hackley DH, Ramm E, Taylor CM, Joung JK, Dervan PB, Pabo CO: Allosteric inhibition of zinc-finger binding in the major groove of DNA by minor-groove binding ligands. *Biochemistry* 43: 3880–3890, 2004
7. Dickinson LA, Gulizia RJ, Trauger JW, Baird EE, Mosier DE, Gottesfeld JM, Dervan PB: Inhibition of RNA polymerase II transcription in human cells by synthetic DNA-binding ligands. *Proc Natl Acad Sci U S A* 95: 12890–12895, 1998
8. Gilbert RE, Wilkinson-Berka JL, Johnson DW, Cox A, Soulis T, Wu LL, Kelly DJ, Jerums G, Pollock CA, Cooper ME: Renal expression of transforming growth factor-beta inducible gene-h3 (beta Ig-h3) in normal and diabetic rats. *Kidney Int* 54: 1052–1062, 1998
9. Yamamoto T, Noble NA, Cohen AH, Nast CC, Hishida A, Gold LI, Border WA: Expression of transforming growth factor-beta isoforms in human glomerular diseases. *Kidney Int* 49: 461–469, 1996
10. Iwano M, Akai Y, Fujii Y, Dohi Y, Matsumura N, Dohi K: Intraglomerular expression of transforming growth factor-beta 1 (TGF-beta1) mRNA in patients with glomerulonephritis: Quantitative analysis by competitive polymerase chain reaction. *Clin Exp Immunol* 97: 309–314, 1994
11. Sporn MB, Roberts AB, Wakefield LM, de Crombrugghe B: Some recent advances in the chemistry and biology of transforming growth factor-beta. *J Cell Biol* 105: 1039–1045, 1987
12. Chen JK, Hoshi H, McKeehan WL: Transforming growth factor type beta specifically stimulates synthesis of proteoglycan in human adult arterial smooth muscle cells. *Proc Natl Acad Sci U S A* 84: 5287–5291, 1987
13. Kasuga H, Ito Y, Sakamoto S, Kawachi H, Shimizu F, Yuzawa Y, Matsuo S: Effects of anti-TGF-beta type II receptor antibody on experimental glomerulonephritis. *Kidney Int* 60: 1745–1755, 2001
14. Yamamoto T, Nakamura T, Noble NA, Ruoslahti E, Border WA: Expression of transforming growth factor beta is elevated in human and experimental diabetic nephropathy. *Proc Natl Acad Sci U S A* 90: 1814–1818, 1993
15. Klahr S, Morrissey J: Obstructive nephropathy and renal fibrosis: The role of bone morphogenic protein-7 and hepatocyte growth factor. *Kidney Int Suppl* 87: S105–S112, 2003
16. Zeisberg M, Hanai J, Sugimoto H, Mammoto T, Charytan D, Strutz F, Kalluri R: BMP-7 counteracts TGF-beta1-induced epithelial-to-mesenchymal transition and reverses chronic renal injury. *Nat Med* 9: 964–968, 2003
17. Tamaki K, Okuda S, Nakayama M, Yanagida T, Fujishima M: Transforming growth factor-beta1 in hypertensive renal injury in Dahl salt-sensitive rats. *J Am Soc Nephrol* 7: 2578–2589, 1996
18. Tahira Y, Fukuda N, Endo M, Suzuki R, Ikeda Y, Takagi H, Matsumoto K, Kanmatsuse K: Transforming growth factor-beta expression in cardiovascular organs in stroke-prone spontaneously hypertensive rats with the development of hypertension. *Hypertens Res* 25: 911–918, 2002
19. Gore-Hyer E, Shegogue D, Markiewicz M, Lo S, Hazen-Martin D, Greene EL, Grotendorst G, Trojanowska M: TGF-beta and CTGF have overlapping and distinct fibrogenic effects on human renal cells. *Am J Physiol Renal Physiol* 283: F707–F716, 2002
20. Matsumoto K, Hatano M: Production of interleukin 1 in glomerular cell cultures from rats with nephrotoxic serum nephritis. *Clin Exp Immunol* 75: 123–128, 1989
21. Yang Y, Mumy M, Romeo D, Wakefield LM: Identification of the start sites for the 1.9- and 1.4-kb rat transforming growth factor-beta1 transcripts and their effect on translational efficiency. *Gene* 219: 81–89, 1998

22. Bando T, Narita A, Saito I, Sugiyama H: Molecular design of a pyrrole-imidazole hairpin polyamide for effective DNA alkylation. *Chemistry* 8: 4781–4790, 2002
23. Magin-Lachmann C, Kotzamanis G, D'Aiuto L, Wagner E, Huxley C: Retrofitting BACs with G418 resistance, luciferase, and oriP and EBNA-1—New vectors for in vitro and in vivo delivery. *BMC Biotechnol* 3: 1–12, 2003
24. Harger JW, Dinman JD: An in vivo dual-luciferase assay system for studying translational recoding in the yeast *Saccharomyces cerevisiae*. *RNA* 9: 1019–1024, 2003
25. Wolf G, Ziyadeh FN: Molecular mechanisms of diabetic renal hypertrophy. *Kidney Int* 56: 393–405, 1999
26. Ying WZ, Sanders PW: Dietary salt modulates renal production of transforming growth factor-beta in rats. *Am J Physiol* 274: F635–F641, 1998
27. Romeo D, Allison RS, Kondaiah P, Wakefield LM: Recharacterization of the start sites for the major human transforming growth factor-beta 1 mRNA. *Gene* 189: 289–295, 1997
28. Geiser AG, Kim SJ, Roberts AB, Sporn MB: Characterization of the mouse transforming growth factor-beta 1 promoter and activation by the Ha-ras oncogene. *Mol Cell Biol* 11: 84–92, 1991
29. Pennacchio LA, Rubin EM: Genomic strategies to identify mammalian regulatory sequences. *Nat Rev Genet* 2: 100–109, 2001
30. Heinemeyer T, Wingender E, Reuter I, Hermjakob H, Kel AE, Kel OV, Ignatieva EV, Ananko EA, Podkolodnaya OA, Kolpakov FA, Podkolodny NL, Kolchanov NA: Databases on transcriptional regulation: TRANSFAC, TRRD and COMPEL. *Nucleic Acids Res* 26: 362–367, 1998
31. Oyoshi T, Kawakami W, Narita A, Bando T, Sugiyama H: Inhibition of transcription at a coding sequence by alkylating polyamide. *J Am Chem Soc* 125: 4752–4754, 2003
32. Shinohara K, Narita A, Oyoshi T, Bando T, Teraoka H, Sugiyama H: Sequence-specific gene silencing in mammalian cells by alkylating pyrrole-imidazole polyamides. *J Am Chem Soc* 126: 5113–5118, 2004
33. Pertovaara L, Sistonen L, Bos TJ, Vogt PK, Keski-Oja J, Alitalo K: Enhanced jun gene expression is an early genomic response to transforming growth factor beta stimulation. *Mol Cell Biol* 9: 1255–1262, 1989
34. Kim SJ, Denhez F, Kim KY, Holt JT, Sporn MB, Roberts AB: Activation of the second promoter of the transforming growth factor-beta 1 gene by transforming growth factor-beta 1 and phorbol ester occurs through the same target sequences. *J Biol Chem* 264: 19373–19378, 1989
35. Best TP, Edelson BS, Nickols NG, Dervan PB: Nuclear localization of pyrrole-imidazole polyamide-fluorescein conjugates in cell culture. *Proc Natl Acad Sci U S A* 100: 12063–12068, 2003
36. Belitsky JM, Leslie SJ, Arora PS, Beerman TA, Dervan PB: Cellular uptake of N-methylpyrrole/N-methylimidazole polyamide-dye conjugates. *Bioorg Med Chem* 10: 3313–3318, 2002
37. Gupta S, Clarkson MR, Duggan J, Brady HR: Connective tissue growth factor: Potential role in glomerulosclerosis and tubulointerstitial fibrosis. *Kidney Int* 58: 1389–1399, 2000
38. Yokoi H, Sugawara A, Mukoyama M, Mori K, Makino H, Suganami T, Nagae T, Yahata K, Fujinaga Y, Tanaka I, Nakao K: Role of connective tissue growth factor in profibrotic action of transforming growth factor-beta: A potential target for preventing renal fibrosis. *Am J Kidney Dis* 38: 134–138, 2001
39. Sanders PW: Salt intake, endothelial cell signaling, and progression of kidney disease. *Hypertension* 43: 142–146, 2004
40. Dahly AJ, Hoagland KM, Flasch AK, Jha S, Ledbetter SR, Roman RJ: Antihypertensive effects of chronic anti-TGF-beta antibody therapy in Dahl S rats. *Am J Physiol Regul Integr Comp Physiol* 283: R757–R767, 2002